FINITE ELEMENT STUDY OF UNSTIFFENED EXTENDED SINGLE PLATE SHEAR CONNECTIONS

By

Ahmad Abou-Zidan

Submitted in partial fulfilment of the requirements
for the degree of Master of Applied Science

at

Dalhousie University
Halifax, Nova Scotia
April 2014

DEDICATION

This work is dedicated to

My Parents, *Galal Abou-Zidan* and *Rulla Aboushahla,*

For their endless love, support and encouragement

TABLE OF CONTENTS

List of Tables

List of Figures

Abstract

Steel shear tabs are commonly used in beam-to-girder and beam-to-column connections where a vertical plate is welded to the column or girder web, and bolt connected to the web of the in-framing beam. The extended shear tab (EST) is one increasingly popular option when it is necessary to bring the bolt line outside of shop applied coatings or encasement. The effect of greater eccentricity resulting from extending the bolt line needs to be accounted for in design.

The current Canadian steel design standard CSA S16-09 does not contain guidelines for design of EST connections. The AISC Manual 2011 provides a design procedure for EST connections based on the bolt effective eccentricity. The effective eccentricity values based on this method have been shown to be overly conservative in some cases, which ultimately leads to underestimation of the connection capacity

This research presents results of a numerical study on the behaviour amd strength of EST connections using finite element modelling. The model is verified with experimental results reported in literature. The parameters studied include the web slenderness ratio of supporting column, distance 'a', plate thickness, double-row of bolts, beam lateral restraint, beam length-to-depth ratio and number of bolts. The effects of these parameters on the behaviour and bolt shear strength are presented and discussed. Results are also used to assess the effectiveness of the AISC design provisions. It shows that in general, the AISC 2011 design procedure is overly conservative in predicting bolt shear for parameters studied. The overall underestimation on the capacity is around 60 to 65% when compared with finite element results. The finite element determined eccentricity is markedly lower than the AISC specified value. If the AISC 2011 design procedure is used but in combination with the finite element determined effective eccentricity, the estimate on bolt shear strength can be improved by approximately 30% for EST coonetions with 3 and 4 bolts. But for higher number of bolts, the AISC design procedure seems to provide adequate bolt strength estimate.

List of Abbreviations and Symbols Used

A_b: Bolt cross-sectional area

AISC: American Institute of Steel Construction

a: Distance between weld and bolt line

C: Number of effective bolts

CISC: Canadian Institute of Steel Construction

C.G: Cener of gravity of bolt group

CST: Conventional shear tab

C': Coefficient from Part 7 for the moment only case

d: Beam depth

d_b: Bolt diameter

d_p: Plate depth

EST: Extended shear tab

e: Bolt eccentricity

$e_{b,AISC}$: Bolt eccentricity from AISC 2011

$e_{b,FE}$: Bolt eccentricity from FE model

e_{weld}: Weld eccentricity

F_a: Vector of applied load

FE: Finite element

F_i^n: Restoring load

F_u: Ultimate connection shear from FE model

$F_{u,AISC}$: Ultimate connection capacity from AISC 2011 design procedure

$F_{u,FE}$: Bolt shear including bolt group reduction factor based on $e_{b,FE}$

F_v: Nominal bolt shear strength from AISC Table J3.2

f_y: Plate yield stress

h: Plate height

h/w: Column web slenderness ratio

ICR: Instantaneous center of rotation

K_i^t: Tangent matrix

L: Beam length

L_{eh}: Horizontal edge distance

L_p: Plate length

L/D: Beam length-to-depth ratio

l_{ev}: Vertical edge distance

n: Number of bolts

R: Bolt shear at a deformation Δ

R_{ult}: Maximum bolt shear at maximum bolt deformation

S: Beam section modulus

SSL: Short-slotted bolt hole

STD: Standard bolt hole

t_{max}: Maximum plate thickness

t_p: Plate thickness

t_w: Beam web thickness

V_t: Shear force to cause twist failure

Z_{pl}: Plastic section modulus of shear tab

ε_e: Engineering strain

ε_{true}: True strain

θ_{beam}: Beam end rotation

θ_{tab}: Shear tabe rotation

θ_{twist}: Plate twist

θ_{web}: Column web rotation

σ_e: Engineering stress

σ_t: True stress

Δ: Bolt deformation

Acknowledgements

I would like to give sincere gratitude to my research advisor, Dr. Yi Liu, who provided valuable guidance throughout the course of this research. I will never forget her generous contributions, understanding and encouragement as I overcome all the obstacles in the completion of this research.

My thanks also go to my thesis committee members Dr. Farid Taheri and Dr. Stephen Corbin for their time spent on reviewing this thesis. I would like to express my thanks to the faculty and staff of the Department of Civil and Resource Engineering for their support.

Lastly, I would like to thank my friends and family, most importantly, my parents who provided me with unparalleled support and inspiration.

CHAPTER 1 Introduction

1.1 Background of Research

In steel construction, connections are used to connect either beams to girders or beams to columns. Connection design is one crucial design component and often more complex than the associated members design. Depending on the level of restraint developed by the connections, they can be categorized into three main types, including rigid, simple and semi-rigid connections. The connection type will affect the distribution of internal forces throughout the structure. A simple connection assumes that the ends of beams and girders are free to rotate in the plane of loading. This allows for the transfer of shear but prevents the buildup of bending moment in the connection. Rigid connections assume that there is no relative rotation between the two connecting members. This allows for the transfer of both shear and bending moment. A semi-rigid connection provides a restraint somewhere in between the simple and rigid connection and thus the shear and bending moment being transferred is dependent on the stiffness of the connection. It should be pointed out that the assumed connection type may not truly reflect the behaviour of the connection in reality. For instance, simple connections may still develop small end moments, which will be transferred to the supporting member. In some cases, as in double angle connections, this moment is small and often ignored in design while in other cases such as shear tab connections, this moment needs to be considered.

1.2 Shear Tab Connection Behaviour

Shear tab connections are also known as single plate connections, which consist of a single rectangular steel plate with pre-punched holes. Figure 1.1 shows a schematic view of a shear tab connection. Shear tabs are often used to frame beams into supporting girder webs or column webs or flanges. The steel plate is often shop-welded to the supporting member and field bolted to the supported beam. It is a simple, inexpensive and popular shear connection for light to moderate end shears. As shown in Figure 1.1, the connection detail leads to an offset between the vertical weld and the centroid of the bolt group. This distance between the weld line and bolt line is referred to as "a". At low load levels, the shear tab is quite stiff. This results in the development of some moment in the connection and the beam, which is equivalent to an eccentric load on the bolts and welds. This eccentricity is based on the location of the point of inflection. As the load on the beam increases and the shear tab begins to yield, the inflection point moves toward the support. The effective bolt eccentricity, e_b, is defined as the distance between the point of inflection in the beam to the bolt line at failure as seen in Figure 1.1. The bolts in shear tab connections should therefore, be designed to resist shear from the supported beam and an eccentric moment equal to the product of the connection shear and e.

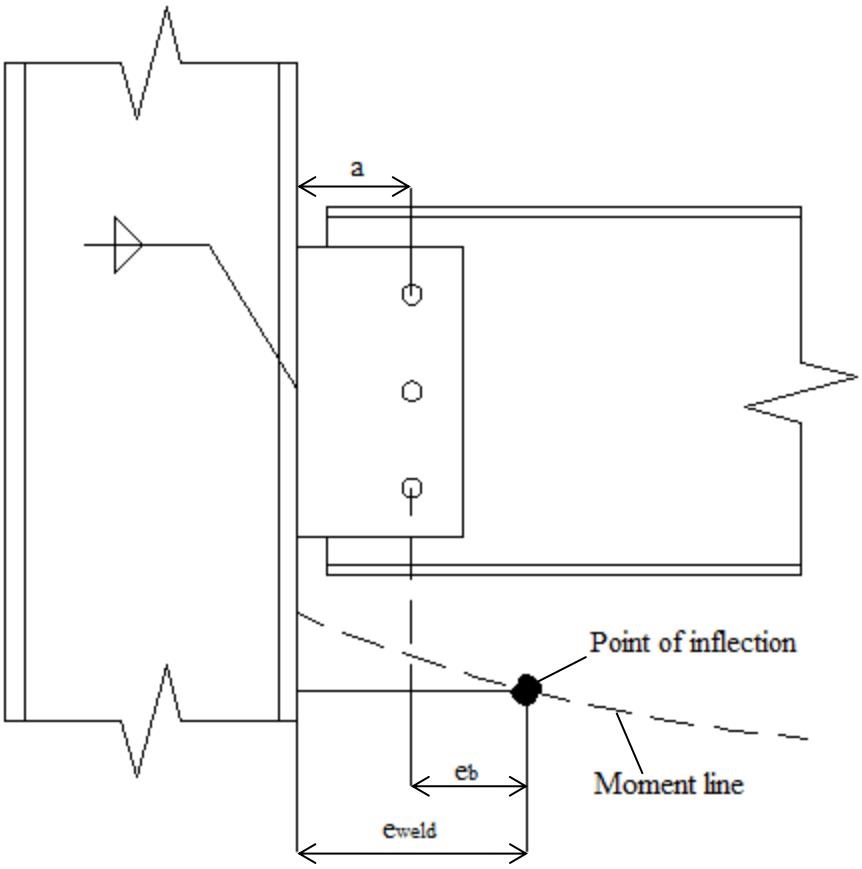

Figure 1.1 Standard shear tab connection

The behaviour and strength of shear tab connections has been studied for the past three decades. The results have shown that the end moments developed depend on many geometric and material properties such as the thickness of the plate; the number, size and arrangement of bolts, and the flexibility of the supporting member. However, majority of the research has been focused on the shear tab connections with "a" ≤ 90mm. These connections are referred to as conventional shear tab connections. The design guidelines and recommendations based on these research were then only applicable to shear tab connections with "a" ≤ 90mm.

1.3 Extended Shear Tab Connections

In recent shear tab application, shear tabs with long distance "a" (> 90mm) are used when it is desired to extend the bolt line outside the supporting member's flange. Extending the shear tab beyond the supporting member's flange eliminates the need to cope the supported beam. Additionally, the extension eases erection, as more space is available to fit bolt wrenches for fastening bolts. The extension results in quickening the erection and fabrication processes, which in turn leads to reduction in costs. To distinguish from the conventional shear tab (CST), the shear tab with an a-distance greater than 90 mm is referred to as extended shear tab (EST). Figure 1.2 illustrates both the CST and EST connection.

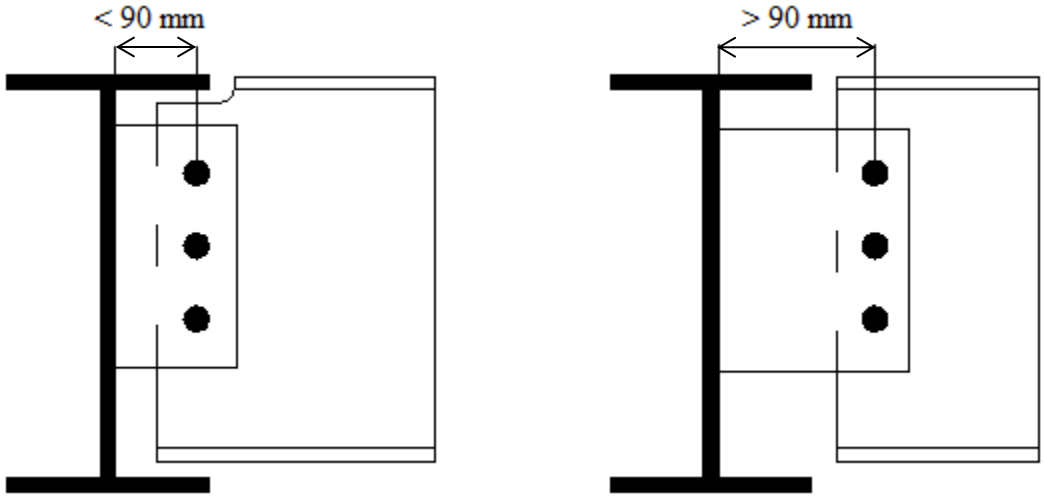

Figure 1.2 CST and EST framing into the supporting girder

Compared with the conventional shear tab connections, the previous research on the extended shear tab connections is limited and experimental studies and the test results are scarce in the reported literature. The few available studies have shown that geometric and

material factors influential for conventional shear tab connection will also affect the behaviour of extended shear tab connection. But the longer shear tabs in ESTs will result in different effective eccentricity and failure modes that were not observed in CSTs, and ultimately affect the capacity. For design practice, the current Canadian steel design standard S16-09 (2010) does not contain guidelines for the design of ESTs. The AISC manual 2011 just included a new section on the design of ESTs but the accuracy of the provision needs to be evaluated with more studies.

1.4 Objectives and Scope

This study is therefore motivated to investigate the behaviour and strength of extended shear tab connections. A numerical study based on finite element modeling is used in this investigation. The model is verified using available test results reported in the literature. A parametric study using the verified model is subsequently conducted to study the effects of several parameters on the behaviour and strength of the connections. The detailed objectives of this research are:

1. to conduct a comprehensive literature review on research relevant to the behaviour and strength of extended shear tabs and collect available test results.
2. to develop a finite element model for the extended shear tab connections.
3. to validate the finite element model using experimental results from available literature.
4. to conduct a parametric study to investigate the effect of parameters including supporting member stiffness, distance “a”, plate thickness, double-row of bolt

arrangement, lateral restraint of the beam, beam length-to-depth ratio and number of bolts on the behaviour and strength of extended sher tab connections.

5. to examine the accuracy of provisions suggested in the AISC manual 2011 on the design of extended shear tab connections and make recommendations as appropriate.

1.5 Outline of Research

This thesis commences with a review of previous research conducted on extended shear tab connections in Chapter 2. Chapter 3 describes the development of the finite element model. The verification of the model with available test results is presented in Chapter 4. Chapter 5 summarizes and discusses the results of parametric study using the finite element model. Chapter 6 provides the summary, conclusions and recommendations from this research.

CHAPTER 2 Literature Review

The research on shear tab connections dated back in 1960s with earlier research being focused on the conventional shear tab connections. In 2000s the research in extended shear tab connections began to attract attention as this type of connections became popular in practice. It should be pointed out that several failure modes of shear tab connections might be possible depending on geometric and material properties of the connection. Previous research on CSTs revealed that in addition of the shear failure of the bolts, yielding of the tab, fracture of the tab, bearing failure of the beam web or shear tab, and fracture of welds need also be checked as other limit states. Since this study focuses on the bolt shear capacity of the connection, the following literature review summarizes the results more pertinent to bolt shear strength.

2.1 Previous Research

Lipson (1968) tested 85 conventional shear tab connections. The number of bolts was varied from 2 to 6 and the 'a' distance was kept at 45 mm (1.75 in) or 65 mm (2.5 in). Moment-rotation curves obtained from test results have shown that single plate connections with two bolts experienced long yielding at a constant connection moment, and as the number of bolts increased the moment increased at a decreasing rate. It was also shown that the flexibility of the connection was entirely due to the bolt displacement in the bolt holes where significant deformations were observed. The center of rotation was found to coincide with the centroid of the bolt group. Some of the single plate shear

connections failed under load by means of cracking in the plate below the bottom bolt, cracking of the weld or cracking in the tension edge of the plate.

Richard et al. (1980) conducted five full-scale beam tests on three, five and seven bolted CST connections. One end of the beam was bolted to a shear tab that was in turn welded to the flange of the supporting column and the other end of the beam rested on a roller support. A concentrated load was applied at mid-span of the beam. The location of the point of inflection as a function of the applied load was experimentally determined. The researchers concluded that the effective eccentricity is a function of number and size of the bolt and the section modulus of the beam.

Young and Disque (1981) developed a set of design tables for the design of CSTs based on results obtained by Richard et al. (1980). The tables were developed with the assumption the connection support is fixed. The eccentricity, e, can be determined through a simple quotient shown below in Equation [2.1]. The $e(s)^{0.4}$ value is obtained from a table according to the L/D, n and bolt size. The $(S)^{0.4}$ value is obtained from another set of tables according to the size of the beam section.

$$e = \frac{e(S)^{0.4}}{S^{0.4}} \qquad [2.1]$$

Richard et al. (1982) conducted research on conventional single plate connections with slotted holes. It was suspected that connection moment would significantly lessen with the use of slotted holes. Fifteen full-scale specimens were tested using 22 mm (7/8-in)

nominal diameter A307 bolts. The bolts were snug-tightened using a wrench in some, and were simply finger-tightened in others. The results showed that the eccentricity, e, was virtually zero for all finger-tightened tests when compared to connections with snug-tightened bolts. It can also be seen from the test results that for the same number of bolts, higher beam length-to-depth ratios resulted in larger eccentricities.

Hormby et al. (1984) conducted eight full-scale tests using a 9.75 m (32 ft) long W24x55 steel section connected to a rigid support at one end with a 9.5 mm (3/8 in) plate and simply supported on a roller on the other end. The experimental eccentricity test results for slotted holes compared well with the predicted design curve eccentricities developed by Richard et al. (1980). It was concluded that the design curve developed by Richard et al. (1980) can be used to determine eccentricities for single plate connections with slotted holes.

Astaneh et al. (1989) tested five full-scale beam-to-column single plate CST connections. It was found that the strength of shear tabs was a function of the stiffness of the supporting member whether being a beam or a column. Shear tabs connected to column flanges were more so restrained from end rotation than when connected to the web of a girder. This resulted in different effective eccentricities on the bolts. Eccentricities were found to be a function of the number of bolts. Shear tabs on flexible supports have larger bolt eccentricities and therefore lower resistances. However, as the number of bolts increases to seven, the effective eccentricities are the same for both rigid and flexible

supports. Astaneh et al. (1989) proposed an analytical solution, expressed in Equations [2.2] and [2.3], for determining the effective eccentricity for bolts.

for rotationally rigid support:

$$e = \left|(n-1)(25mm) - a\right| \qquad [2.2]$$

for rotationally flexible support:

$$e = \left|(n-1)(25mm) - a\right| \geq a \qquad [2.3]$$

The authors developed a design procedure for single plate shear connections. The procedure ensures that ductile yielding of plate precedes the brittle fracture of bolts, tab and welds. The design procedure developed by Astaneh et al. (1989) was adopted by the Canadian steel design standard S16-09 for conventional shear tab connection design.

Porter and Astaneh (1990) conducted experimental testing of conventional shear tab connections in short slotted holes. Four CST connections with 3, 5, 7 and 9 bolts in slotted holes were tested. The researchers recommended the following equations for CST connections with short-slotted holes.

$$e = \left|\frac{2n}{3} - a\right| \qquad \text{for a rigid support with short slotted holes} \qquad [2.4]$$

$$e = \left|\frac{2n}{3} - a\right| \geq a \qquad \text{for a flexible support with short slotted holes} \qquad [2.5]$$

The design equations recommended by Astaneh et al. (1989) and Porter and Astaneh (1990) were adopted in the AISC *Manual of steel construction, Load and Resistance Factor Design* (1994) single plate shear connection design procedure.

Sherman and Ghorbanpoor (2002) tested full-scale connection specimens to develop a design procedure for extended shear tabs welded to the webs of supporting girders or columns. This was the first reported literature on EST connections. They concluded that for three and five-bolt connections, the calculated connection ultimate capacities based on measured eccentricities correlated better with experimental results than capacities calculated using the eccentricity values of the AISC 1994 equations for CST connections. As the number of bolts increases to six and eight, the AISC eccentricity equations predicted the experimental eccentricities much closer. Therefore, Sherman and Ghorbanpoor recommended Equation [2.6] and [2.7] for determining the effective bolt eccentricity for EST connections where e_b is in inches.

$$e = n \leq a, \text{ in} \qquad \text{for } n \leq 6 \qquad [2.6]$$

$$e = 3 + n/2 \leq a, \text{ in} \qquad \text{for } n > 6 \qquad [2.7]$$

They also indentified two additional limit states that may govern the design of unstiffened extended shear tab connections framing into column webs. A bending failure of the column web support and twisting failure of the shear tab were identified. The twisting of the shear tab is caused due to the eccentricity of the shear force to the centroid of the shear tab as the beam web is connected to one side of the extended shear tab. The twisting shear stress becomes increasingly pronounced as the shear tab becomes longer

and deeper. When the beam at connection location is not laterally braced, the twisting of the shear tab may lead to failure. They proposed the following equation to estimate the capacity for the twisting failure of shear tab.

$$V_t = 0.3 d_p t_p f_y \quad [2.8]$$

Where

V_t = Maximum allowable shear force

f_y = Shear tab yield stress

d_p = Shear tab depth

t_p = Shear tab thickness

Ashakul (2004) conducted a finite element (FE) analysis on both CST and EST connections using software ABAQUS. Several parameters were considered such as the a-distance, plate thickness, and double-row bolt connections. It was concluded that the eccentricity was not a function of the a-distance and those connections that did not satisfy the plate ductility criteria would result in significant moments. Additionally, it was found that force redistribution takes place for double-row connections. However, redistribution did not occur when plates were thick, resulting in bolts of the farther row from the supporting member fracturing, whereas the other row resisting much less force.

Creech (2005) conducted ten full scale conventional single plate connections and results were used to quantify the effective eccentricity. The ten specimens included flexible and rigid support conditions and STD and SSL holes. A key observation made by Creech was

that eccentricity can be neglected for connections with more than three bolts if the 20% bolt strength reduction factor is included in the nominal bolt shear strength. The AISC Specification (2005) incorporates the 20% reduction factor to the nominal bolt shear strength to account for non-uniform load distributions in connections.

Rahman et al. (2007) showed that the finite element modeling can be used to simulate the behaviour of EST connections. The model developed provided results in good agreement with the experimental results. The authors pointed out that the details of the connection such as boundary conditions, load application, coefficient of friction between surfaces, and pretension of bolts should be accurately modeled to produce satisfactory results. However, no parametric study was conducted using the model.

2.2 Eccentrically Loaded Bolt Groups

When the bolt group is subjected to an eccentric load, the bolts must be designed to resist the combined effect of the direct shear and induced moment. There are two main analysis methods for design, i.e., the elastic method and the instantaneous center of rotation (ICR) method. The elastic method is more simplified but may be excessively conservative because it neglects ductility of the bolt group and the potential for load redistribution. The ICR method is more accurate but calculations are more tedious and requires iterations to the solution.

In the elastic method, the eccentrically applied load in a single plate shear connection is resolved into a direct shear, P, acting through the center of gravity (C.G) of the bolt group

and a moment, P*e, where e is measured from the C.G of the bolt group to the load P. The magnitude of force in each bolt is then the result of the load P plus the couple P*e. The moment is assumed to cause the plate to rotate about the C.G of the bolt group. Each bolt is assumed to resist an equal share of the direct shear and a share of the eccentric moment proportional to its distance from the C.G. The amount of rotation or strain at a particular bolt is proportional to its distance from the C.G. This means that stress is the greatest at the bolt furthest from the C.G of the bolt group since stress is proportional to strain in the elastic range. There are two key assumptions in the elastic method. Firstly, the elastic method assumes a linear relationship between the loads and deformations in the bolts. Additionally, this method assumes that the yield stress is not exceeded when the ultimate load on the connection is reached.

In the instantaneous center of rotation method, the combined effect of rotation and translation is equivalent to a rotation about a point defined as the ICR. This concept was first introduced by Yarimci and Slutter (1963) based on riveted connections and the material was assumed elastic. The ICR is located a certain distance e' from the center of gravity (C.G) of the bolt group as shown in Figure 2.1. The ICR falls on a horizontal line through the center of gravity of the bolt group and is found by trial and error. The bolt deformations are assumed to vary in proportion to their distance from the ICR. Based on experimental data the maximum bolt deformation is set to be 8.6 mm (0.34 in). The nominal shear strength of the bolt group is the sum of the individual strengths of all bolts. The individual resistance of each bolt is assumed to act on a line perpendicular to ray passing through the ICR and the centroid of that individual bolt. The correct location of

the ICR is determined when the three equations of equilibrium are satisfied ($\sum F_x = 0$, $\sum F_y = 0$, $\sum M = 0$). This method no longer assumes a linear relationship between the load and bolt deformation as was assumed in the elastic method.

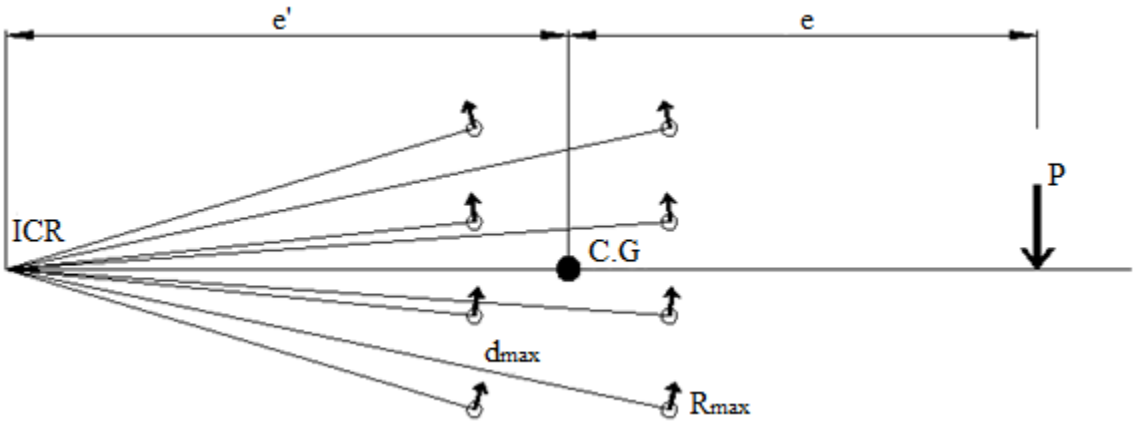

Figure 2.1 Illustration for instantaneous center of rotation method

For calculating the shear of a bolt at any given deformation, Crawford and Kulak (1968) proposed the Equation [2.9] as follows:

$$R = R_{ult}(1 - e^{-10\Delta})^{0.55} \qquad [2.9]$$

where

R = Nominal shear strength of one bolt at a deformation Δ, kips

R_{ult} = Ultimate shear strength of one bolt, kips

Δ = Total deformation, including shear bearing and bending deformations in the bolt and bearing deformation of the connection elements, in

Equation [2.9] developed by Crawford and Kulak (1968) and the ICR method developed by Yarimci and Slutter (1963) are the basis of procedures in the current AISC 2011, *Steel Construction Manual* for design of EST connections. A set of tables entitled 'Coefficients C for Eccentrically Loaded Bolt Groups' are the expansion of these concepts. The coefficient C, known as the number of effective bolts, is extracted from these tables depending on the bolt pattern, bolt spacing, eccentricity and angle of inclined loading. This coefficient predicts the number of 'effective' bolts in the single plate shear connection.

2.3 Single Plate Design Procedure in Standards

As mentioned, early research on the ultimate capacity was focused on conventional shear tab connections. The design standards of North America were developed based largely on empirical interpretation of experimental results on specimens satisfying certain geometric restraints. The following sections present design methods specified in the Canadian steel design standard CSA S16.09 (2010) and AISC manual 2011. These methods are used in the later calculation in Chapter 5.

2.3.1 CSA S16-09

The Canadian steel design standard S16-09 does not provide an explicit design provision for CST connections. Instead, it provides a factored load resistance table for CST connections satisfying specific plate geometry and bolt configurations. The table is based on the test results and design recommendations suggested by Astaneh et al. (1989). The table is only applicable for CST connections with an "a" distance of 75 mm between the

bolt line and the weld line. There are currently no guidelines for the design of EST connections in the CSA S16-09.

2.3.2 AISC Manual 2011

The design method for CSTs in the earlier edition of AISC manual 2005 was based on the work by Astaneh et al. (1989) and Creech (2005) where the bolt eccentricity is implicitly considered by reducing the nominal bolt group shear strength by 20%. However, the nominal bolt shear strength was increased by 10% in the AISC specification 2010, so overlooking the bolt group eccentricity was no longer suitable. The main changes made to the CST design procedure were based on research done by Muir and Thornton (2011). In this edition, design values of the effective eccentricity for conventional single plate shear connections are no longer ignored. The eccentricity values for CST connections are listed in Table 2.1. They are dependent on the number of bolts and the hole type (STD or SSLT).

Table 2.1 Design values for conventional single plate shear connections

n	**Hole Type**	**e, in**	**Maximum t_p or t_w, in**
2 to 5	SSLT	a/2	None
	STD	a/2	$d_b/2+(1/16)$
6 to 12	SSLT	a/2	$d_b/2+(1/16)$
	STD	a	$d_b/2-(1/16)$

For the design of extended shear tab connections, no limitations are placed on the number of rows or the number of bolts used in the connection. Most importantly the distance from the weld line to the bolt line closest to the support is not limited. The AISC manual

2011 EST design procedure states that the bolt eccentricity is to be taken equal to the distance from the weld line to the bolt line (distance 'a'). The EST connections needs to be checked for plate shear yielding, shear rupture, block shear rupture and plate buckling.

2.4 Concluding Remarks

The literature review shows that most of available research has been conducted to study the behaviour of conventional shear tab connections. The research on extended shear tab connections only began in 2000s which led to limited technical and scientific information available. Moreover, the design procedures developed were largely based on previous research results for shear tab connections with certain geometric and material properties and thus the validity of these procedures applied to other situations is questionable. The finite element modeling has been shown to be an effective tool to investigate a wide range of parameters and results can be used to supplement the test data. However, the parameters considered in previous finite element studies are limited. Additionally, there is little data on the effect of the lateral support on the twisting on EST connections. More information on the beahaviour and strength of extended shear tab connections as affected by influential parameters is needed.

CHAPTER 3 Finite Element Model

3.1 General

The numerical simulations were conducted using the finite element software ANSYS 13.0 (2010). ANSYS is capable of simulating the nonlinear structural response incorporating various geometric and material characteristics. The finite element model developed in this study consists of a beam framing into the web of a supporting column with a single plate shear connection. The following sections describe the element selection, finite element mesh, material properties, boundary conditions, load application, and analysis technique. The finite element model was verified with experimental results on CSTs obtained by Astaneh et al. (1989) and on ESTs obtained by Sherman and Ghorbanpoor (2002).

3.2 Element Selection

Several finite elements were investigated in determining which elements can most efficiently simulate the nonlinear structural response of the connection. The aim was to generate a model that can achieve a balance between running time and structural response accuracy. The first order SOLID185 and second order SOLID186 finite elements were examined. The SOLID185 is a three-dimensional eight-node structural solid with three translational degrees of freedom per node, suitable for modeling large rotation and large strain nonlinearities. The high order SOLID186 finite element is similar to SOLID185 except that it is a 20-node solid with three translational degrees of freedom per node.

They are shown in Figure 3.1. The SOLID186 exhibits quadratic displacement behaviour and is able to capture the stresses and strains more accurately in vicinities of high stress concentrations. However, the use of SOLID186 increases the simulation time significantly due to the quadratic displacement behaviour and number of nodes. The 3-bolt CST connection tested by Astaneh et al. (1989) was simulated using both SOLID185 and SOLID186. Figure 3.2 illustrates the shear versus beam end rotation of the connection using the two elements. It can be seen that the beam rotation response obtained using both elements were identical. The total computing time for the first order SOLID185 was approximately 3 hours and for the SOLID186 was 7 hours. Therefore, the SOLID185 elements were used in the model.

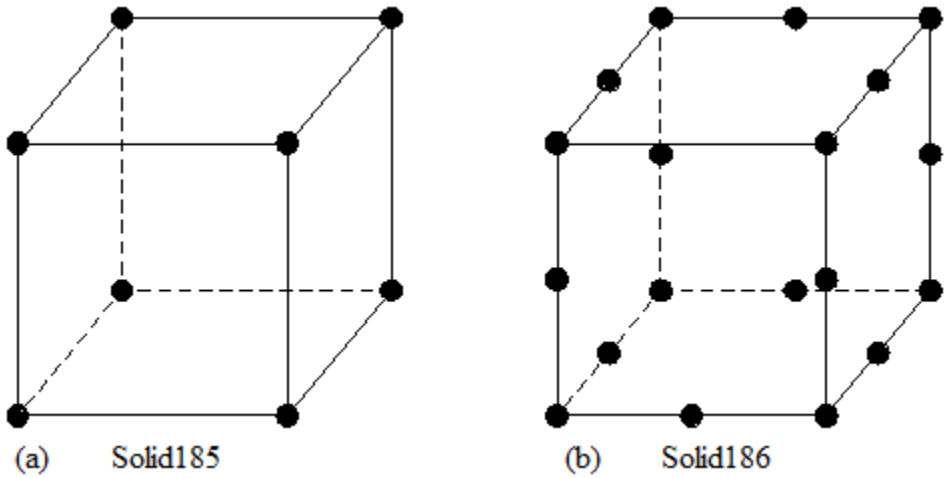

Figure 3.1 Three-dimensional structural solid finite elements

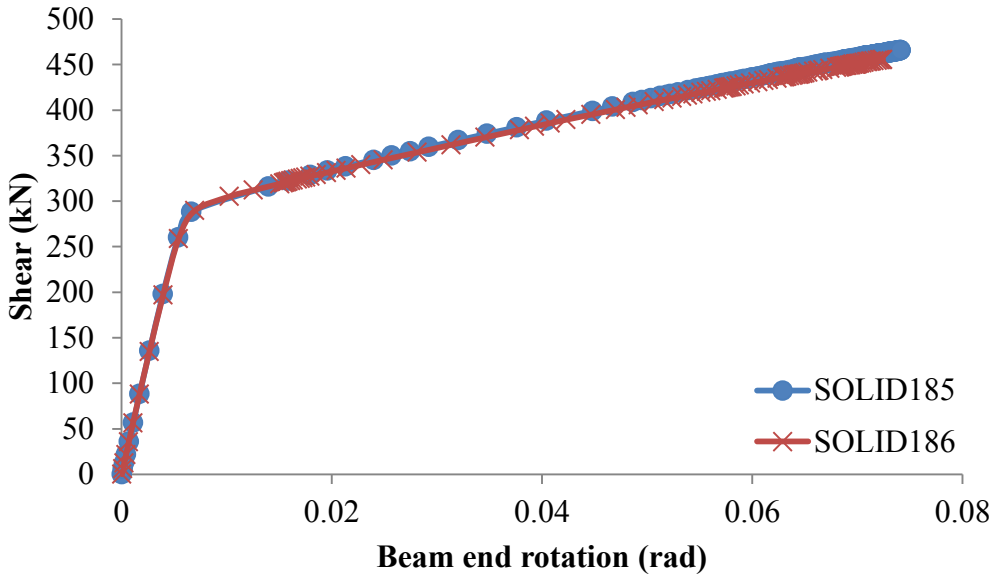

Figure 3.2 Beam end rotation of SOLID185 and SOLID186

Targe170 and Conta174 are surface to surface contact elements which overlay solid elements to simulate the physical transfer of force through contact and friction between the two bodies. Targe170 and Conta174 are 4-node quadrilateral element. Contact elements were used on the adjacent surfaces of the shear tab and beam web, the bolt shank and shear tab holes, the bolt shank and web holes, the bolt head and shear tab and finally the nut and beam web surfaces. The PRETS179 element was used to define the pretension section within the meshed high strength bolts. This element has one translational degree of freedom. The pretension force was applied normal to the cross-section of the bolt shank (in the z-direction). Figure 3.3 illustrates the pretension surface for a 3-bolt CST connection. A summary of the various elements used in the analysis is provided in Table 3.1.

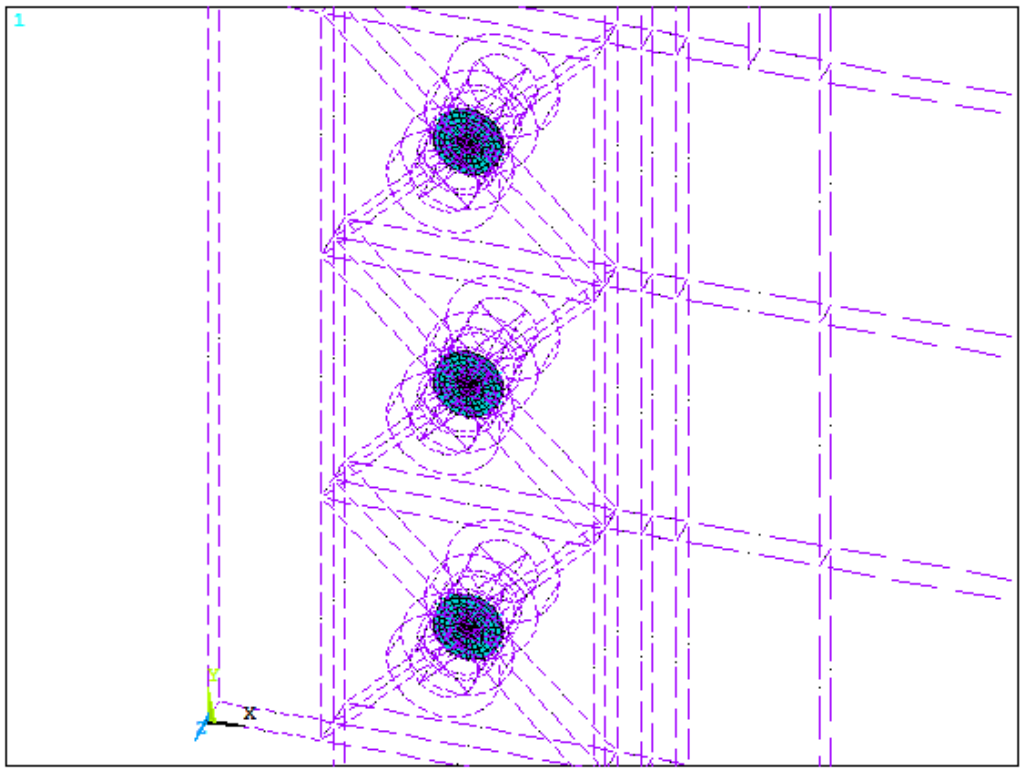

Figure 3.3 Pretension surface for CST connection

Table 3.1 Element type summary

Element Name	Number of Nodes	Degrees of Freedom
SOLID185	8	UX,UY,UZ
SOLID186	20	UX,UY,UZ
TARGE170	8	UX,UY,UZ
CONTA174	8	UX,UY,UZ
PRETS179	3	User Defined

3.3 Mesh Refinement

Since the behaviour of the shear tab connection rather than the global behaviour of the beam is the focus of the study, the mesh density for the shear tab is more important.

Therefore, a mesh density study was carried out for the shear tab. The 3-bolt connection tested by Astaneh et al. (1989) was modelled with three different shear tab mesh densities. The mesh densities had a maximum element width of 9.5, 4.8 and 2.4 mm Figures 3.4, 3.5 and 3.6 illustrate the three meshes. The shear tab was restrained from translations in the x, y and z-directions along the weld line.

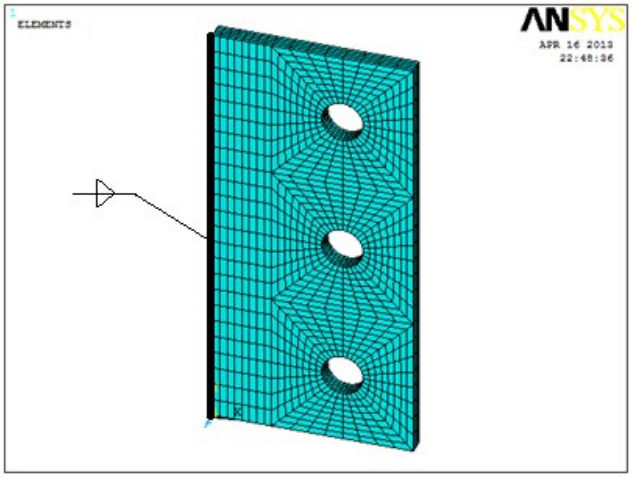

Figure 3.4 FE mesh with maximum element width of 9.5 mm

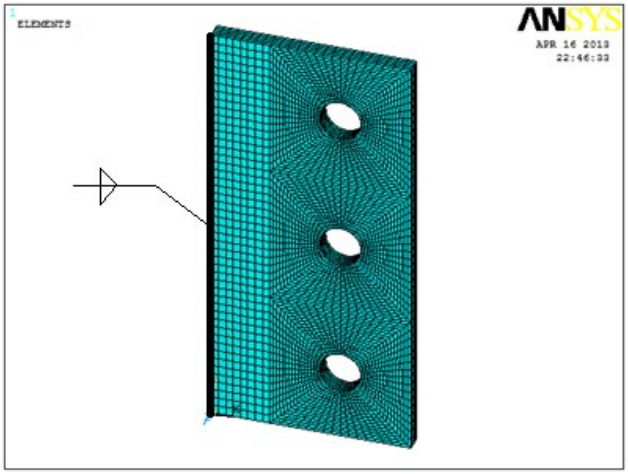

Figure 3.5 FE mesh with maximum element width of 4.8 mm

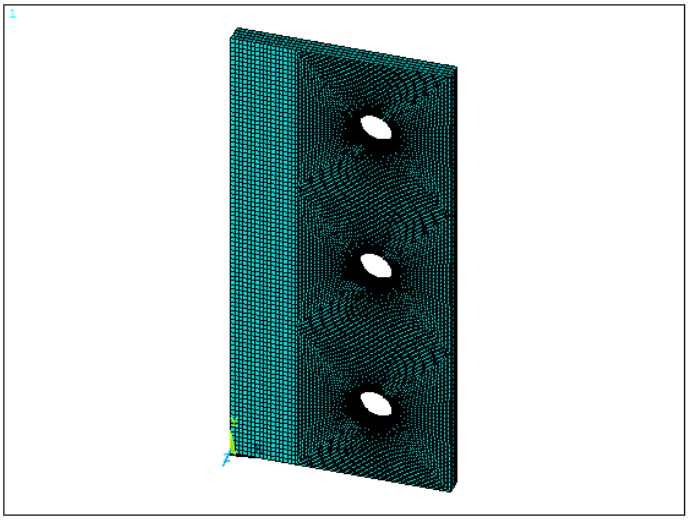

Figure 3.6 FE mesh with maximum element width of 2.4 mm

To ensure smooth contact between the bolt shank and the holes, the bolt had the same mesh size as the plate. The bolt, bolt head and nut were modelled as one solid body as shown in Figure 3.7. Additionally, a 2 mm gap was provided between the bolt shank and the holes in the shear tab and beam web. This was to mimic the true geometry of the shear connection where the punched holes are commonly 2 mm bigger in diameter than the bolts. The contact elements, Targe170 and Conta174, were used to simulate the physical transfer of force through contact and friction between the two bodies.

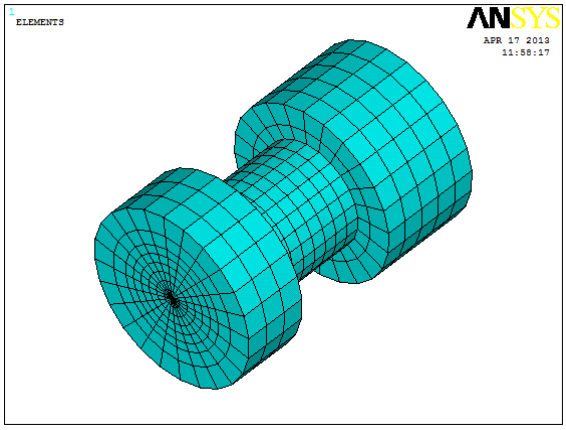

Figure 3.7 Bolt mesh

Two mesh sizes were implemented for the beam. In the vicinity of the bolts a fine mesh was needed to capture the high stress concentrations with element dimensions of 9.5 mm by 10mm. Away from the bolt line, the mesh dimension increased to 17 mm by 19 mm. The beam flange was modelled with 6 elements across the width of the beam. Figure 3.8 illustrates the mesh configuration of the beam and the connection.

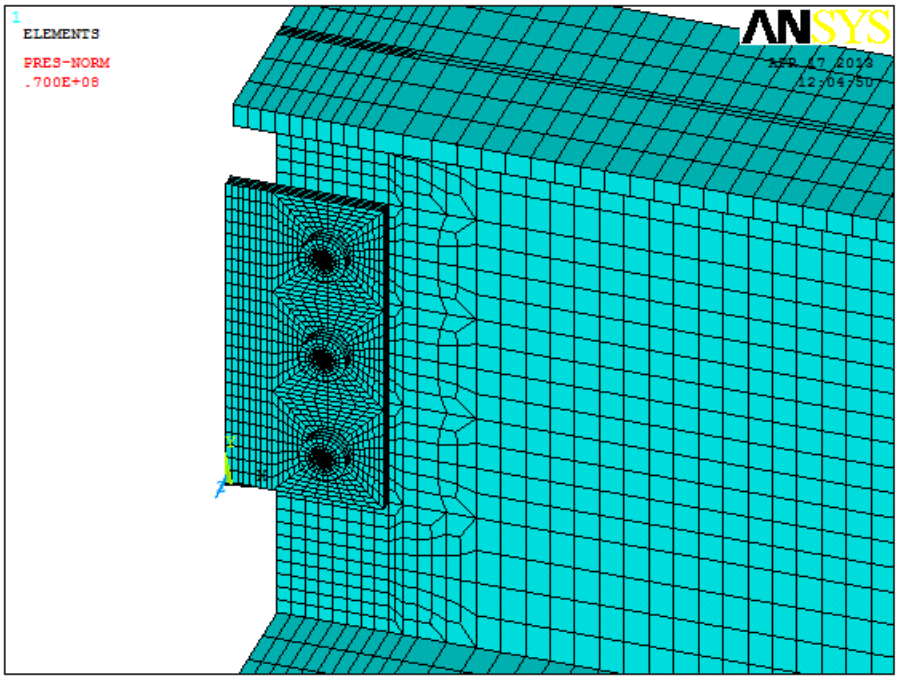

Figure 3.8 Mesh configuration for CST verification model (Astaneh et al. 1989)

The supporting member, column, has the same mesh configuration as the shear tab. This allows for the nodes along the end of the shear tab to be merged with the nodes of the supporting member.

The connection shear versus shear tab rotation along the bolt line was produced for the three single plate mesh densities. As shown in Figure 3.9, it can be seen that the 9.5mm

element mesh produces almost the same result as the two other finer mesh. However, the finer meshes allow the contacts to be simulated more smoothly and effectively. Additionally, the finer meshes graphs flatten once maximum shear is reached. The 2.4 and 4.8 element widths produced identical results. However the computation time for the mesh with 2.4mm element width resulted in a longer computation time. Therefore, the 4.8 mm mesh density is used in all simulations, for both the validation study of the FE model and in the parametric study.

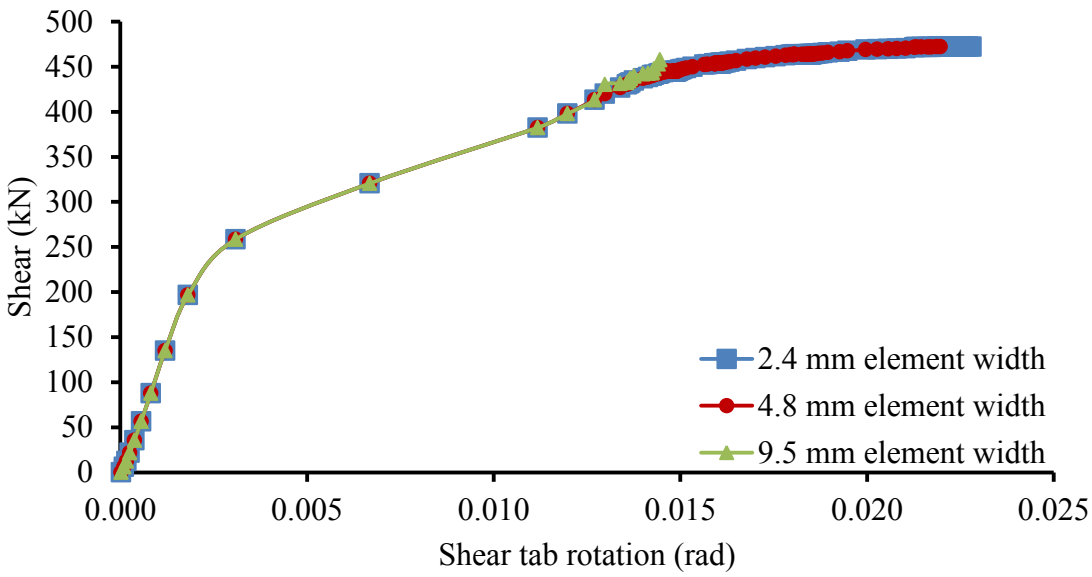

Figure 3.9 Shear versus rotation at bolt line for fine and very fine mesh densities

3.4 Boundary Conditions

Boundary conditions assumed for the FE model to verify with test results were modelled to be consistent with the experimental setup (Astaneh et al. 1989; Sherman and Ghorbanpoor 2002). In the test setup of Astaneh et al. (1989), the beam was subjected to

a single point load at its midpsan. At two end supports, the shear tab was weld connected to the center of the flange of the supporting column which was fixed to concrete walls. This setup resulted in a relatively rigid connection along the weld line for the shear tab. Therefore, the shear tab was modelled to be restrained against translation in the x, y and z-directions along the weld line. Using the symmetric state of loading, only half of the beam was modelled and the mid-span nodes were restrained from translation in the x-direction. Furthermore, the top and bottom flanges were restrained along the length of the beam to prevent lateral torsional buckling.

For the subsequent parametric study and EST validation study (Sherman and Ghorbanpoor 2002), the supporting column was modeled and the shear tab is connected to the centerline of the web of the column. The supporting member (column) is assumed to be fixed at two ends where all nodes ends are restrained against translations in the x, y and z-directions. The beam top flange along the length of the beam was restrained in the lateral direction (z-direction) to prevent lateral torsional buckling unless otherwise stated. In the EST validation study the load was offset from center to simulate a shear and end rotation equivalent to a beam subjected to a uniformly distributed load. The full beam length was modelled and the support at the far end was restrained against translations in the x, y and z-directions to idealize a simply supported member. Figure 3.10 and 3.11 below illustrates the fully assembled EST connection mesh detail at the beam-to-column web and the overall setup of the beam including the loading and far end boundary condition. Figure 3.12 shows the mesh and applied boundary condition at the simply supported end of the beam for the EST validation and parametric study.

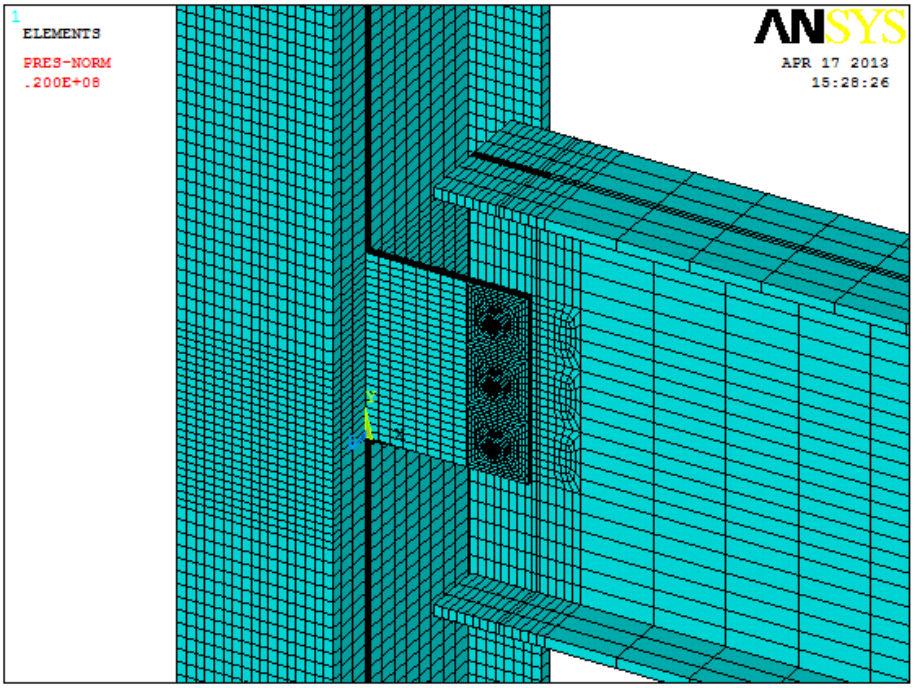

Figure 3.10 Assembled extended shear tab connection

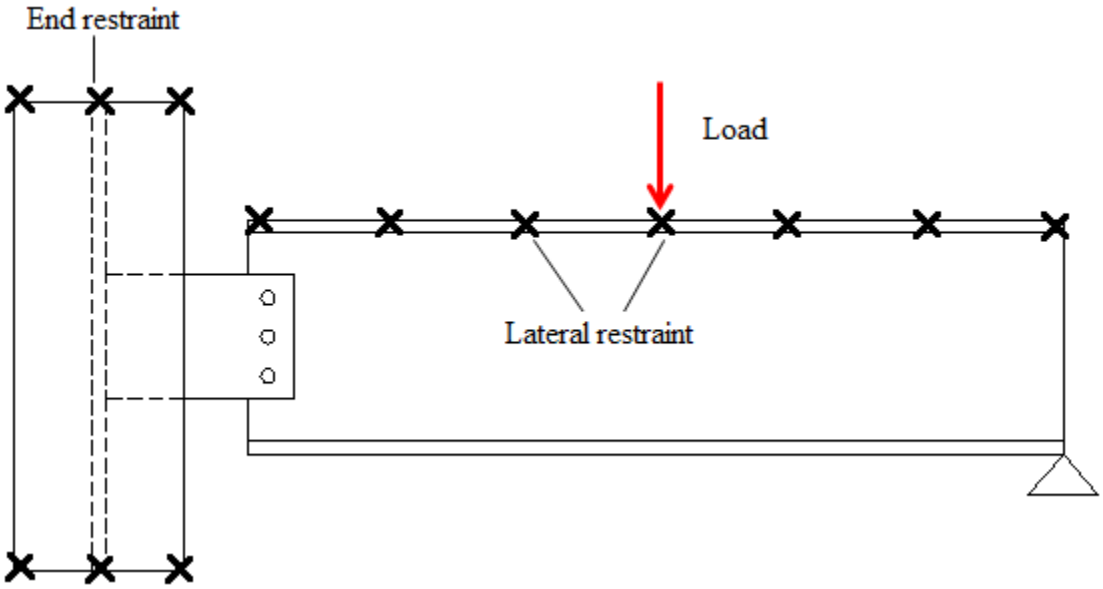

Figure 3.11 EST connection illustrating loading appication and beam far end support

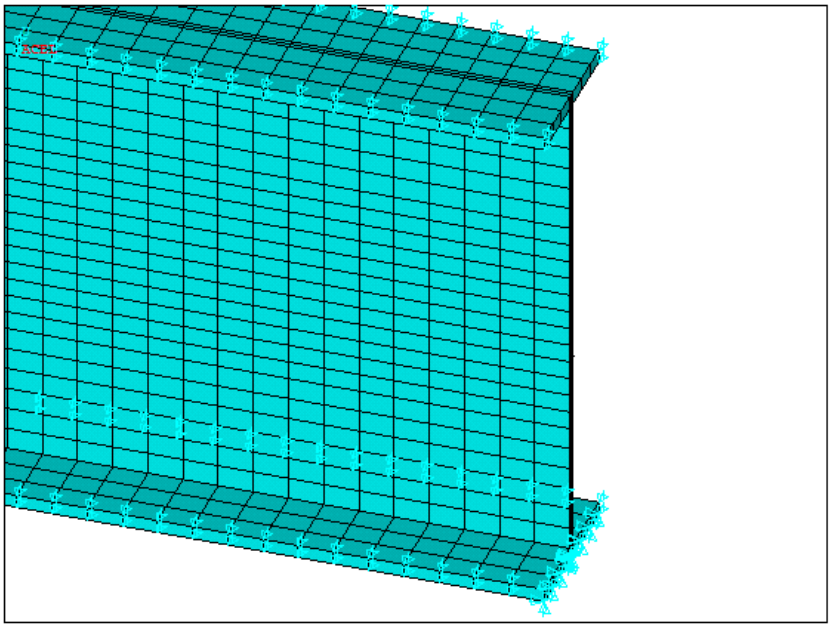

Figure 3.12 Mesh and boundary conditions at simply supported end of beam for EST connections

3.5 Material Properties

An isotropic multi-linear material model was used for the beam, supporting member and the shear tab. This material model consists of an elasto-plastic strain relationship with a strain hardening portion. The modulus of elasticity, E, is taken as 200,000 MPa with a Poisson ratio of 0.3 for all structural steel. The stress-strain curve for the tab, beam and supporting member is shown in Figure 3.13. It is noted that a yield stress of 250 MPa was used to verify the finite element model with experimental results (Astaneh et al. 1989; Sherman and Ghorbanpoor 2002). In the case of the parametric study, the material model assumed a yield stress of 350 MPa for the tab, beam material and supporting member. As for the high strength bolts, the stress strain relationship is shown in Figure 3.14. An

ultimate strength of 945 MPa for the high strength A325 bolts was used for the validation models.

The stress-strain relationships were converted into true stress and strain as required in ANSYS (2010). The true stress, σ_t, and true strain, ε_{true}, were calculated from engineering stress and engineering strain using Equations [3.2] and [3.3].

$$\sigma_t = \sigma_e(1 + \varepsilon_e) \quad [3.2]$$

$$\varepsilon_{true} = \ln(1 + \varepsilon_e) \quad [3.3]$$

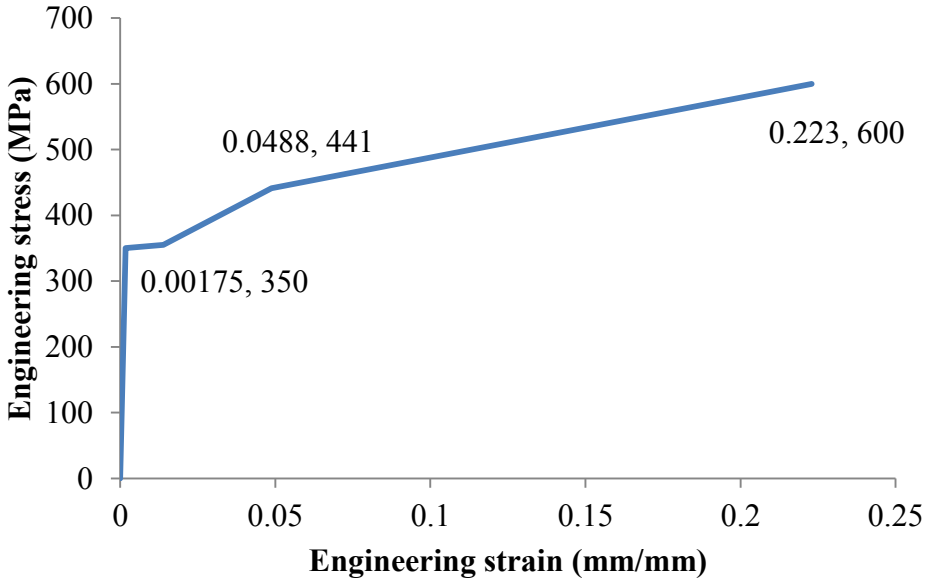

Figure 3.13 Stress-strain curve for 350W steel (Ashakul 2004)

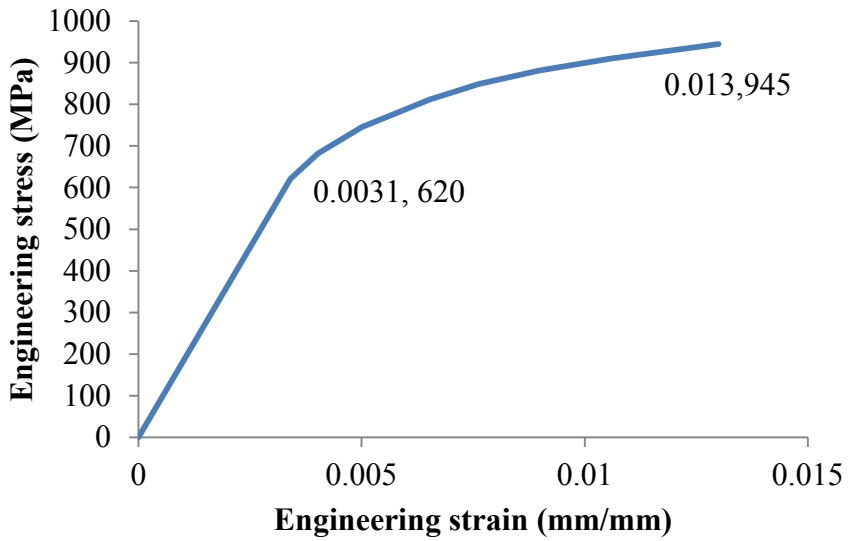

Figure 3.14 Stress-strain curve for A325 high strength bolts (Rahman et al. 2003)

3.6 Loading Analysis

Loading was applied in two main load steps. The first load step involved the pretensioning of the bolts to simulate the snug-tightened condition. Although ASTM standard A325M (2013) provides a definition of "the snug-tightened condition", it does not specify a minimum applied pretension force, only that the two bodies are visually in firm contact. The snug-tightened condition is simulated by applying a pretensioning force value of 50 kN per bolt based on recommendations by Kulak and Grondin (2010). The purpose of the pretension force was to establish firm contact between all adjacent surfaces such as contact between the shear tab and beam web, the bolt head and shear tab, bolt nut and beam web. The pretension force clamps the beam web together with the shear tab and induces a tensile force in the bolts.

The second load step was the application of the transverse loading. In experimental testing, a concentrated load was applied at beam midspan. If this loading was applied as a concentrated load on a single node, excessive element deformation would result which may lead to wrong solution of the model. Alternately, the concentrated transverse load was applied as a distributed pressure load on a small area on the top flange in order to prevent local failure during the finite element analysis. In addition, stiffeners are modelled underneath the pressure loading on both sides of the beam web to increase the web buckling capacity and ensure the failure occurring in the connection. The mesh configuration of the stiffeners is similar to that of the beam to allow for nodal merging. Figure 3.15 shows the pressure loading and the stiffener underneath the flange.

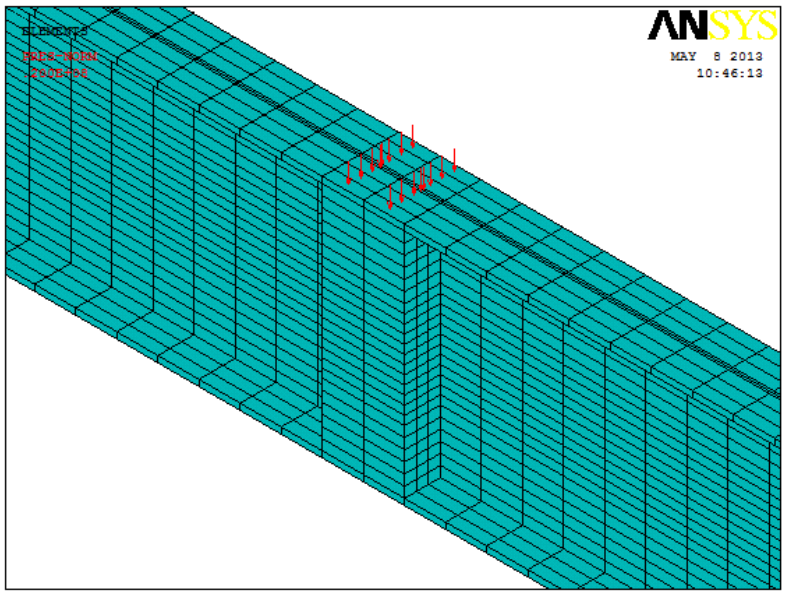

Figure 3.15 Distributed pressure loading including stiffeners

A nonlinear static analysis using the full Newton-Raphson method was employed. During each load substep, a number of equilibrium iterations were performed where the out-of-

balance vector, which is the difference between the restoring forces (the loads corresponding to the element stresses) and the applied loads was evaluated for convergence. The out of balance stiffness matrix is the right hand side of Equation [3.4]. The convergence criterion was set such that the out of balance vector is less than 0.0001. If the convergence criterion is not satisfied, the $\{\Delta u_i\}$ is calculated using Equation [3.4] using the tangent matrix, $[K_i^T]$, and restoring load, $\{F_i^{nr}\}$ from the previous converged solution. $\{\Delta u_i\}$ is then added to $\{u_i\}$ from the previous converged solution. Using the updated nodal displacements, the stiffness matrix and restoring load vector are recalculated and another equilibrium iteration is performed until convergence criterion is satisfied. Once a solution is obtained the next loading increment is applied. The maximum number of equilibrium iterations allowed per substep was limited to 30 iterations. If the maximum number of equilibrium iterations is exceeded for the substep the load increment is bisected and this process is repeated until convergence. The load stepping can be automated using features available in ANSYS. The auto time step scheme ensures that the time step variation is neither too aggressive (resulting in many bisections) nor too conservative (substep increment too small).

$$[K_i^T]\{\Delta u_i\} = \{F^a\} - \{F_i^{nr}\} \qquad [3.4]$$

Where:

$[K_i^T]$ = Tangent stiffness matrix

$\{\Delta u_i\}$ = Displacement vector

$\{F^a\}$ = Vector of applied load

$\{F_i^{nr}\}$ = Vector of restoring loads corresponding to the element internal loads

The augmented Lagrangian method was selected as the contact algorithm for solving the contact problem since the augmented Lagrangian method usually leads to better conditioning and is less sensitive to the magnitude of the contact stiffness coefficient (ANSYS 2010). For the augmented Lagrangian method a normal contact stiffness factor is required. The amount of penetration between the contact and the target surface depends on this factor. A higher stiffness factor reduces the amount of penetration between the two adjacent surfaces but could lead to convergence difficulties. A lower stiffness factor could lead to a certain amount of penetration and result in an inaccurate solution. A normal stiffness factor of 1.0 specified in ANSYS was used.

Moreover, as the bolt shank surface and bolt hole surface are initially not in contact, adjustments to the initial contact conditions is required, otherwise warning messages of "zero or negative pivot" or "excessively large displacements" would terminate the analysis. ANSYS can automatically bring two surfaces into contact by initiating the "close gap" option in the initial contact adjustment controls.

3.7 Failure Criteria

As reported in the literature, the limit states that govern CST connections are bolt shear, plate shear yielding, plate bearing and plate shear fracture. EST connections can additionally be governed by web failure of the supporting member and twisting of the shear tab. Not all limit states are monitored in this study, a justification for the exclusion of certain limit states is given in the following.

Plate bearing - the bearing stress on the plate is a means to achieve ductility in the connection; this limit state does not result in the failure of the connection. Although the bearing of the bolts on the shear tab is visible in the finite element simulation, it is difficult to assess at which load bearing failure has occurred. Therefore, this limit state is not considered in this study.

Plate shear rupture - shear rupture of the plate was not reported as being a recurring failure mode provided that sufficient bolt spacing and edge distance is provided.

The limit states of interest in this study are bolt shear rupture, plate shear yielding, the web failure of supporting member and twisting of shear tab. The monitoring of these limit states is discussed as follows.

Bolt shear rupture is monitored by the fluctuation of shear stress along the centerline of all the bolts in the connection. Bolt shear rupture is deemed to have occurred once the shear stress of any one bolt showed irreversible decrease. The finite element simulation does not have the capability of physically fracturing the bolt; instead it redistributes the applied load to the remaining bolts in the connection. As the load is gradually applied an increase in shear stress can be detected along the centerline of the bolt. Once the bolt reaches its maximum strength, a decrease in shear stress is detected in the following substep. Additionally, as a result of the redistribution of force in the connection, an increase in the shear stress along the centerline of the second bolt will be detected at the same substep. A decrease in this stress will occur immediately thereafter and this process

will repeat for all remaining bolts.

Twisting of the shear tab is monitored by observing the relative rotation, θ_{twist}, between the either sides of the top flange. Figure 3.16 below illustrates the twisting of the plate.

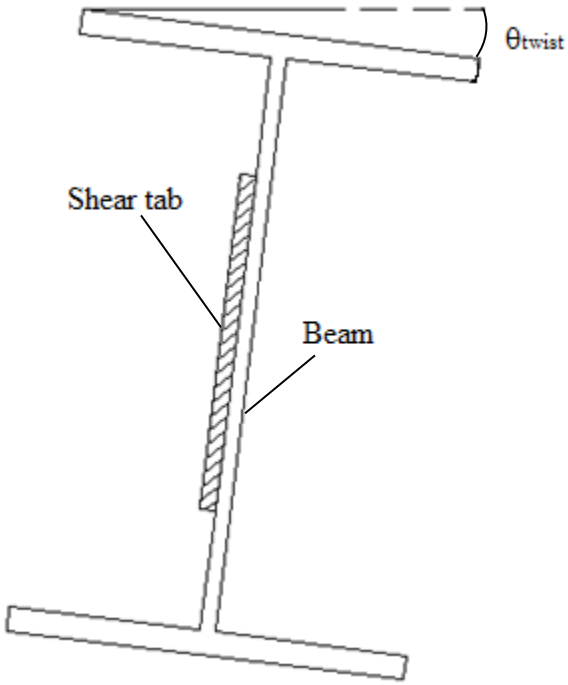

Figure 3.16 Twisting rotation for shear tab

The web failure limit state can be characterized using the shear versus web rotation curve along the weld line θ_{web}, where the shear tab frames into the supporting member. If the shear vs. web rotation curve indicates significantly high values for rotation in the supporting member for a small increase in load, then a web mechanism failure is identified as the critical failure mode. The shear yielding of the plate can be defined by generating a shear versus shear tab rotation θ_{tab} along the line of bolts. The weld rupture

limit state is monitored by generating a moment at weld line versus beam end rotation θ_{beam}. The weld-moment can be calculated as the summation of all the x-component element forces along the weld line multiplied by the respective vertical distance of each node to the centerline of the shear tab. Figure 3.17 illustrates different rotation angles that are used in the failure monitoring.

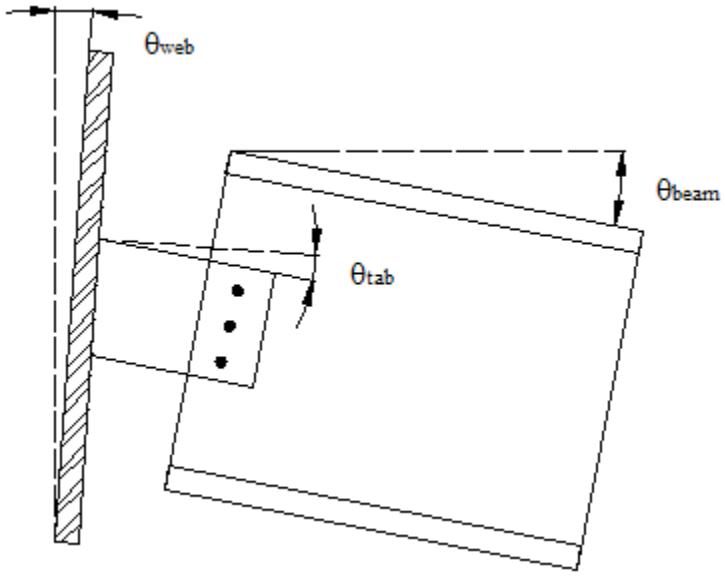

Figure 3.17 Connection rotations

In summary, the failure modes that were considered in the parametric study are the bolt shear rupture, plate yielding, weld fracture, tab twisting and the supporting member web failure.

CHAPTER 4 Validation of the Finite Element Model

4.1 Introduction

The finite element model developed in Chapter 3 is validated using the experimental results obtained by Astaneh et al. (1989) on CST connections and by Sherman and Ghorbanpoor (2002) on EST connections. The details of the four models are presented in Table 4.1. The dimensions reported in the published literature were in imperial units and they have been converted to SI units for consistency in this report. All bolts are 20 mm (3/4 in) A325 type high strength bolts. The mesh for the CST and EST connections are shown in Figures 4.1, 4.2, 4.3 and 4.4. As discussed earlier, the shear tab in the CST connection was assumed fixed in the finite element model whereas the shear tab in the EST connection model is framed into the column web, which is a more flexible support. The CST connections were modelled using half symmetry as load symmetry was present, whereas the full beam was modelled in the EST connections as load symmetry did not exist. Figures 4.5 and 4.6 illustrate the load location and boundary condition applied for the CST and EST validation models, respectively.

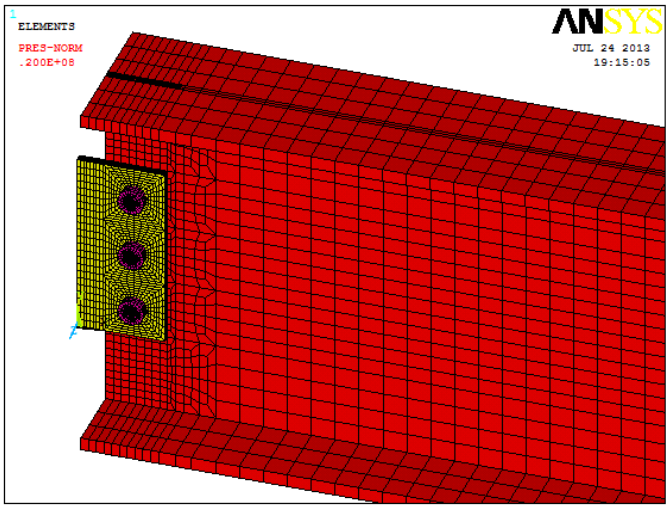

Figure 4.1 FE mesh configuration for the 3-bolt CST connection tested by Astaneh et al. (1989)

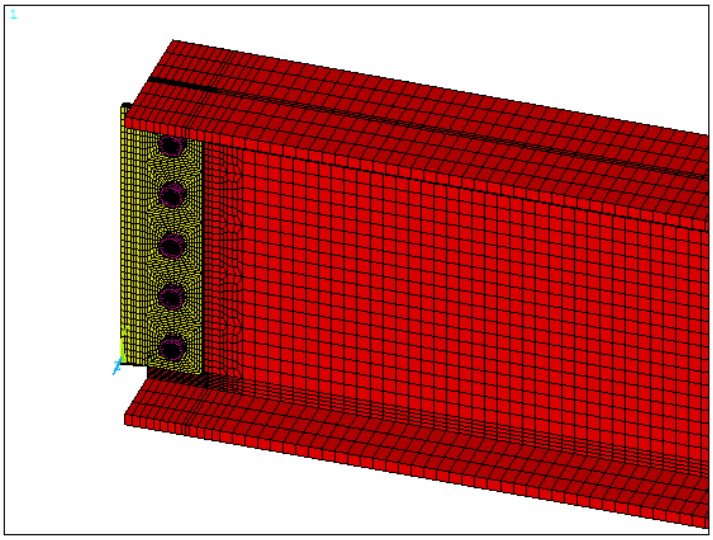

Figure 4.2 FE Mesh configuration for the 5-bolt CST connection tested by Astaneh et al. (1989)

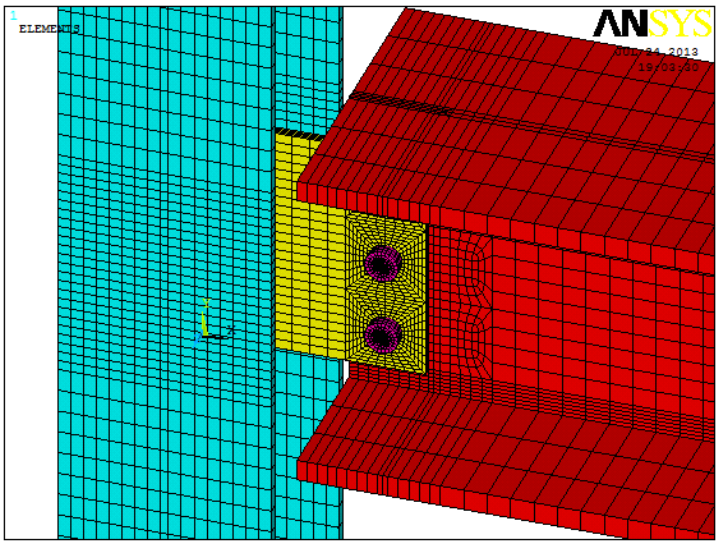

Figure 4.3 FE mesh configuration for the 3-bolt EST connection tested by Sherman and Ghorbanpoor (2002)

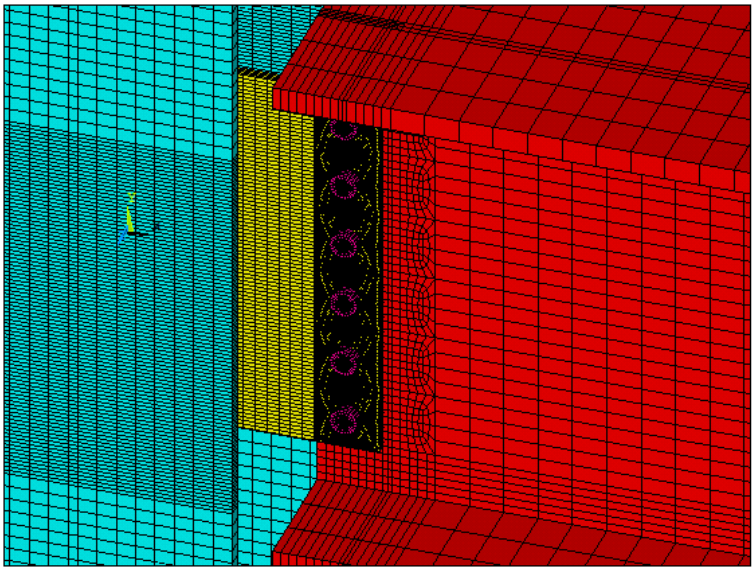

Figure 4.4 FE mesh configuration for the 6-bolt EST connection tested by Sherman and Ghorbanpoor (2002)

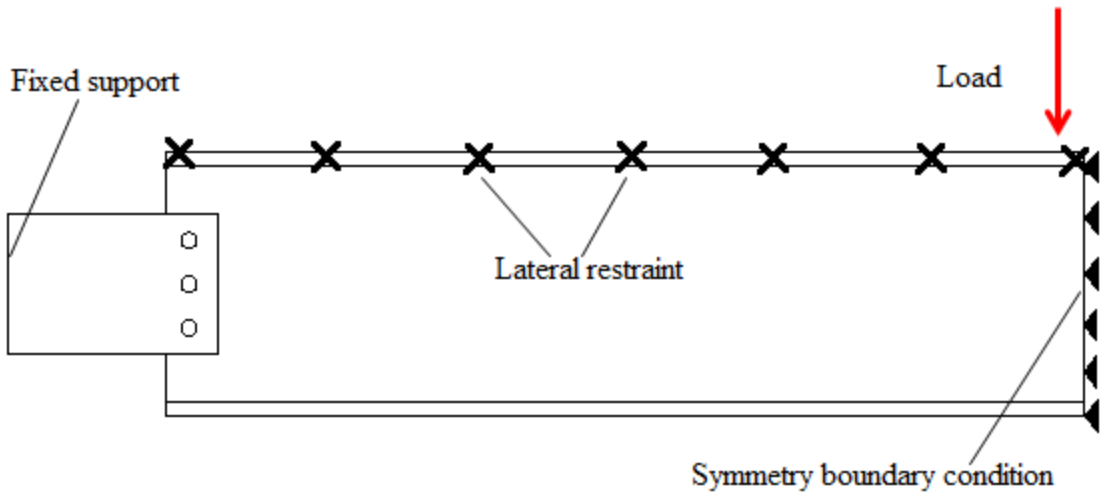

Figure 4.5 Boundary conditions and load application for the 5-bolt CST connection tested by Astaneh et al. (1989)

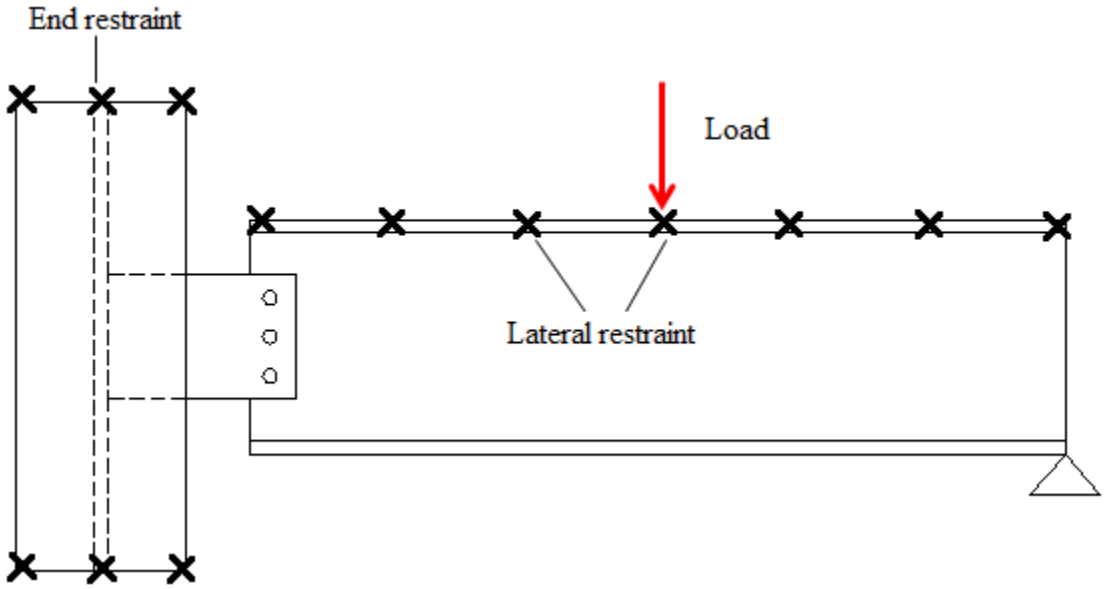

Figure 4.6 Boundary conditions and load application for the 3-bolt EST connection tested by Sherman and Ghorbanpoor (2002)

Table 4.1 Details of finite element verification model

Test	Supported member			Bolts	Shear tab				Weld-bolt distance (mm)	Reference
	Size	Span (m)	Type	Num.	t (mm)	L_p (mm)	d_p (mm)	Type		
1	W18x55	3	A36	3	9.5	108.0	228.6	A36	69.9	Astaneh et al. (1989)
2	W18x55	3	A36	5	9.5	108.0	381	A36	69.9	
3	W12x87	9	Gr.50	3	9.5	212.3	228.6	A36	174.2	Sherman and Ghorbanpoor (2002)
4	W24x146	10	Gr.50	6	12.7	292.1	457.2	A36	254.0	

4.2 Validation of the Finite Element Model

4.2.1 Three-bolt CST Connection

Figure 4.7 compares the beam behaviour where the shear vs. beam end rotation is plotted. The shear force is equal to the applied force for the CST simulation. It shows that the model agrees reasonably well with the experimental behaviour in the linear portion. The test results showed that the beam remained elastic up to a shear force of 262 kN with a beam rotation of 0.0163 rad. At this point the beam midspan began to yield. The ANSYS simulation predicts a similar beam behaviour up to the experimental yield point. However, the ANSYS solution deviates slightly from the experimental data in the post yielding region where the finite element simulation experienced a larger rotation at a given load level. This disparity may be attributed to the difference in the material properties between the model and the test specimen. Astaneh et al. (1989) only specified the beam steel to be A36 but did not provide the detailed stress-strain curves. The stress-strain relationship in the finite element simulation was assumed to be elastic perfectly plastic with a strain hardeing phase typical of the A36 steel.

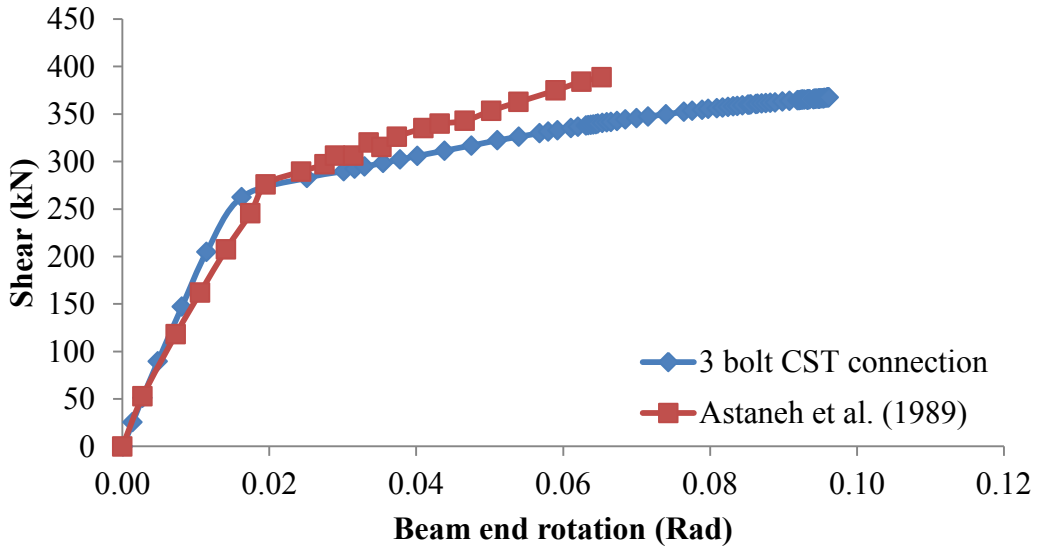

Figure 4.7 Comparison of connection shear versus beam end rotation of 3-bolt CST connection Astaneh et al. (1989)

Figure 4.8 shows the moment at the weld line in the connection. The moment along weld line is calculated as the summation of the nodal x-direction reaction force multiplied by the nodes' respective distance to the center of the shear plate. The maximum moment reached was 43.7 kN-m whereas the maximum moment recorded by Astaneh et al. (1989) was 39.5 kN-m (350 kips). This results in a 9% difference between the experimental test and numerical model.

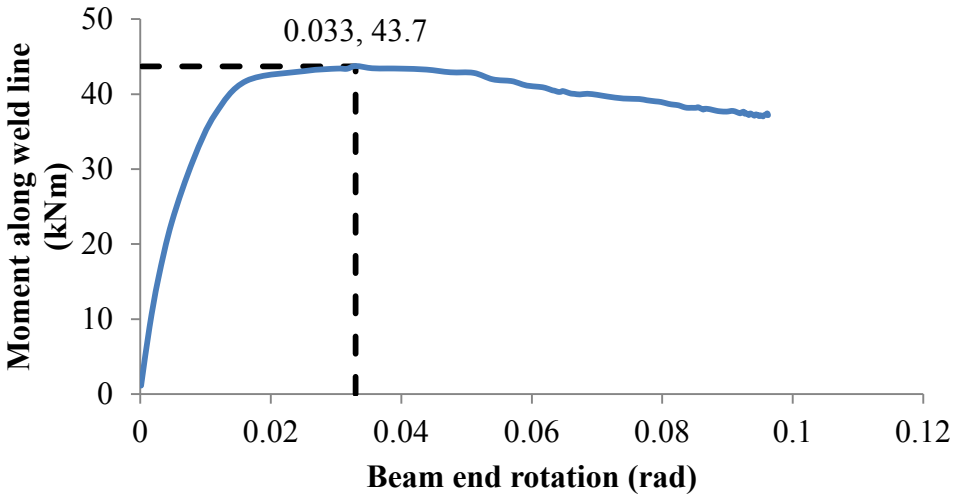

Figure 4.8 Moment at weld line of 3-bolt CST connection

Bolt fracture is predicted by observing the fluctuation of bolt shear stresses. As shown in Figure 4.9, an irreversible decrease in shear stress of the top bolt (Bolt 1) is detected at a shear load of 368 kN and a bolt shear stress of 385 MPa. The connection is deemed to fail by bolt fracture of the top bolt at 368 kN. An increase in shear stress is observed in the remaining bolts in the connection thereafter indicating that the remaining bolts pick up the load but a stress drop is observed immediately thereafter. The 3-bolt CST connection tested by Astaneh et al. (1989) was reported to have failed by bolt fracture at 418 kN (94 kips). There is a 12% difference between the experimental test and the FE model. This difference is acceptable as nominal bolt shear strength was assumed.

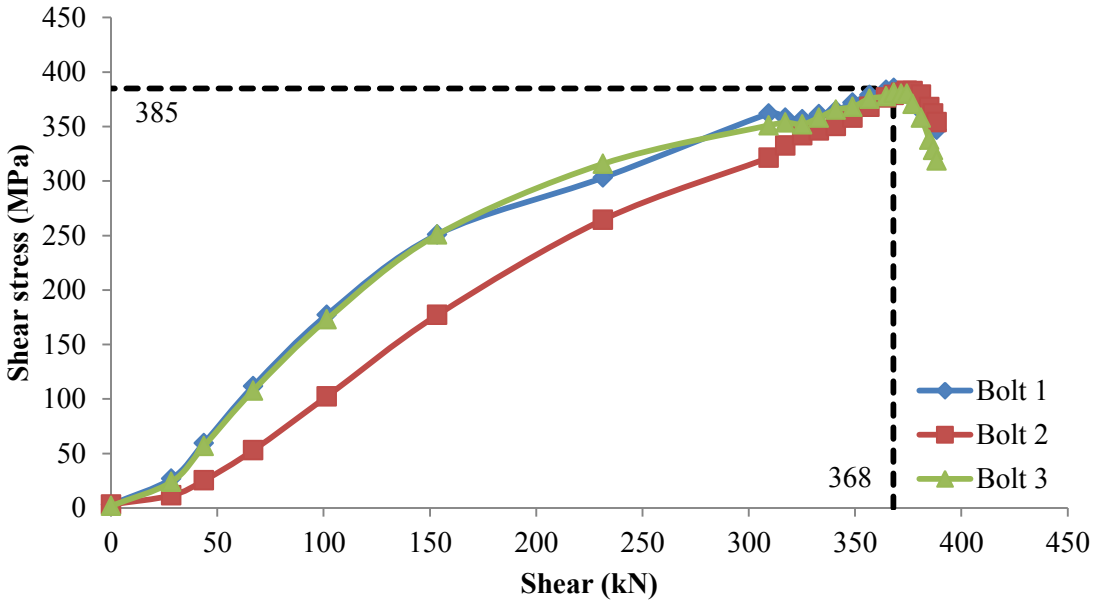

Figure 4.9 Shear stress versus connection shear of 3-bolt CST connection Astaneh et al. (1989)

The finite element bolt eccentricity at failure was determined to be 40 mm whereas the experimental value was 44 mm. The determination of inflection point is explained in Figure 4.10. Nodes, n_1, n_2, n_3 and n_4 represent nodes along the centerline of the beam flange. The strain changes from positive (i.e tension) to negative (i.e. compression) in the bottom flange when approaching the support. A linear interpolation is done between the two adjacent nodes with opposite signs to determine the location of the inflection point.

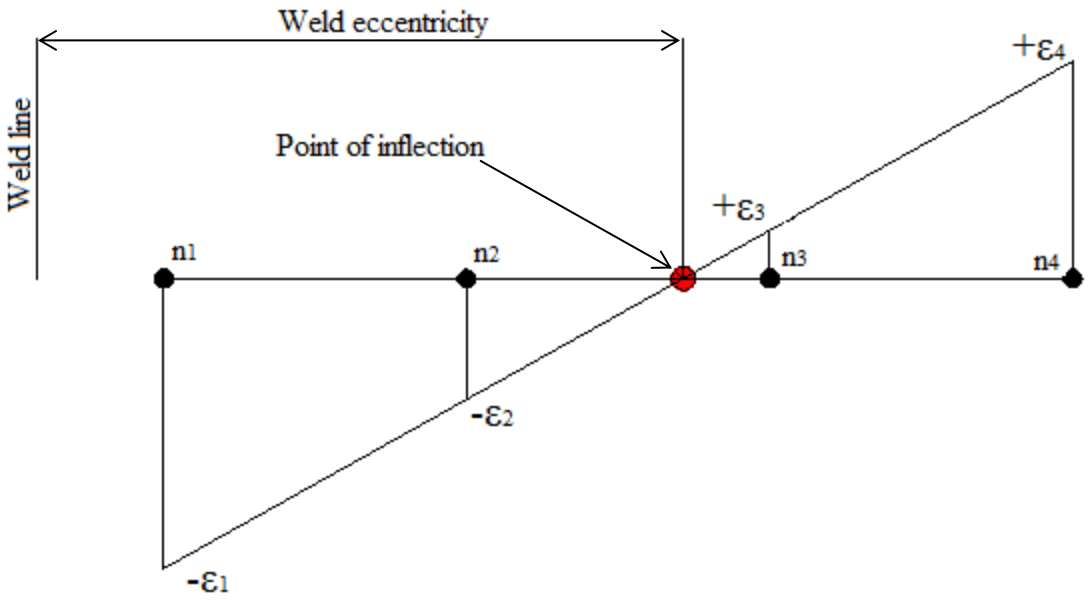

Figure 4.10 Determination of point of inflection from ANSYS

4.2.2 Five-bolt CST Connection

Figure 4.11 is a plot of the shear versus beam end rotation for the 5-bolt CST connection tested by Astaneh et al. (1989). The FE result predicts the experimental behaviour reasonably well. The FE results indicates that beam begins to yield at 485 kN at a beam end rotation of 0.016 rad whereas, the experimental results for beam yielding occurred at 461 kN with a beam end rotation of 0.018. The FE model also compares well with test results in the post-yield region but the experimental data showed a larger beam end rotation than the FE model.

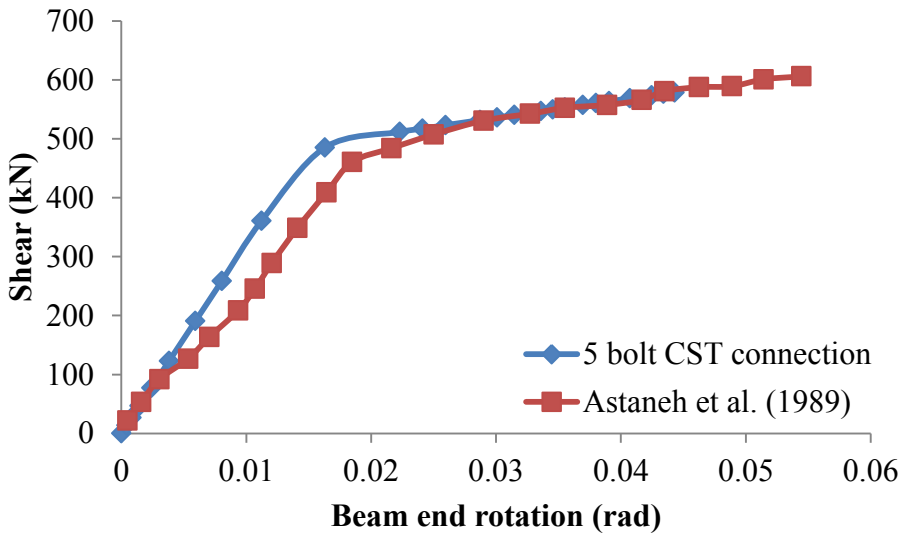

Figure 4.11 Comparison of connection shear versus beam end rotation of 5-bolt CST connection by Astaneh et al. (1989)

Figure 4.12 is a plot of the connection shear versus the shear stress across all five bolts for the 5-bolt CST connection. The dotted line in Figure 4.12 depicts the maximum shear stress and corresponding failure load for bolt 1. The 5-bolt CST connections failed by bolt fracture of the top bolt (Bolt 1) at a shear load of 578 kN. The shear stress of the top bolt at failure was 419 MPa. The experimental failure was by bolt fracture and occurred at a load of 608 kN (137 kips). There is a 5% difference between the FE and experimental result.

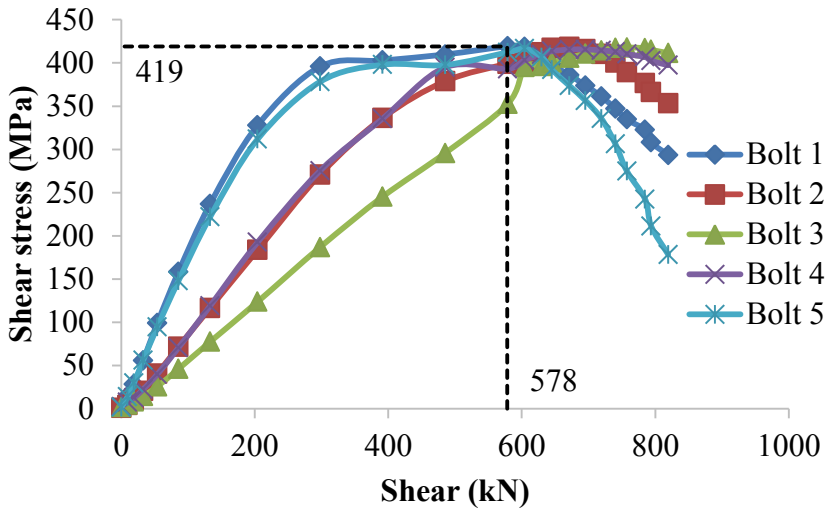

Figure 4.12 Shear stress versus connection shear of 5-bolt CST connection (Astaneh et al. 1989)

The finite element bolt eccentricity at failure was determined to be 50 mm whereas the experimental value was 32 mm.

4.2.3 Three-bolt EST Connection

Figure 4.13 compares the shear versus beam end rotation response for the 3-bolt EST connection by Sherman and Ghorbanpoor (2002). In this case, the shear force in the connection is calculated as the difference between the total applied load and the summation of the nodal y-direction reaction forces at the simply supported far end. Both the finite element simulation and the test results indicate a linear behaviour with similar stiffness.

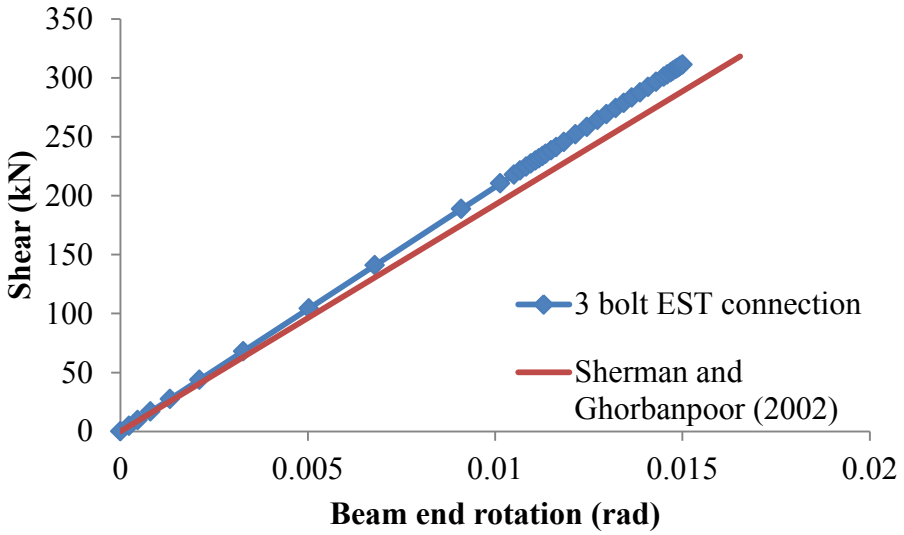

Figure 4.13 Comparison of connection shear versus beam end rotation of 3-bolt EST connection by Sherman and Ghorbanpoor (2002)

Figure 4.14 below illustrates the fluctuation of shear stress acting across the face of each bolt. The shear stress values were obtained from nodes along the centerline of the three bolts. The bolt group is deemed to have failed when the connection shear force reached 250 kN. As shown in Figure 4.14, the shear stress of the top bolt (Bolt 1) reached its maximum value of 473 MPa at the shear connection load of 250 kN. The shear stress decreases thereafter as more load is applied and the additional load is resisted by the other two bolts, as shown by the increase in shear stress for bolts 2 and 3. The ultimate load reported by Sherman and Ghorbanpoor (2002) is 261 kN (58.6 kips) which results in a 5% difference from the FE solution.

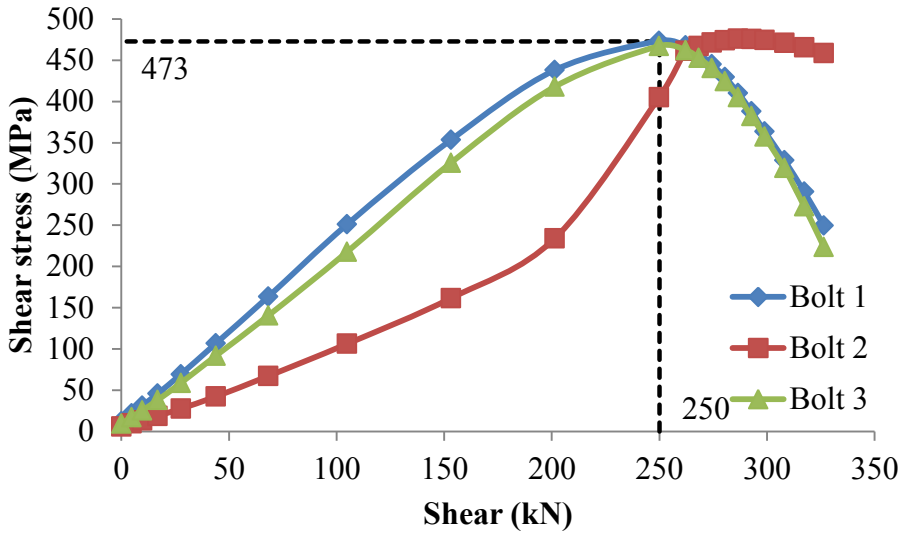

Figure 4.14 Shear stress versus connection shear for validation study for 3-bolt EST connection

The finite element determined bolt eccentricity, e_b, at failure is 41 mm whereas experimental results had a bolt eccentricity of 84 mm. This discrepancy is believed to be attributed to the measurement method employed in the test. Sherman and Ghorbanpoor (2002) determined the point of inflection in the beam by using 3 strain gauges along the top flange of the beam measuring compressive strains. The point of inflection was determined by extrapolating the line of best fit to the point of zero strain and the distance of the inflection point to the weld line was determined. It is suspected that there was a potential for error in the experimental measurement where it may have missed the negative strains in the vicinity of the bolt line.

4.2.4 Six-bolt EST Connection

Figure 4.15 compares the connection shear versus beam end rotation response for the 6-bolt EST connection. The beam showed elastic beahviour during testing. The FE model compares well with the experimental data.

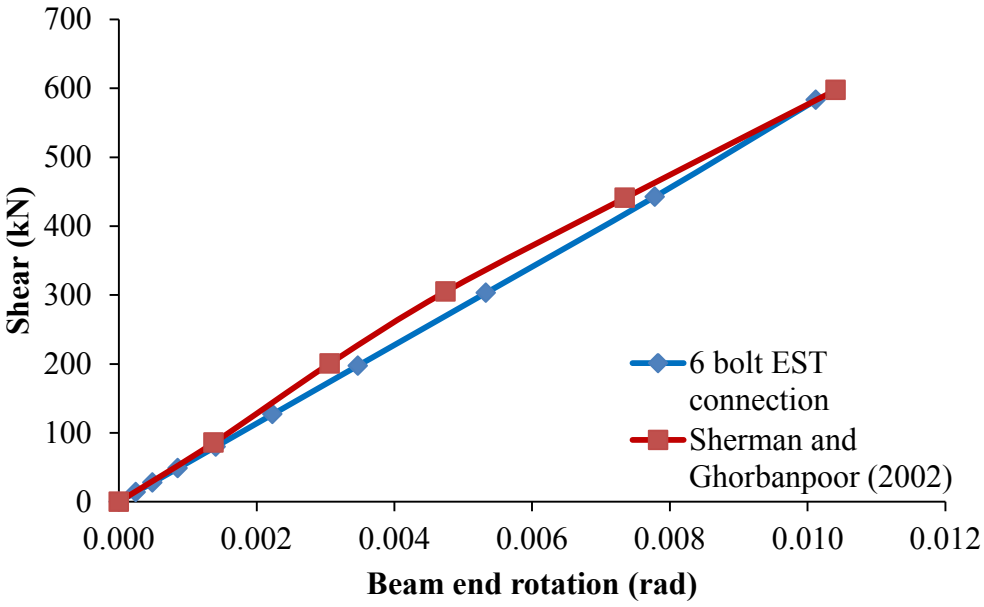

Figure 4.15 Comparison of connection shear versus beam end rotation of 6-bolt EST connection by Sherman and Ghorbanpoor (2002)

Figure 4.16 below illustrates the fluctuation of shear stress acting across the face of each bolt for the 6-bolt EST connection. The bolt group is deemed to have failed when the connection shear force reached 583 kN. As shown in Figure 4.16, the shear stress of the top bolt (Bolt 1) reached its maximum value of 462 MPa at the shear connection load of 583 kN. The ultimate load reported by Sherman and Ghorbanpoor (2002) is 605 kN (136 kips). This results in a difference of 4% between the FE model and the experimental test.

The researchers reported a bolt fracture failure mode similar to that predicted by the FE model.

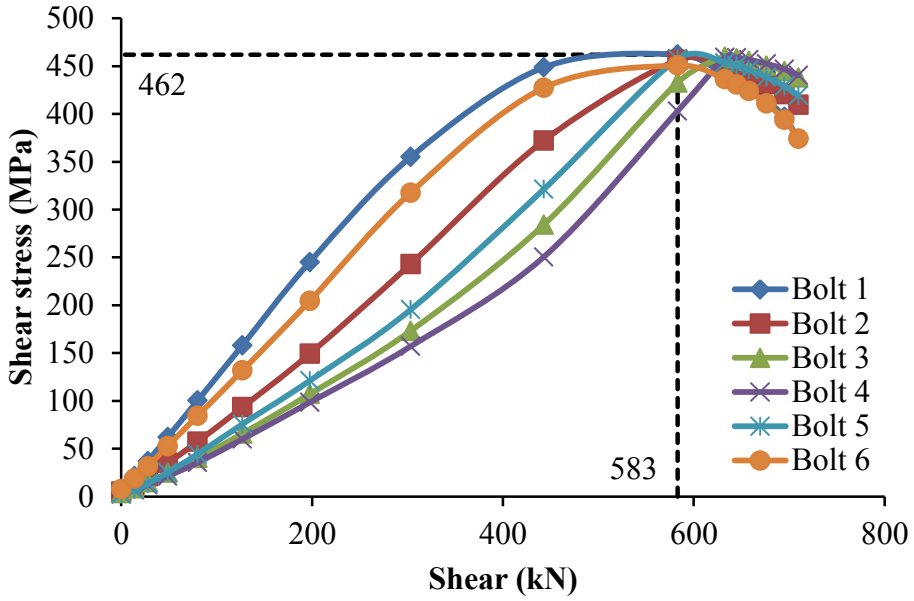

Figure 4.16 Shear stress versus connection shear for validation study for 6-bolt EST connection

The finite element determined bolt eccentricity at failure is 82 mm whereas the experimental value is 127 mm.

4.3 Summary

In this Chapter, the finite element model presented in Chapeter 3 was validated using the experimental test results from Astaneh et al. (1989) and Sherman and Ghorbanpoor (2002). The ultimate load capacity of the single plate shear connections were reasonably predicted by the numerical model. The model was also capable of simulating the behaviour of the connection to an acceptable degree of accuracy. Table 4.5 summarizes

the test results with the FE model. The differences between the finite element ultimate capacity and test values are 5% and 12% for the 3-bolt CST and 5-bolt CST connections, respectively and 5% and 4% for the 3-bolt and 6-bolt EST connections respectively.

Table 4.2 Summary of validation of FE model

Type	**Bolts**	**Failure Mode**		**Ultimate load (kN)**		**Ansys / Experiment**	**Source**
		Test	Ansys	Test	Ansys		
CST	3	Bolt fracture	Bolt fracture	418	368	0.95	Astaneh et al. (1989)
	5	Bolt fracture	Bolt fracture	608	578	0.88	
EST	3	Bolt fracture / Bolt bearing	Bolt fracture	261	250	0.95	Sherman and Ghorbanpoor (2002)
	6	Bolt fracture	Bolt fracture	605	583	0.96	

CHAPTER 5 Parametric Study

5.1 Introduction

A parametric study is conducted on EST connections using the FE model developed in Chapter 3. The parameters investigated include the web slenderness ratio of the supporting column, distance 'a', plate thickness, double bolt rows, beam lateral restraint, beam length-to-depth ratio and number of bolts. Figure 5.1 illustrates a typical EST connection used in the parameteric study. All supported beam sections are kept as W530x74. Supporting columns are all W460x144 except for simulations 1, 2, 4 and 5 where column section is varied for web thickness. Table 5.1 and Table 5.2 lists the details for all FE simulations where the symbols are depicted in Figures 5.1 and 5.2. The highlighted simulation 3 in Table 5.1 is the control simulation for all varying parameters. Cells highlighted in grey indicate the parameters being varied from the control simulation.

An elasto-plastic material model with a strain hardening phase was employed for all W-sections and shear tab where a yield stress of 350 MPa and a modulus of elasticity of 200,000 MPa are assumed as shown in Figure 5.3. All bolts are ¾ in A325 type high strength bolts. The stress-strain graph for the high strength bolts can be referred to in Figure 5.4 where a modulus of elasticity of 200,000 MPa and an ultimate load of 945 MPa are assumed.

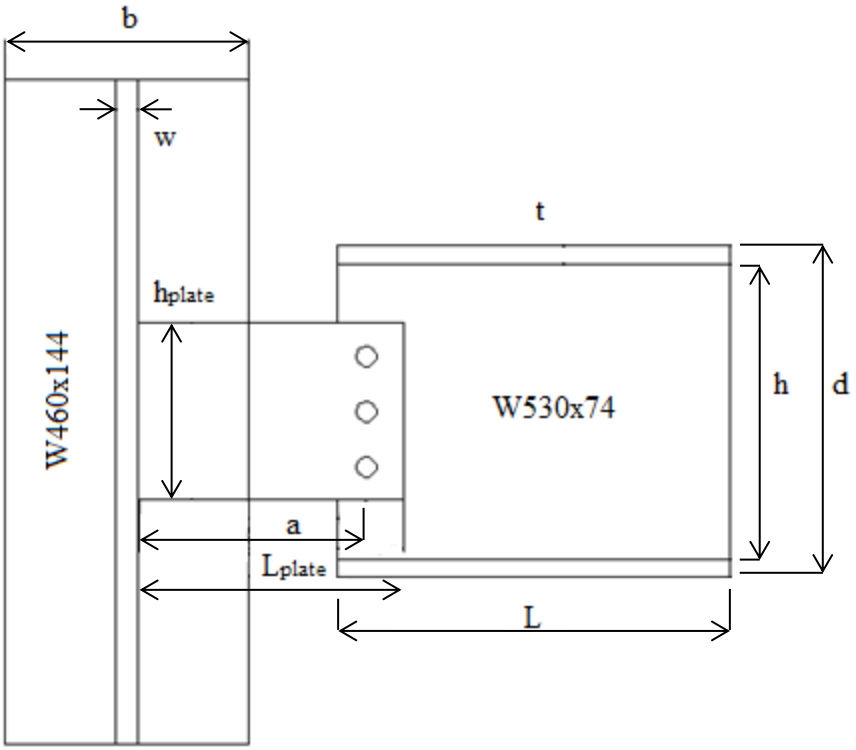

Figure 5.1 Typical EST connection for parametric study

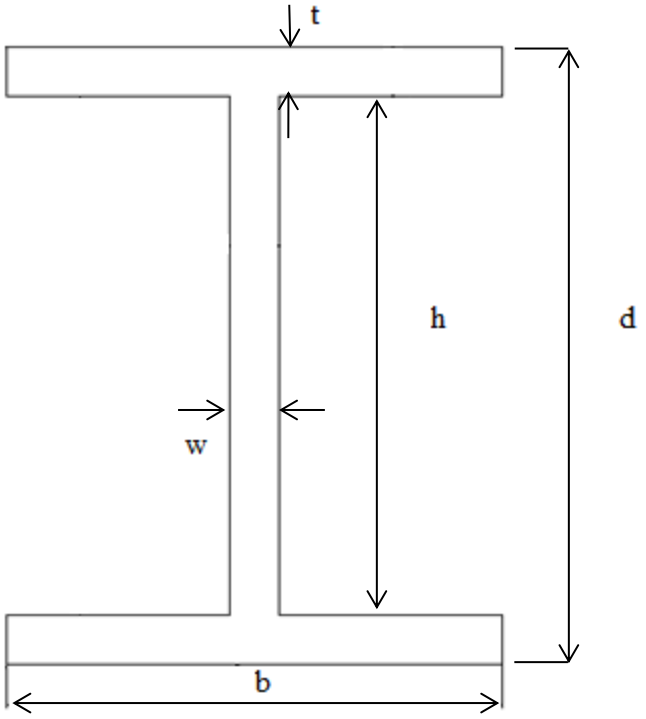

Figure 5.2 Symbols for typical beam/column crossection

Table 5.1 Details of finite element simulations

Simulation	Web slenderness	Distance 'a' (mm)	Plate thickness (mm)	Number of vertical rows	Beam lateral restraint	Beam L/d ratio	Number of bolts in a single row
1	11.1	162	10	Single	Full lateral restraint	17	3
2	20.8						
3	31.5						
4	40.8						
5	53.5						
6	31.5	172					
7		182					
8		200					
9		250					
10		162	8				
11			6				
12			12				
13			10	Double			
14			12	Double			
15			10	Single	Mid-span restraint		
16					Endpoint restraint		
17					Mid-span and endpoint restraint		
18					Full lateral restraint	9.5	
19						13	
20						17	4
21							5
22							6

Table 5.2 Details of beam/column sections

	W section	d	b	t	h	w
Beam	530x74	529	166	13.6	502	9.7
Column	460x464	567	305	69.6	428	38.6
	460x235	501	287	36.6	428	20.6
	460x144	472	283	22.1	428	13.6
	460x89	463	192	17.7	428	10.5
	460x60	455	153	13.3	428	8

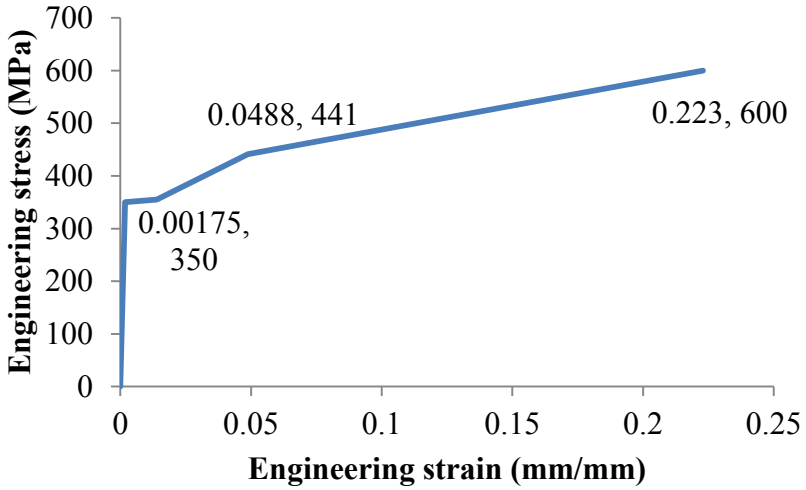

Figure 5.3 Stress-strain relationship for W-sections and shear tab in parametric study

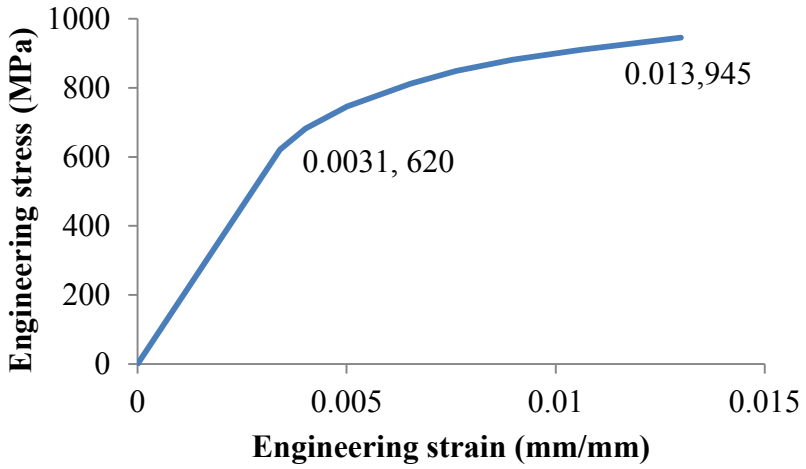

Figure 5.4 Stress-strain relationship for A325 bolts in parametric study

5.2 Web Slenderness Ratio of the Supporting Column

The web slenderness of the supporting column is varied by changing the web thickness while maintaining the web depth. This ensures that the column flange confining effect on the web rotation remained the same for all simulations. The web slenderness ratio, h/w, is varied from 11.1 to 53.5 with simulation 1 having the lowest slenderness ratio and simulation 5 having the highest slenderness ratio.

Figure 5.5 shows the connection shear versus web rotation for all tested slenderness ratios. It shows that an increase in web slenderness resulted in a reduction in connection shear capacity and also a change in connection behavior. At a low web slenderness indicating a thick web (simulation 1), the response remained almost linear up to the ultimate load. As the slenderness increases (web becomes thinner), the responses showed evident non-linearity and the onset of this nonlinearity began increasingly earlier in the loading history. The nonlinear behaviour is characterized by yielding in the web. An increase in web slenderness results in an increase in web rotation for the same load level.

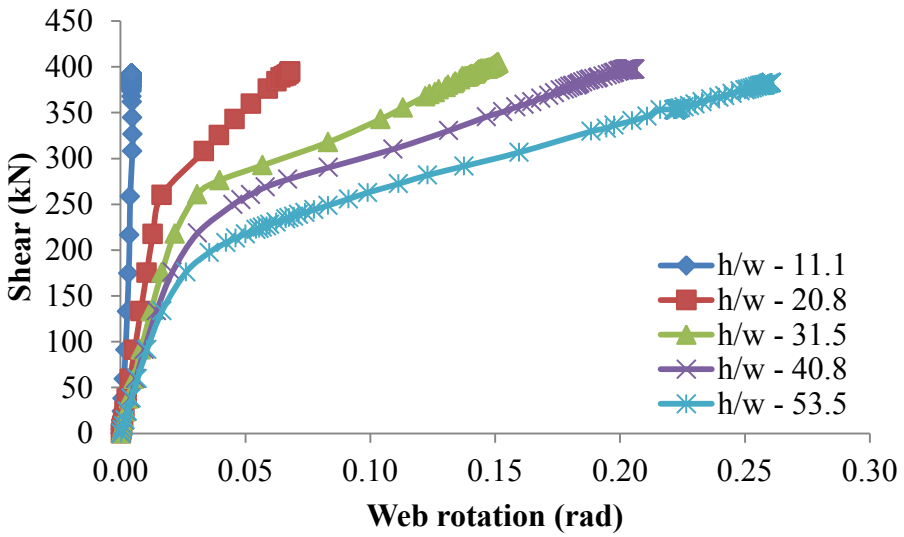

Figure 5.5 Connection shear vs. web rotation for varying web slenderness

Figure 5.6 is a depiction of the nonlinear web rotation that is experienced by slender webs of columns. The plot is of simulation 5 with an h/w ratio of 53.5. The column flanges are excluded for clarity. The high slenderness results in a deformation in the column web where the top and bottom portions of web experience pulling and pushing actions resulting in tensile forces at the top and compressive forces at the bottom. The manner of deformation also indicates that the tensile forces are greater than the compressive forces since the pulling deformation is more significant than the pushing deformation. Figure 5.7 illustrates the von Mises stress in Pascals for the column web where the stress in the top portion of the web is much higher than that in the bottom portion.

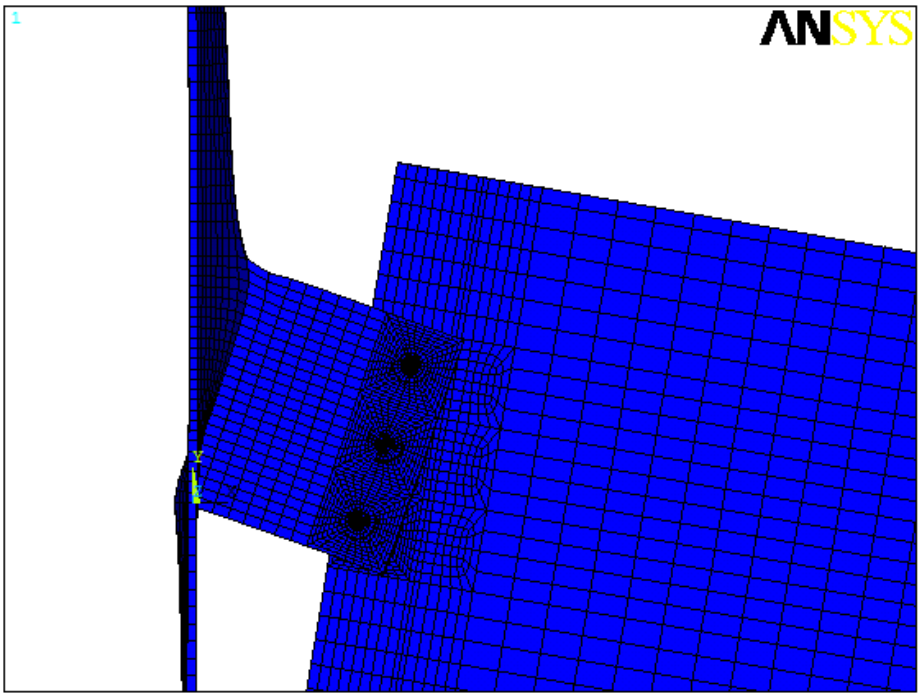

Figure 5.6 Column web rotation deformation for h/w=53.5

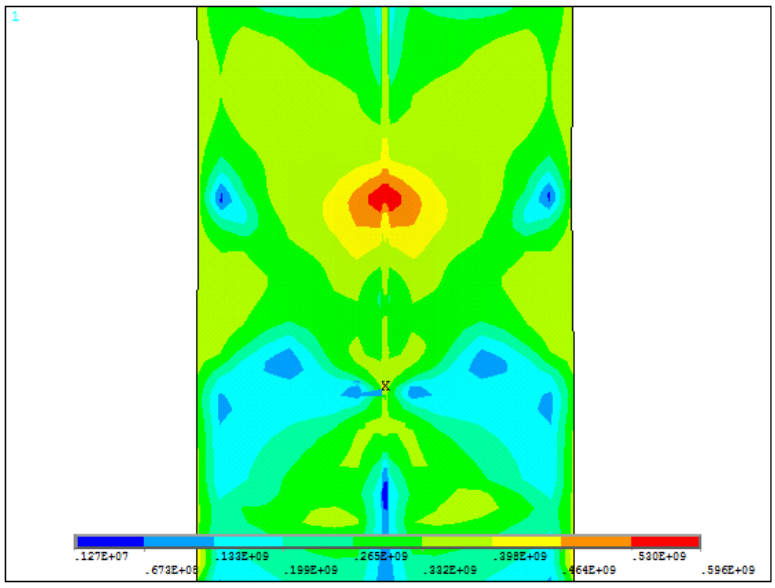

Figure 5.7 Column web von Mises stress distribution for h/w=53.5

Figure 5.8 shows the connection shear vs. beam end rotation responses for the five web slenderness ratios. The initial phase of all 5 models had the same stiffness. At approximately 260 kN the beam sections began to yield. Post yield stiffness is higher for connections with a lower slenderness ratio (thicker column web) than connections with a high slenderness ratio (thinner column web). The column web thickness only affects the beam rotation after the yielding of the beam section.

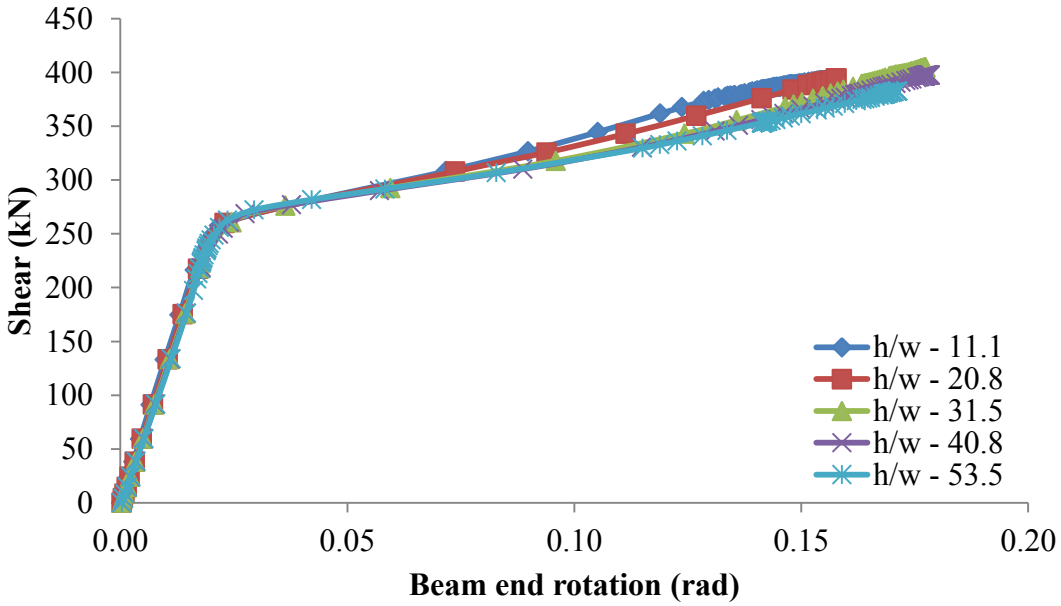

Figure 5.8 Connection shear versus beam end rotation for varying web slenderness

The connection shear strength is determined using the shear stress in the bolts. The connection is deemed to fail once the shear stress of any one of the bolts showed an irreversible drop in magnitude with an increase of external applied load. Figure 5.9 plots the shear stress versus connection shear for simulation 3 where bolt 1, 2, and 3 indicates the top, middle, and bottom bolt. Similar plots for simulations 1, 2, 4 and 5 are presented

in Appendix A. Figure 5.9 shows that the shear stress in the bottom bolt increases with load until the shear stress reaches 457 MPa. Afterwards, the shear stress begins to decrease in the bottom bolt. Hence, the EST connection fails by bolt fracture of the bottom bolt at a load of 368 kN as illustrated in the figure. From the same figure the middle bolt also experiences a decrease in shear stress however the decrease occurs after the decrease is observed in the bottom bolt.

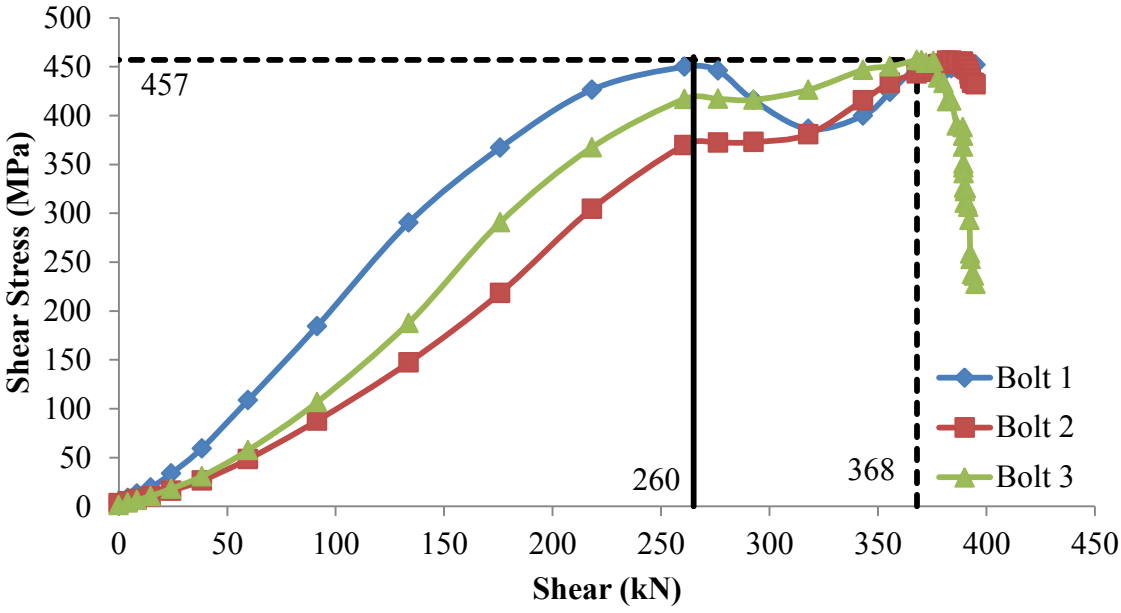

Figure 5.9 Shear stress versus connection shear for simulation 3

In Figure 5.9, bolt 1 shows a dip in shear stress at the connection shear of 260 kN but followed by an increase. The 260 kN coincides with the beam yield point shown in Figure 5.8. At this point, the horizontal shear stress component of the top bolt began to decrease due to the yielding of the beam and rotation of the web. The resulted total shear stress therefore showed reduction but fracture did not occur in the top bolt. The variation of horizontal shear stress is illustrated in Figure 5.10 for all three bolts. Prior to yielding

of the beam web, rotations are relatively small, the horizontal shear force in the top bolt is directed away from the support and in the bottom bolt is directed towards the support. Once yielding commences, the web rotations become larger, the horizontal shear stresses in the top bolt decreases and ultimately changes direction to direct towards the support. The dotted black line in the figure represents the shear force level at which beam yielding is reached. To the left of the dotted line, the horizontal shear force is positive (directed away from the support) and increasing for bolt 1. After beam yield, the horizontal shear stress of the top bolt decreases and eventually changes its direction to be directed towards the support.

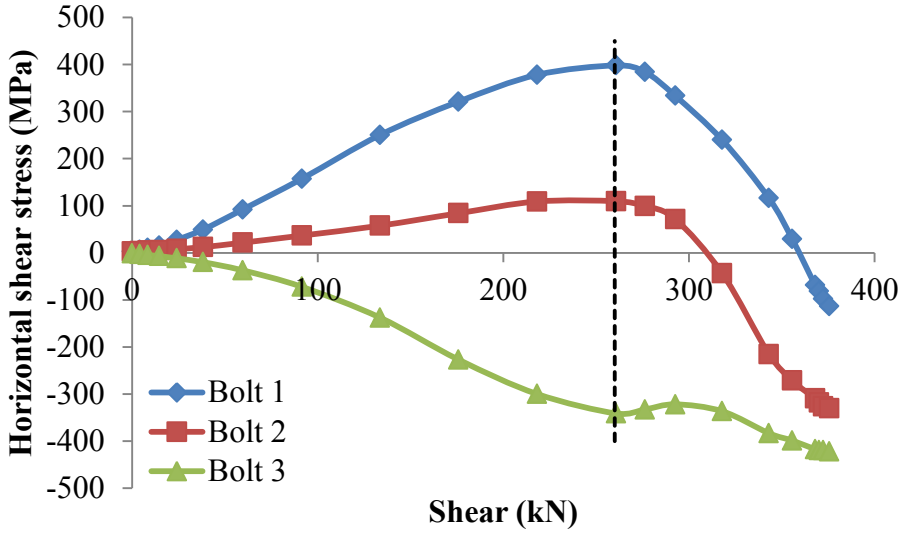

Figure 5.10 Horizontal shear stress versus connection shear for simulation 3

Table 5.3 lists the shear stress distribution across all three bolts for simulations 1 to 5 at ultimate load. The table confirms that the connection ultimate capacity decreases with the increase in slenderness. The shear stress is more evenly distributed among the three bolts

for thicker column webs. Simulations 1, 2, 3, 4 and 5 have a shear stress standard deviation of 4, 5, 7, 14 and 36 MPa, respectively.

The outer bolts resist most of the shear due to the high geometric nonlinearity in the EST connection. The top and bottom bolts mainly resist the horizontal shear stresses due to rotations and middle bolt resists more of the vertical shear. As the column web becomes stiffer, less web rotation is experienced, hence resulting in a more evenly distributed shear stress.

Table 5.3 Shear stress, MPa, distribution across 3 bolts for simulations 1 to 5

Simulation	1	2	3	4	5
Top Bolt	456	452	451	444	440
Middle Bolt	453	448	443	429	397
Bottom Bolt	445	457	457	457	456
Standard Deviation	4	5	7	14	36
Ultimate Load (kN)	377	376	368	330	208

Figure 5.11 illustrates the movement of the inflection point in the beam as the load increases where the y axis indicates the weld line and black line indicates the bolt line. It shows that the point of zero moment follows a similar trend for all simulations. In the low load region, the increase in the load causes the inflection point to move toward the support (weld line), which is understandable since at the zero load, the inflection point is considered infinitely away from the support. However, as the load increases, the inflection point moves away from the support. A larger range in movement is noticed for simulation 1 with a low slenderness ratio (i.e. higher support stiffness) than with simulations with a higher slenderness ratio. The bolt effective eccentricity is defined as the distance from the inflection point at ultimate to the bolt line. According to the figure,

the column web slenderness has an effect on the bolt effective eccentricity. The higher the web slenderness, the greater the bolt effective eccentricity.

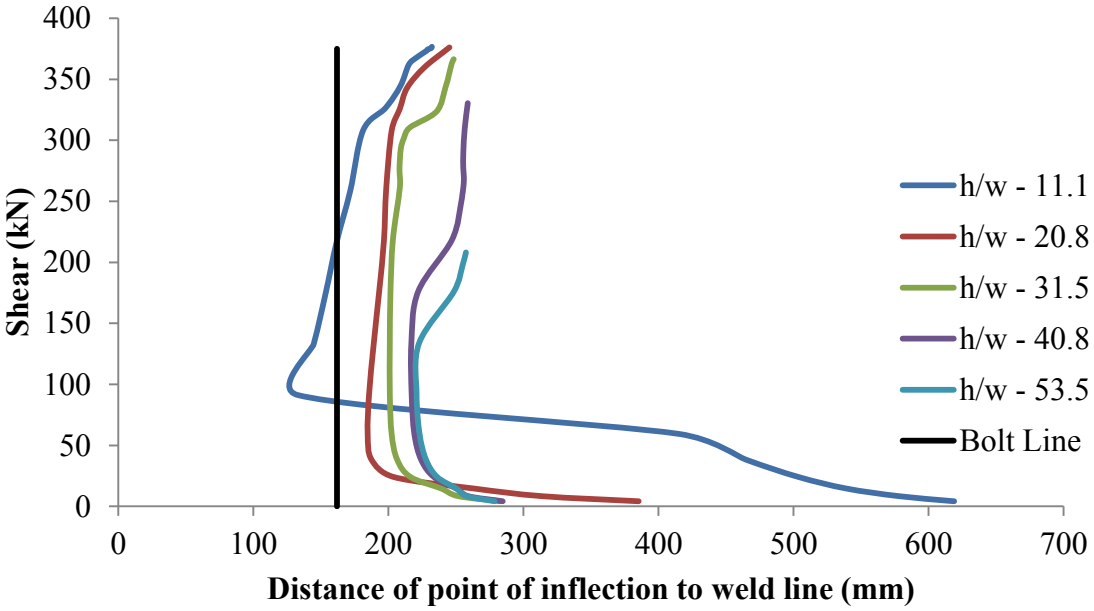

Figure 5.11 Distance of point of inflection to weld line for varying web slenderness

Figure 5.12 shows the column web slenderness ratio versus the effective bolt eccentricity, $e_{b,}$ at ultimate. A more or less linear increase in e_b is realized with an increase in web slenderness. This indicates that as the support becomes more flexible, the effective eccentricity becomes larger.

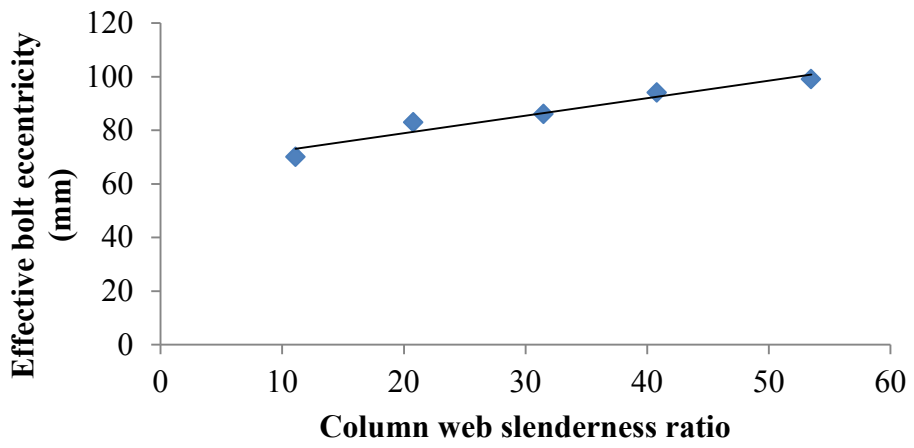

Figure 5.12 Slenderness ratio versus measured e_b

The AISC manual 2011 states that the bolt effective eccentricity, e_b, is to be taken equal to the distance 'a'. Table 5.4 lists the predicted e_b from both the finite element simulations and the AISC recommendation together with the finite element and AISC ultimate load. In the table, $F_{u,FE}$ is the bolt shear capacity calculated using the effective bolt eccentricity, $e_{b,FE}$, obtained from the FE simulation whereas $F_{u,AISC}$ and $F_{u,CISC}$ are the ultimate capacities calculated using the distance 'a' as the effective bolt eccentricity. The $F_{u,FE}$ and $F_{u,AISC}$ are are calculated using procedures recommended in AISC manual 2011. Whereas, $F_{u,CISC}$ is calculated using the tables for eccentrically loaded bolts in the CISC manual. The $F_{u,AISC}$ and $F_{u,CISC}$ ultimate bolt capacities were the same as they were both based on the ICR procedure. F_u is the ultimate load at which bolt failure occurs based on the FE analysis. Table 5.4 shows that the $F_u/F_{u,AISC}$ ratio ranged from 0.37 for the stiffer supports (thicker web) to 0.67 for the more slender supports (thinner web). This suggests that the e_b recommended in AISC manual 2011 is overly conservative. On the other hand, using the procedure specified in AISC but with e_b values obtained from the FE

simulations improved the prediction significantly. The $F_u/F_{u,FE}$ ratios for simulations 1, 2, 3, 4 and 5 are 0.75, 0.67, 0.66, 0.69 and 1.04, respectively. Bolt shear failure occurs in the top bolt for simulation 1 whereas simulations 2, 3, 4 and 5 had bolt shear failure occurring in the bottom bolt.

The AISC manual 2011 does not specify a design check to evaluate the stiffness of the column web. The influence of the flexibility of the web is not included in the bolt shear deisgn calculation. This study suggests that a limit of h/w less than 40 is required to ensure that the calculation of the bolt shear using measured e_b does not result in an unsafe design. A sample of the AISC manual 2011 design procedure for EST configuration is presented in Appendix B for simulation 3.

Table 5.4 Summary of effect of web slenderness

Simu.	**h/w**	**Web Rotation (rad)**	**Bolt Failure**	$e_{b,FE}^{(1)}$	$e_{b,AISC}^{(2)}$	$F_{u,FE}^{(3)}$	$F_{u,AISC}^{(4)}$	$F_{u,CISC}$	$F_u^{(5)}$	$F_{u,FE}/F_u$	$F_{u,AISC}/F_u$
1	11.1	0.0045	Top	70	162	283	139	139	377	0.75	0.37
2	20.8	0.0068	Bottom	83	162	251	139	139	376	0.67	0.37
3	31.5	0.0150	Bottom	86	162	244	139	139	368	0.66	0.38
4	40.8	0.2060	Bottom	94	162	228	139	139	330	0.69	0.42
5	53.5	0.2610	Bottom	99	162	217	139	139	208	1.04	0.67

1 Bolt effective eccentricity according to FE simulation, mm
2 Bolt effective eccentricity according to AISC 2011, mm
3 Bolt shear including bolt group reduction factor based on $e_{b,FE}$, kN
4 Connection ultimate capacity based on AISC 2011 design procedure, kN
5 Ultimate connection shear for FE simulation, kN

5.3 Distance ‘a’

Five different ‘a’ distances are selected to investigate the effect of varying length of plate on the behaviour and ultimate load of EST connections. Simulations 3, 6, 7, 8 and 9 have ‘a’ distances of 162, 172, 182, 200 and 250 mm, respectively. The distance ‘a’ is the distance between the bolt line and weld line.

Figure 5.13 and Figure 5.14 compare the connection shear versus column web rotation responses and connection shear versus the beam end rotation responses for all five simulations. Both figures show that for studied distance ‘a’ up to 182 mm, the increase in this distance does not affect the overall beam behaviour. However, for distance “a” in the range of 200 to 250 mm, an increase in the distance results in an onset of yielding in the web occurring much earlier in the loading history. On the other hand, the linear behaviour of the beam end rotation remains practically identical for all distances. However, as the distance increases, the beam has less ability to sustain end rotation after yielding and at distance “a” of 250 mm, no post yielding rotation can be observed.

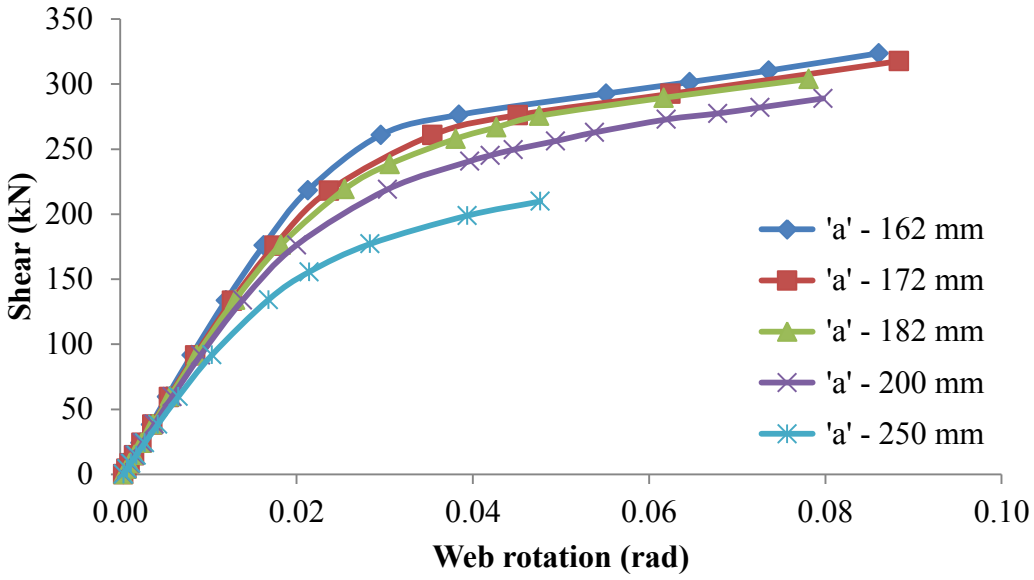

Figure 5.13 Shear vs. web rotation for varying distance 'a'

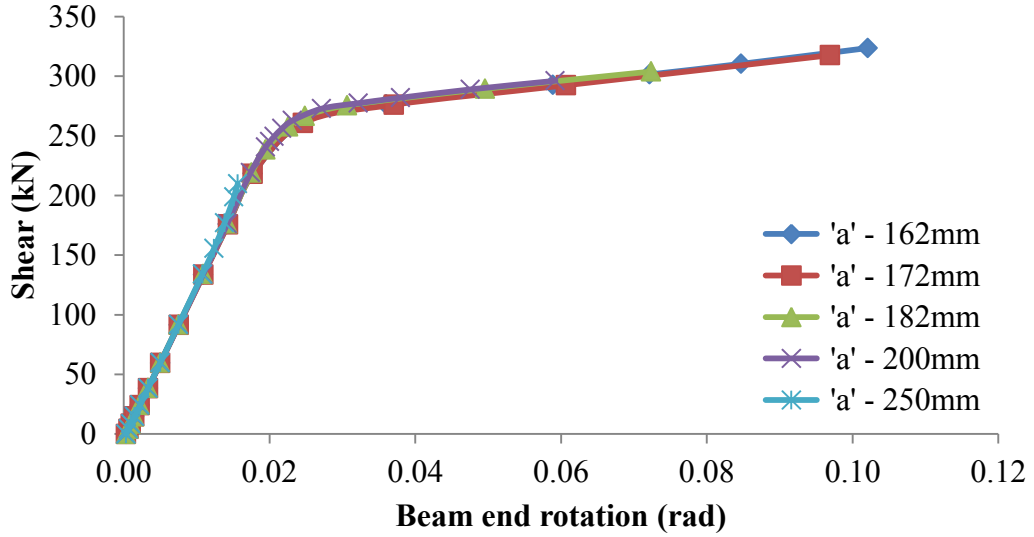

Figure 5.14 Shear versus beam end rotation for varying distance 'a'

Table 5.5 lists the shear stress for all the bolts at failure, the ultimate connection capacity and the standard deviations of stresses for the three bolts. Simulations 3, 6, 7, 8 and 9

achieved ultimate loads of 368, 352, 348, 297 and 209 kN, respectively. The bolt shear stress was more evenly distributed for shorter connection lengths than longer ones. The standard deviation across the three bolts for simulations 3, 6, 7, 8 and 9 were 7, 7, 18, 24 and 64 MPa respectively. The increase in distance 'a' resulted in a reduction in the bolt shear capacity.

Table 5.5 Shear stress, MPa, distribution across 3 bolts for simulations 3, 6, 7, 8 and 9

Simulation	**3**	**6**	**7**	**8**	**9**
Distance 'a' (mm)	162	172	182	200	250
Top Bolt	451	449	419	412	344
Middle Bolt	443	443	445	450	451
Bottom Bolt	457	457	456	457	458
Standard Deviation	7	7	18	24	64
Ultimate Load (kN)	368	352	348	297	209

As expected, an increase in distance 'a' results in a greater distance between the point of inflection to the weld line due to the geometric offset of the bolt group, as shown in Figure 5.15. The movement of the beam inflection point with the increase in the load followed a similar path as discussed previously. The inflection point moves towards the support and then reverses direction away from the support. It is realized that the bolt effective eccentricity, e_b, increases with the increase in the 'a' distance. At failure the e_b values for simulations 3, 6, 7, 8 and 9 are 86, 96, 101, 104 and 105 mm.

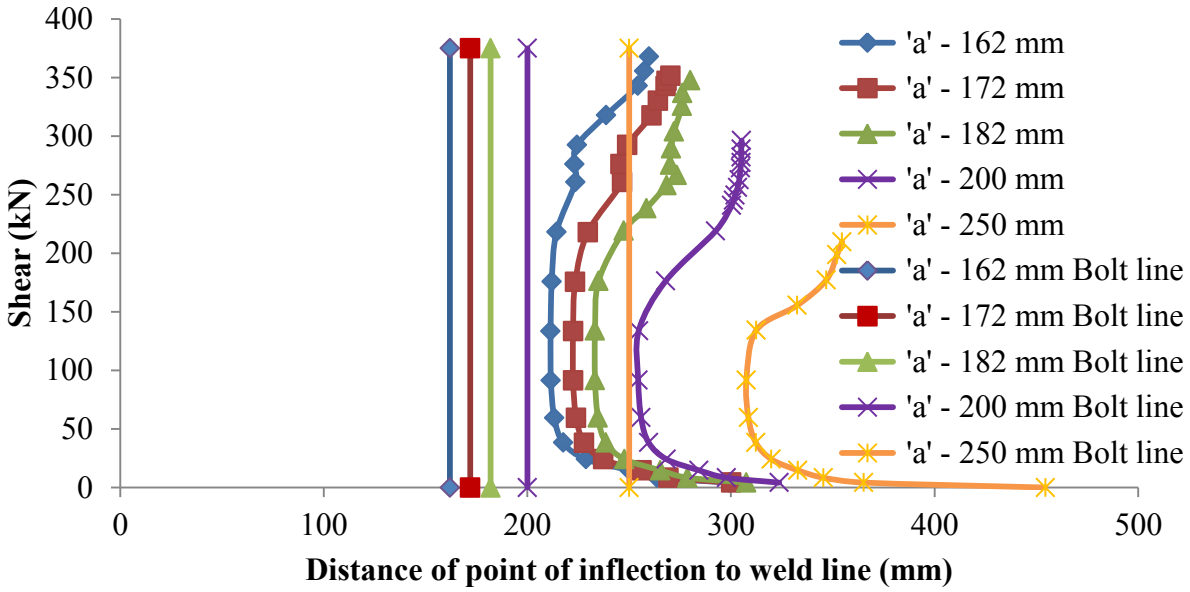

Figure 5.15 Distance of point of inflection to weld line for varying distance 'a'

Figure 5.16 is a graph of the distance 'a' versus the measured effective bolt eccentricity, e_b, at failure. It shows that the e_b increases with an increase in distance 'a' up to a maximum bolt eccentricity value of 105 mm.

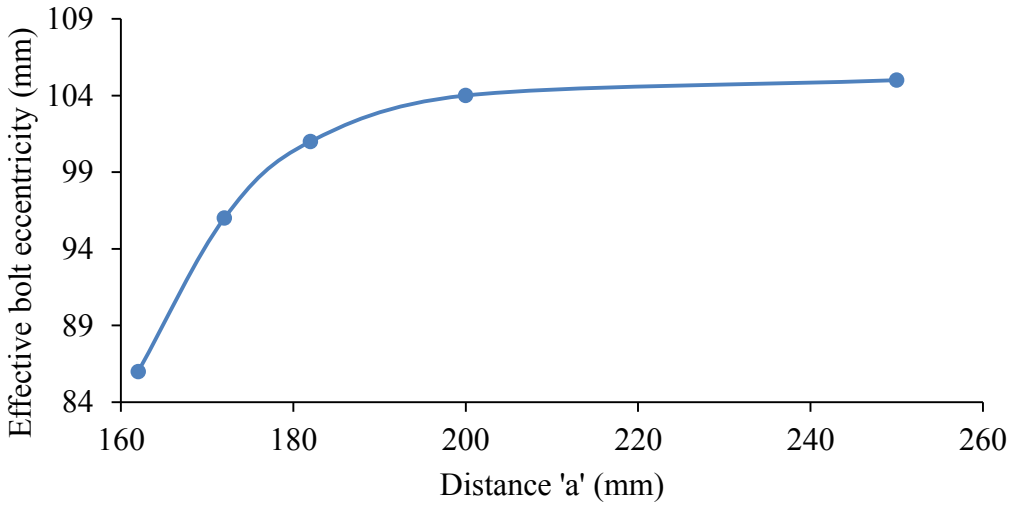

Figure 5.16 Distance 'a' versus FE measured e_b

Table 5.6 lists the predicted e_b and ultimate loads from both the FE simulations and the AISC recommendation. It shows that the AISC design procedure is conservative in estimating the effective bolt eccentricity, which results in underestimating the connection shear capacity with an average of $F_{u,AISC}/F_u$ ratio of 0.38. The calculated bolt shear capacity using FE effective bolt eccentricities compares better with the FE ultimate loads, having an average $F_{u,FE}/F_u$ ratio of 0.73 which is approximately twice the shear load predicted by the standard.

Table 5.6 Summary of effect of distance'a'

Simu.	'a' Distance	Bolt Failure	$e_{b,FE}^{(1)}$	$e_{b,AISC}^{(2)}$	$F_{u,FE}^{(3)}$	$F_{u,AISC}^{(4)}$	$F_u^{(5)}$	$F_{u,FE}/F_u$	$F_{u,AISC}/F_u$
3	162	Bottom	86	162	244	139	368	0.66	0.38
6	172	Bottom	96	172	223	131	352	0.63	0.37
7	182	Bottom	101	182	213	123	348	0.64	0.35
8	200	Bottom	104	200	209	113	297	0.70	0.38
9	250	Bottom	105	250	208	91	209	1.00	0.43

1 Bolt effective eccentricity according to FE simulation, mm
2 Bolt effective eccentricity according to AISC 2011, mm
3 Bolt shear including bolt group reduction factor based on $e_{b,FE}$, kN
4 Connection ultimate capacity based on AISC 2011 design procedure, kN
5 Ultimate connection shear for FE simulation, kN

5.4 Plate Thickness

Four different shear tab thicknesses are selected to investigate the effect of varying the plate thickness on the behaviour and ultimate load of EST connections. Simulations 3, 10, 11 and 12 have plate thicknesses of 10, 8, 6 and 12 mm respectively. Figure 5.17 plots the connection shear versus vertical deflection of the shear tab. The deflection was measured at the bottom of the shear tab as illustrated in Figure 5.18. Figure 5.17 shows that the onset of nonlinearity for the 6 mm plate commences at much lower load and

attained a significantly lower capacity than the other three plate thicknesses. For the other three plate thickness, as the plate thickness increases, the vertical displacement decreases.

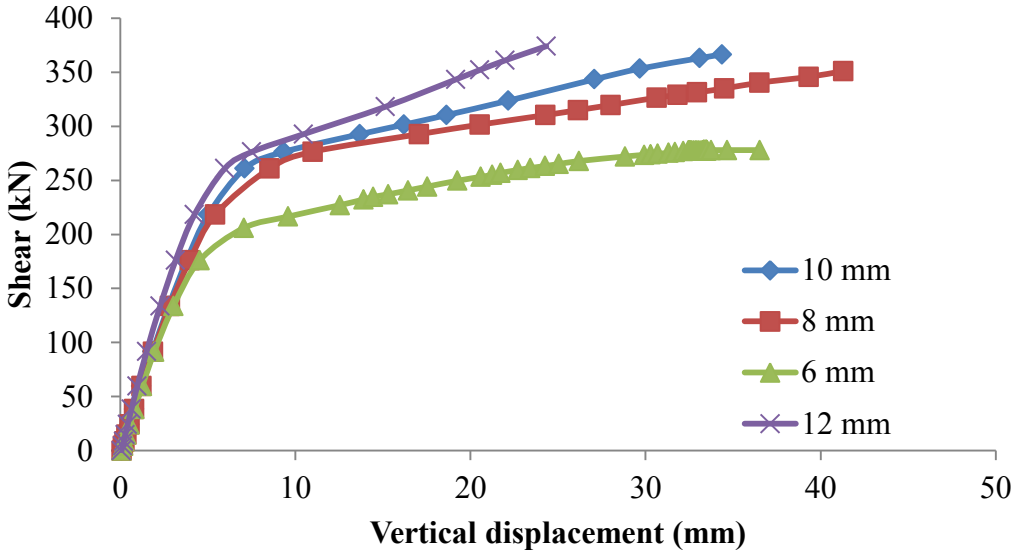

Figure 5.17 Shear versus vertical displacement for varying plate thickness

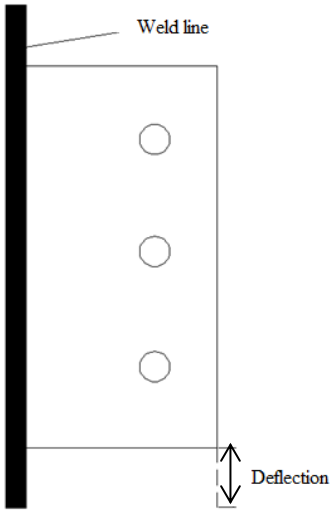

Figure 5.18 Location of shear tab deflection measurment

Figure 5.19 is a plot of the connection shear versus shear tab rotation for four plate thicknesses. Once again it can be seen that onset of nonlinear behaviour commences earlier for simulation 11 with the 6 mm plate. For simulation 11, the shear tab rotation plot flattens at 275 kN whereas simulations 3, 10 and 11 with the thicker plates, are capable of resisting higher shear loads.

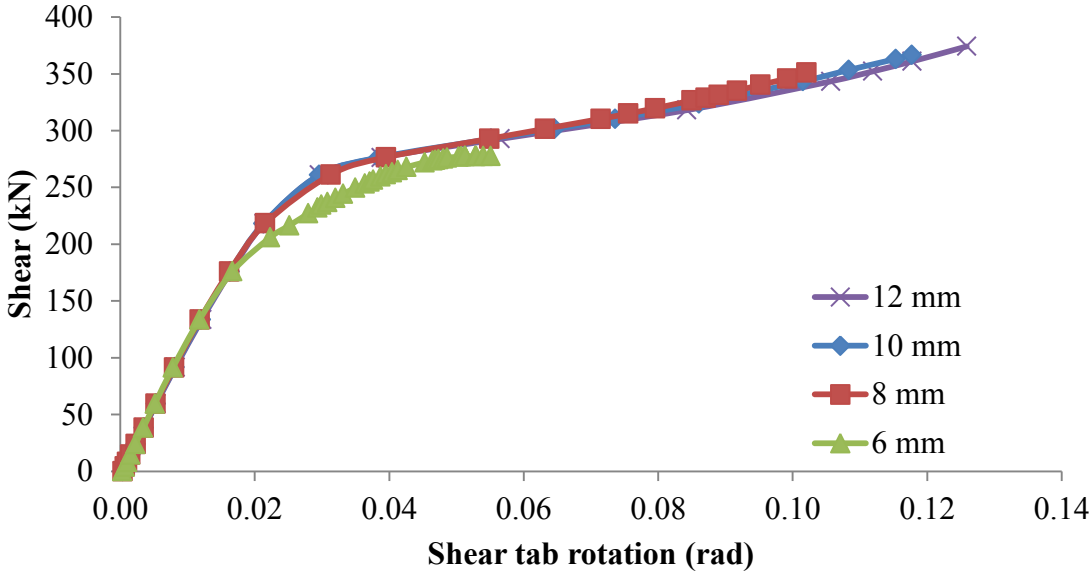

Figure 5.19 Connection shear versus shear tab rotation for varying plate thickness

Figures 5.20, 5.21 and 5.22 are plots of the connection shear versus the shear stress across all three bolts for simulations 10, 11 and 12, respectively. Similar to the shear stress plot for simulation 3 (Figure 5.9), simulation 10 demonstrates a drop in shear stress in the bottom bolt after fracture at a connection shear load of 351 kN. The dotted line in Figure 5.20 depicts the maximum shear stress and corresponding failure load for bolt 3.

For simulation 11 shown in Figure 5.21 the shear stress does not reach shear stress levels large enough to cause bolt fracture. Instead an instability of the plate occurs at the 275 kN marked by the dotted line in Figure 5.21. After this point the shear stress fluctuates erratically with load indicating an instability. At the 275 kN the shear versus vertical deflection plot for simulation 11 in Figure 5.17 flattens signifying plate yielding. Hence, the reduced thickness of simulation 9 resulted in a plate shear yielding failure at 275 kN.

Simulation 12 with the 12 mm thick plate reached bolt fracture at 371 kN with a maximum shear stress of 457 MPa as illustrated in Figure 5.22.

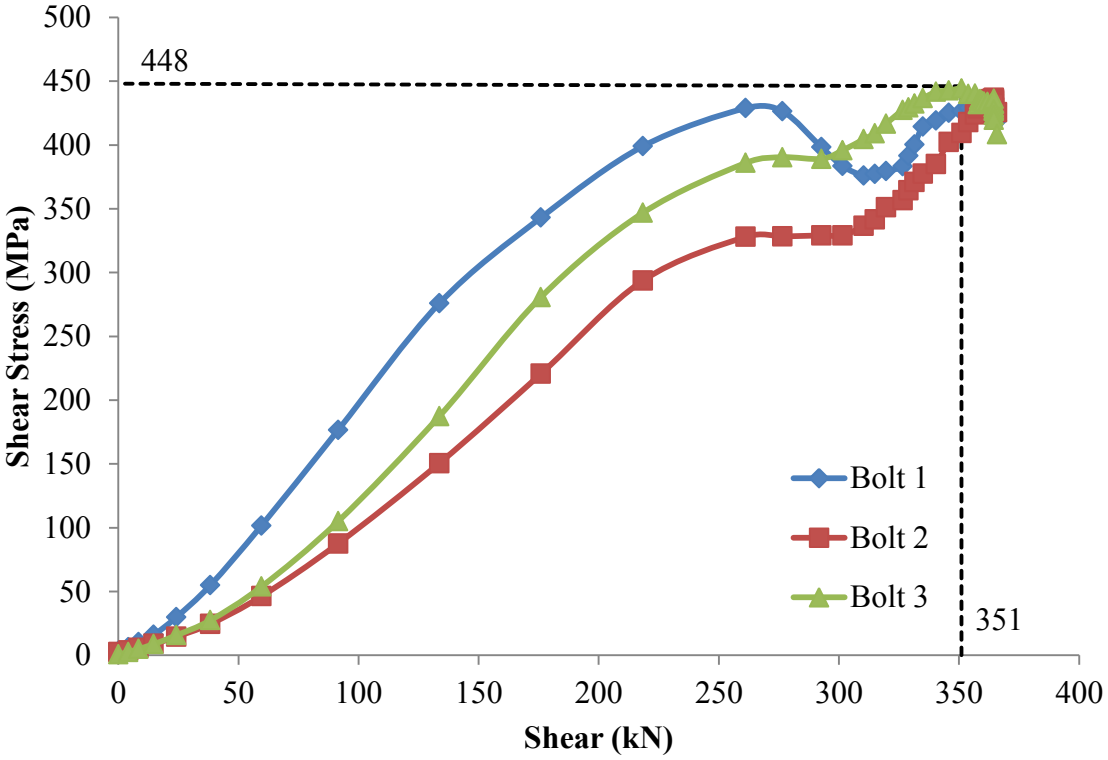

Figure 5.20 Connection shear versus shear stress for simulation 10

(plate thickness = 8 mm)

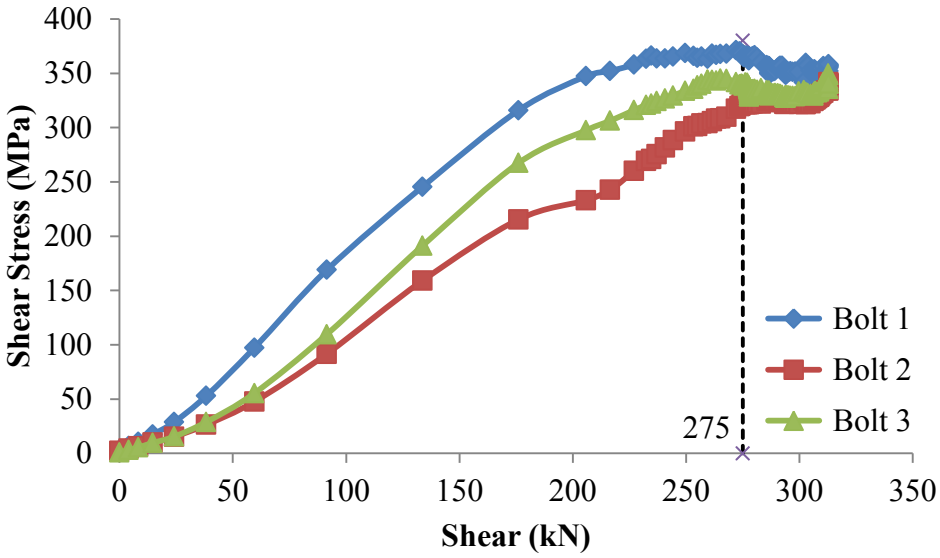

Figure 5.21 Connection shear versus shear stress for simulation 11

(plate thickness = 6 mm)

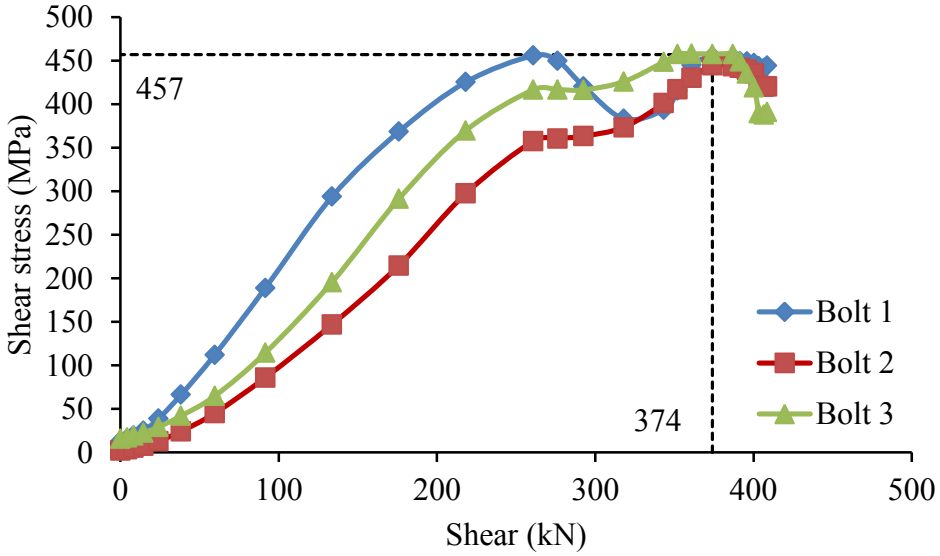

Figure 5.22 Connection shear versus shear stress for simulation 12

(plate thickness = 12 mm)

Table 5.7 lists the shear stress for all bolts at ultimate load for simulations 3, 10 and 12. The shear stress standard deviation for simulation 3, 10 and 12 were 7, 19 and 6 MPa, respectively. As theplate thickness increases, the distribution of shear stress in three bolts becomes more even.

Table 5.7 Shear stress, MPa, distribution across 3 bolts for simulations 3, 10, 11 and 12

Simulation	**3**	**10**	**11**	**12**
Plate thickness (mm)	10	8	6	12
Top Bolt	451	426	-	454
Middle Bolt	443	409	-	445
Bottom Bolt	457	448	-	457
Standard Deviation	7	19	-	6
Ultimate Load (kN)	368	351	275	374

Figure 5.23 illustrates the movement of the point of inflection for simulation 3, 10, 11 and 12. As shown, the change in plate thickness does not influence the overall movement trend of the inflection point. Furthermore, the inflection point of simulation 11 does not reverse direction away from the bolt line as in simulations 3, 10 and 12 since the shear yielding governed the connection capacity prior to bolt shear failure.

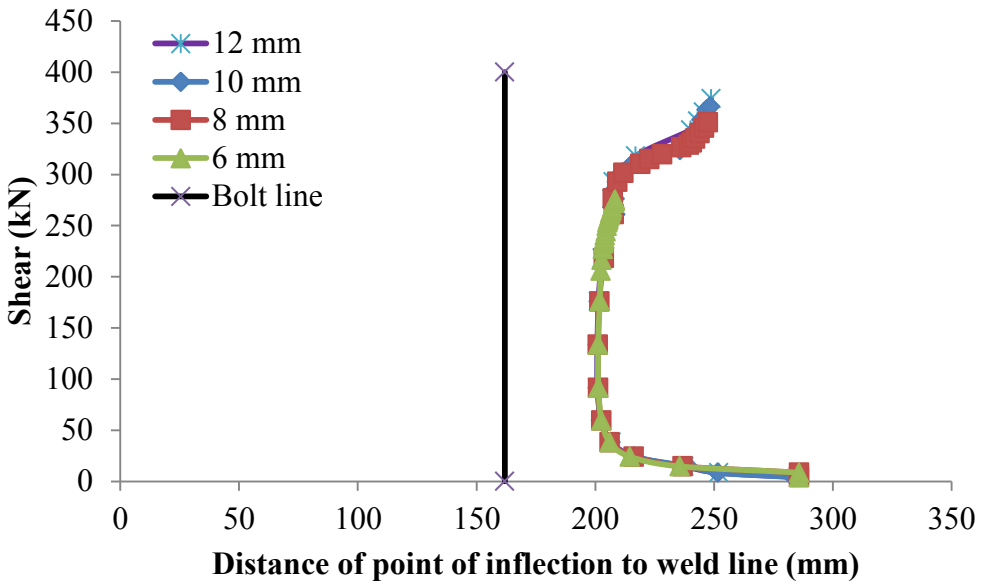

Figure 5.23 Distance of point of inflection to weld line for varying plate thickness

Table 5.8 summarizes the FE results for the parametric study of plate thickness. Bolt fracture governed simulation 3, 10, and 12 whereas simulation 11 was governed by plate shear yield. The FE ultimate connection capacities were 368 kN, 351 kN, 275 kN and 374 kN for simulations 3, 10, 11 and 12 respectively. The calculated ultimate capacities using the AISC procedure when taking e_b to be equal to distance 'a' predicted a bolt shear failure of 139 kN for all four connections. However, when the bolt effective eccentricities obtained from the FE simulation were used, simulations 3, 10 and 12 were governed by bolt shear with ultimate loads of 244 kN, 243 kN and 244 kN, resulting in $F_{u,FE}/F_u$ ratios of 0.66, 0.69 and 0.66, respectively. Compared with the average ratio $F_{u,AISC}/F_u$ of 0.38, the use of FE e_b markedly improved the estimate of the connection capacity by bolt fracture. This also underscore the importance to have a minimum plate thickness requirement in order to ensure a bolt shear failure.

For simulation 11, the AISC manual 2011 predicted bolt shear to be the governing limit state at 139 kN. The plate shear yielding limit state according to the AISC Specification (2010) yields a value of 290 kN for plate yielding. The finite element simulation predicted plate yield at 275 kN, which is within 5% of the AISC value.

Table 5.8 Summary of effect of plate thickness

Sim.	Plate thickness (mm)	Vertical deflection (mm)	Failure	$e_{b,FE}^{(1)}$	$e_{b,AISC}^{(2)}$	$F_{u,FE}^{(3)}$	$F_{u,AISC}^{(4)}$	$F_u^{(5)}$	$F_{u,FE}/F_u$	$F_{u,AISC}/F_u$
3	10	34	Bolt fracture	86	162	244	139	368	0.66	0.38
10	8	41	Bolt fracture	87	162	243	139	351	0.69	0.39
11	6	36	Plate yield	-	-	-	139/290	275	-	-
12	12	24	Bolt fracture	86	162	244	139	371	0.66	0.38

1 Bolt effective eccentricity according to FE simulation, mm
2 Bolt effective eccentricity according to AISC 2011, mm
3 Bolt shear including bolt group reduction factor based on $e_{b,FE}$, kN
4 Connection ultimate capacity based on AISC 2011 design procedure, kN
5 Ultimate connection shear for FE simulation, kN

5.5 Double-Row of Bolts

A single plate shear connection with two vertical bolt rows was investigated. Figure 5.24 identifies rows 1 and 2 in the connection. The distance between the first row of bolts and the weld line remained 162 mm as in simulation 3.

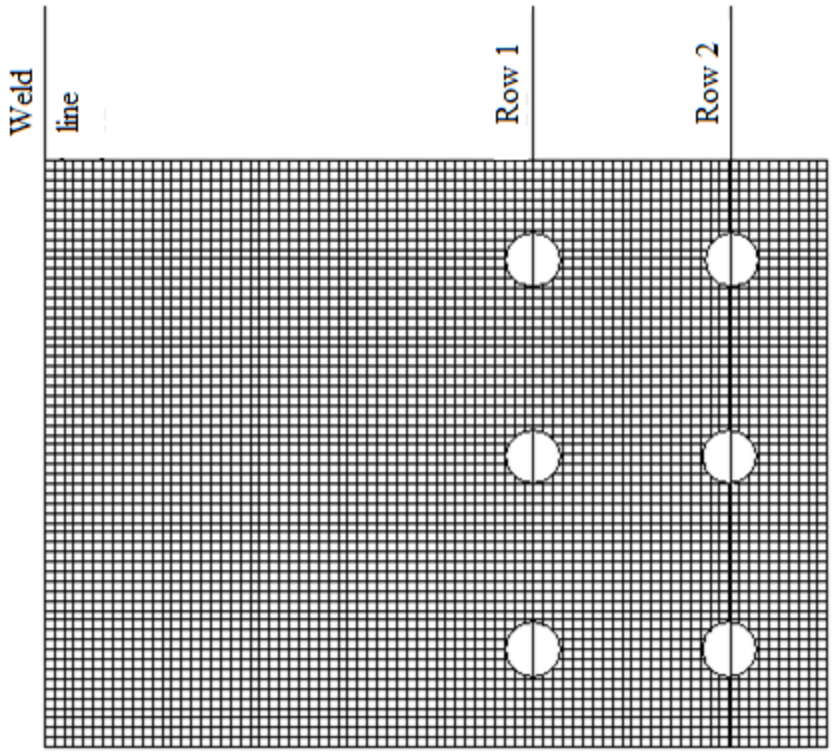

Figure 5.24 EST with double vertical bolt rows

Figure 5.25 illustrates the connection shear versus the beam end rotation for simulations 3, 13, and 14. Simulation 3 has one single row and simulation 13 with two rows but both have a plate thickness of 10 mm. Simulation 14 has two rows of bolts but with a plate thickness of 12 mm. Beams in simulations 3, 13 and 14 all yield at approximately 260 kN marked by the dotted black line. The double-row connection shows beam behaviour similar to that of simulation 3 but attains greater beam end rotation. In the case of double-row connection, the use of a thicker plate (simulation 14) results in a higher connection load and a greater post-yield rotation than the thinner plate (simulation 13).

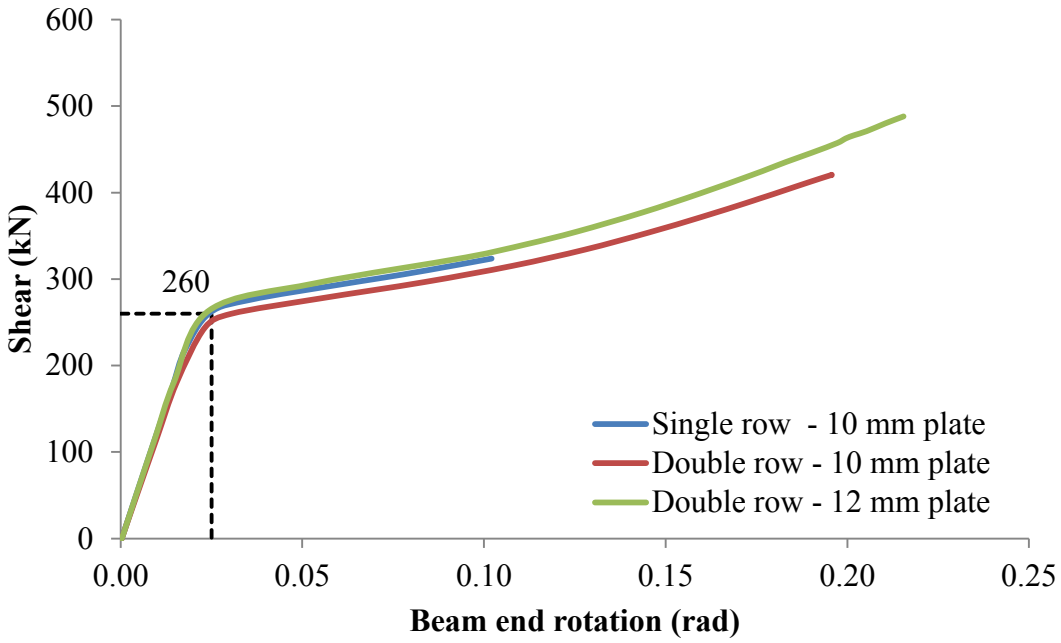

Figure 5.25 Shear versus beam end rotation for double bolt row

Figure 5.26 illustrates the shear stress distribution for the double-row connection for simulation 13. It is evident that in general, the bolts in row 1 resist more shear than bolts in row 2. Additionally, in a single line of bolts the topmost bolt initially carries more of the shear than the bolts in the middle or bottom of the row. The FE model failed to converge at 420 kN shear load marked by the dotted black line in the Figure 5.26. At this point shear stresses are not high enough to cause a bolt shear failure. At the 420 kN load, the shear tab rotation became excessive resulting in high stress concentrations between the EST and column web. Figure 5.27 is the von Mises stress distribution at 420 kN for the shear tab from FE results. The large rotation results in a high stress concentration along the top left corner of the shear tab. The high stress traces along the entire column web.

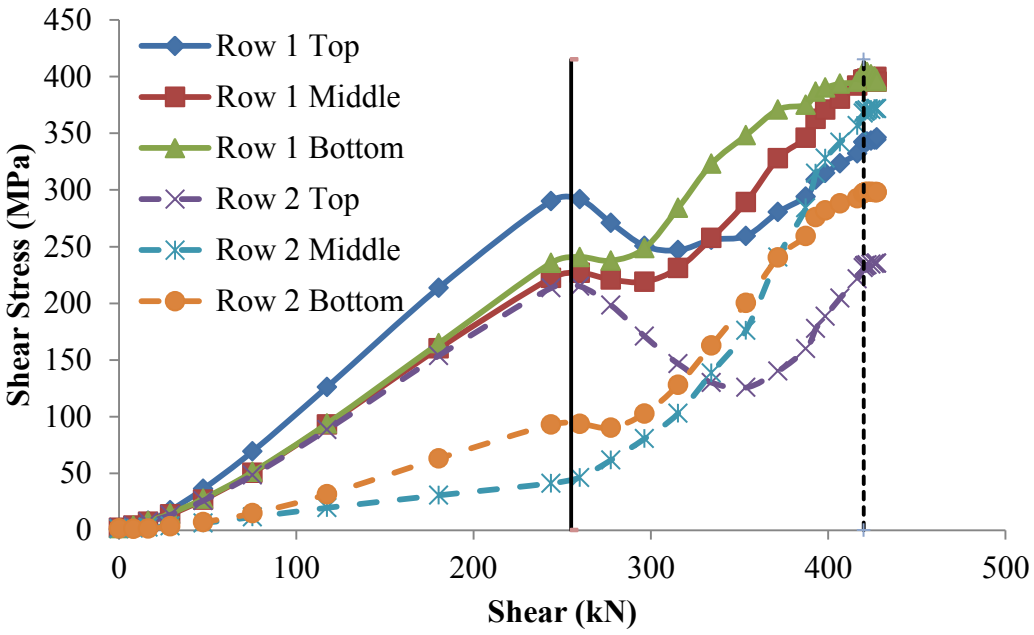

Figure 5.26 Connections shear versus Shear stress fluctuation for simulation 13

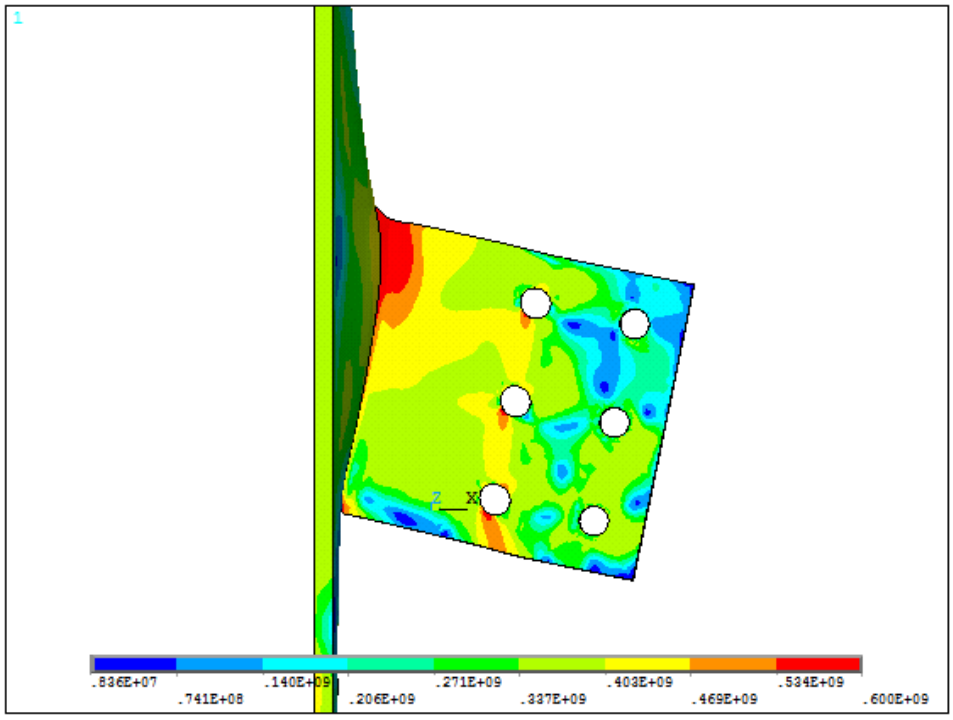

Figure 5.27 Von Mises stress, Pa, distribution for simulation 13 at 420 kN

Figure 5.28 below is a plot of the horizontal shear stress component versus connection shear for simulation 13. It shows that the top and bottom bolts resist horizontal shear forces due to the shear tab rotation for both rows. The middle bolts experience a small positive shear force which suggests that the center of rotation does not lie exactly at mid-depth of the shear tab. In addition, the second row of bolts appears to attained slightly higher horizontal shear stress. Referring to Figure 5.26 which shows that the first row of bolts attained much greater total shear stress prior to the yielding of beam web, this indicates that the most vertical shear stress is resisted by the first row of bolts before yielding. Force redistribution is evident when at failure the second row of bolts picks up the load significantly.

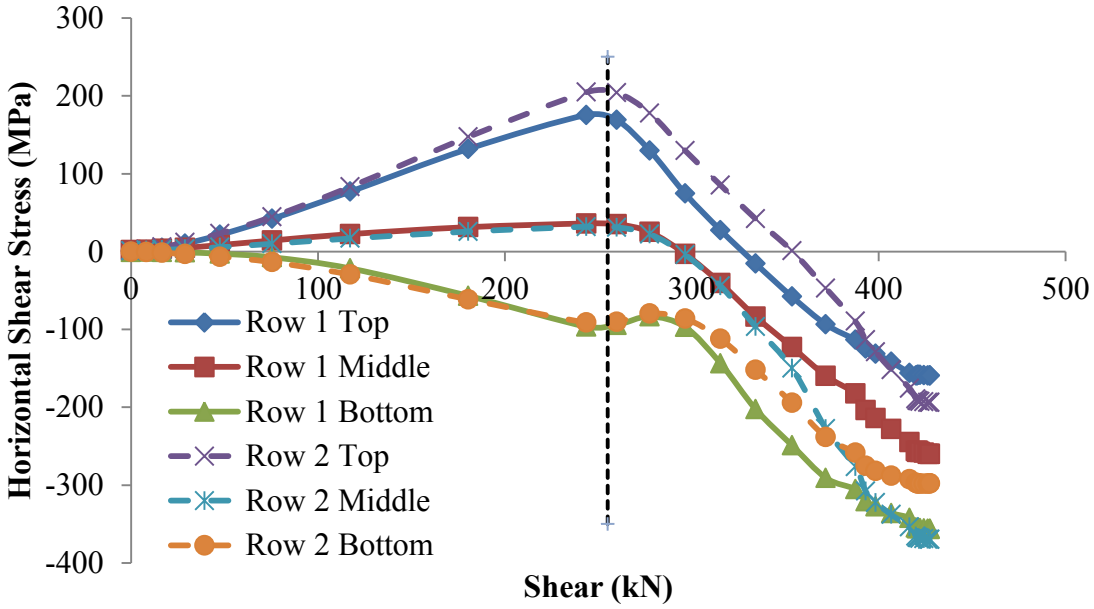

Figure 5.28 Connection shear versus horizontal shear stress for simulation 13

The fluctuation of the shear stress for simulation 14 is illustrated in Figure 5.29. A similar variation trend to simulation 13 is observed but a close examination shows that the

connection failed by bolt shear failure at 488 kN. It suggests that when the connection becomes stiffer using more rows of bolts, the plate thickness needs to be increased to ensure a bolt shear failure.

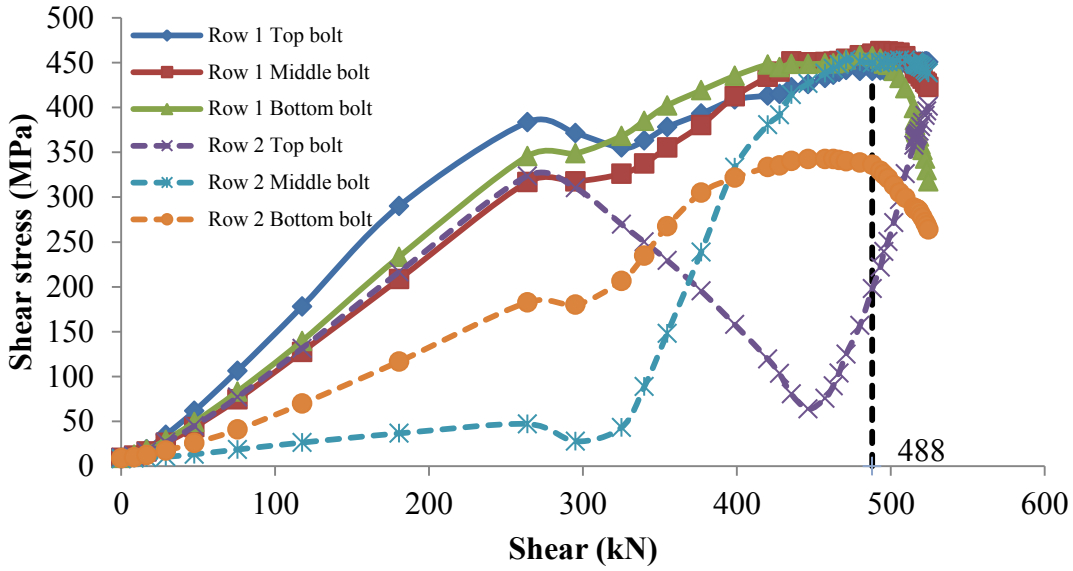

Figure 5.29 Connections shear versus shear stress fluctuation for simulation 14

The shear stress variation across each bolt at failure is summarized in Table 5.9 for the single row and double row connections. It is evident that the single-row bolts attain shear stress higher than the double-row connection. The bolts in row 1 in a double row arrangement resist more shear than bolts in row 2. Comparing simulation 13 and 14, it shows that the use of a thicker plate enables failure at a higher load caused by bolt failure and a thinner plate results in a failure load 14% lower. The bolt strength is not fully utilized.

Table 5.9 Shear stress, MPa, distribution across 3 bolts for simulations 3, 13 and 14

Simulation	**3**	**13**		**14**	
Row	-	1	2	1	2
Top Bolt	451	334	228	440	157
Middle Bolt	443	388	363	457	451
Bottom bolt	457	395	287	458	339
Ultimate Load (kN)	368	420		488	

Figure 5.30 compares the movement of the inflection point with the loading history for simulations 3, 13 and 14. Both single-row and double-row EST connections show a similar trend in the movement of the inflection point. Table 5.10 summarizes the results for the single and double-row simulations. As simulation 13 was governed by plate plasticity and not bolt fracture, the $e_{b,FE}$ and $F_{u,FE}$ cannot be extracted from the FE simulation. The e_b values at failure for simulations 3, and 14 are 86, and 104 mm, respectively. Bolt shear governed the AISC 2011 design procedure for the double-row connections with an ultimate load of 325 kN. Considering simulations 3 and 14 which are also governed by bolt shear failure from FE model, the average $F_{u,AISC}/F_u$ is about 0.53 with the thicker plate showing a better agreement. An even better agreement with a mean ratio of 0.8 can be obtained if the FE determined e_b is used with the AISC design procedure. In the case of simulation 13, the AISC design check for the yielding due to flexure predicts a maximum connection shear force of 421 kN for simulation 13 (10 mm plate), which agrees well with the FE result. However, since the bolt shear failure governs the AISC capacity, the design based on AISC procedure would be again conservative.

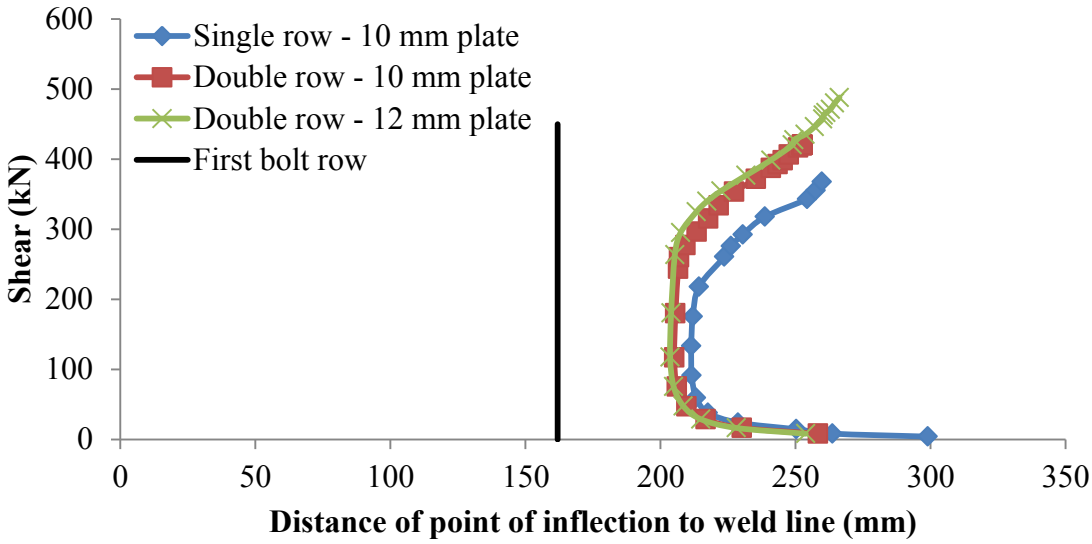

Figure 5.30 Distance of point of inflection to weld line for double vertical row

Table 5.10 Summary of effect of single and double-row bolts

Simu.	Failure	$e_{b,FE}^{(1)}$	$e_{b,AISC}^{(2)}$	$F_{u,FE}^{(3)}$	$F_{u,AISC}^{(4)}$	$F_u^{(5)}$	$F_{u,FE}/F_u$	$F_{u,AISC}/F_u$
3	Bolt fracture	86	162	246	139	368	0.67	0.38
13	Plate yield	-	162	-	325/ 421	420	-	0.77
14	Bolt fracture	104	162	454	325	488	0.93	0.67

1 Bolt effective eccentricity according to FE simulation, mm
2 Bolt effective eccentricity according to AISC 2011, mm
3 Bolt shear including bolt group reduction factor based on $e_{b,FE}$, kN
4 Connection ultimate capacity based on AISC 2011 design procedure, kN
5 Ultimate connection shear for FE simulation, kN

5.6 Beam Lateral Restraint

A potential failure mode for unstiffened EST is the twisting of the plate. As discussed in Chapter II, twisting is due to the offset of the shear force to the centroid of the shear tab

as the beam web is only connected to one side of the EST. The twisting of the plate will result in the twisting of the beam web, which in turn cause the beam flange to twist as well. Figure 5.31 illustrates the twisting of the shear tab when no lateral end restraint is provided where the legend is the lateral deflection in meters.

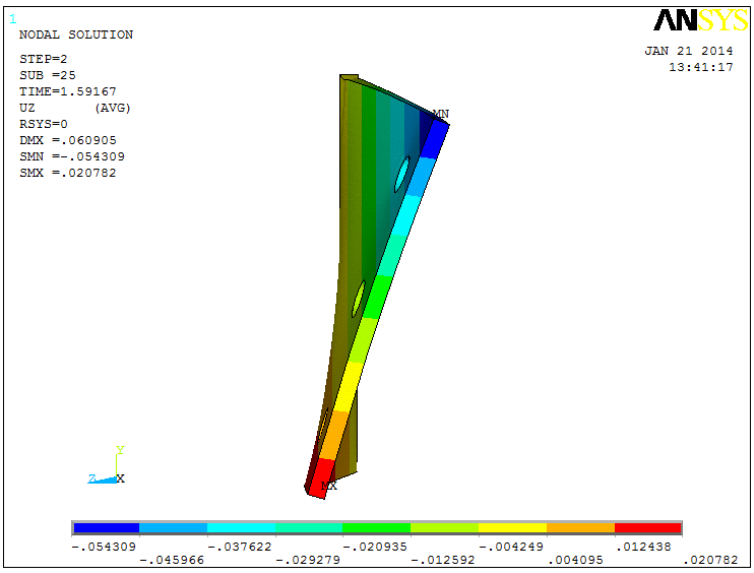

Figure 5.31 Shear tab twist for simulation 15

In this section, the effect of lateral restraint provided at the beam top flange on the capacity of the EST connection is studied. Four different beam lateral restraint cases are examined. The beam in simulation 3 was fully laterally restrained. Simulation 15 was laterally braced at the midspan. Simulation 16 was laterally braced at the end points and simulation 17 was restrained at both midspan and endpoints. Figure 5.32 shows the different beam restraint simulated in the FEM.

(a) Simulation 3

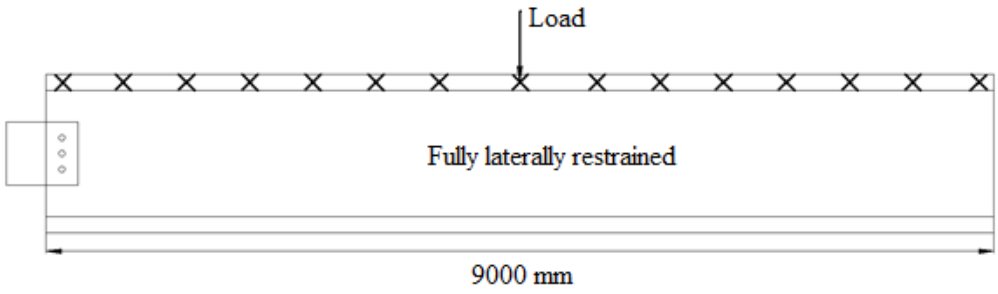

(b) Simulation 15

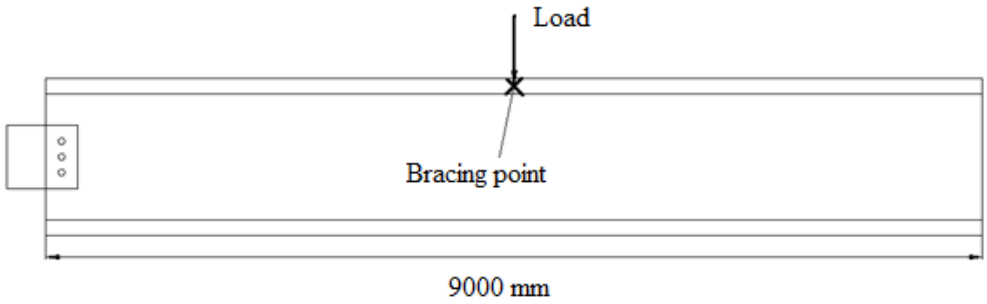

(c) Simulation 16

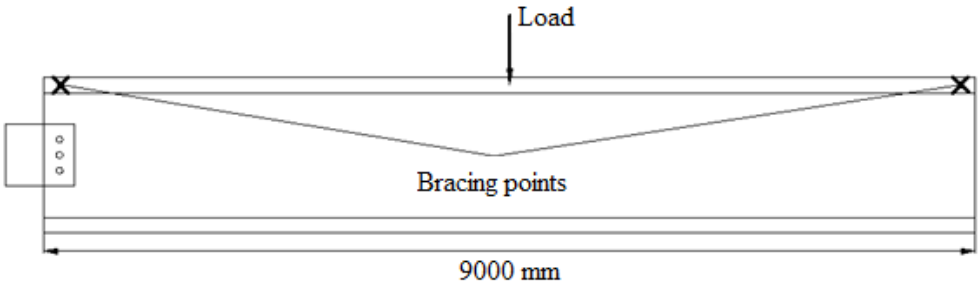

(d) Simulation 17

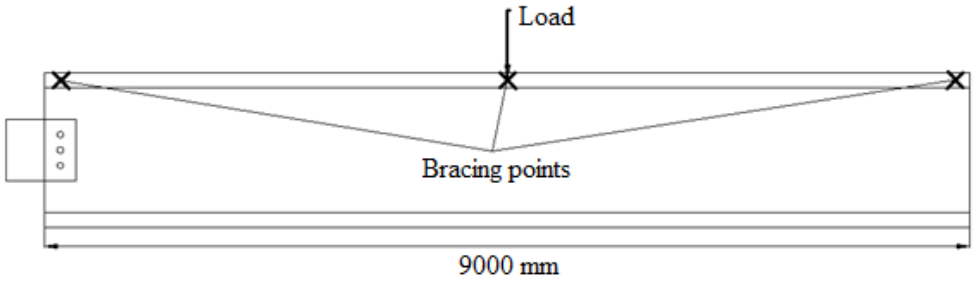

Figure 5.32 Beam lateral restraint locations

Figure 5.33 illustrates the beam behaviour for each of the four simulations. Simulation 3 with the fully laterally supported beam began to yield at 260 kN whereas the other simulations predict yielding of the beam at 220 kN.

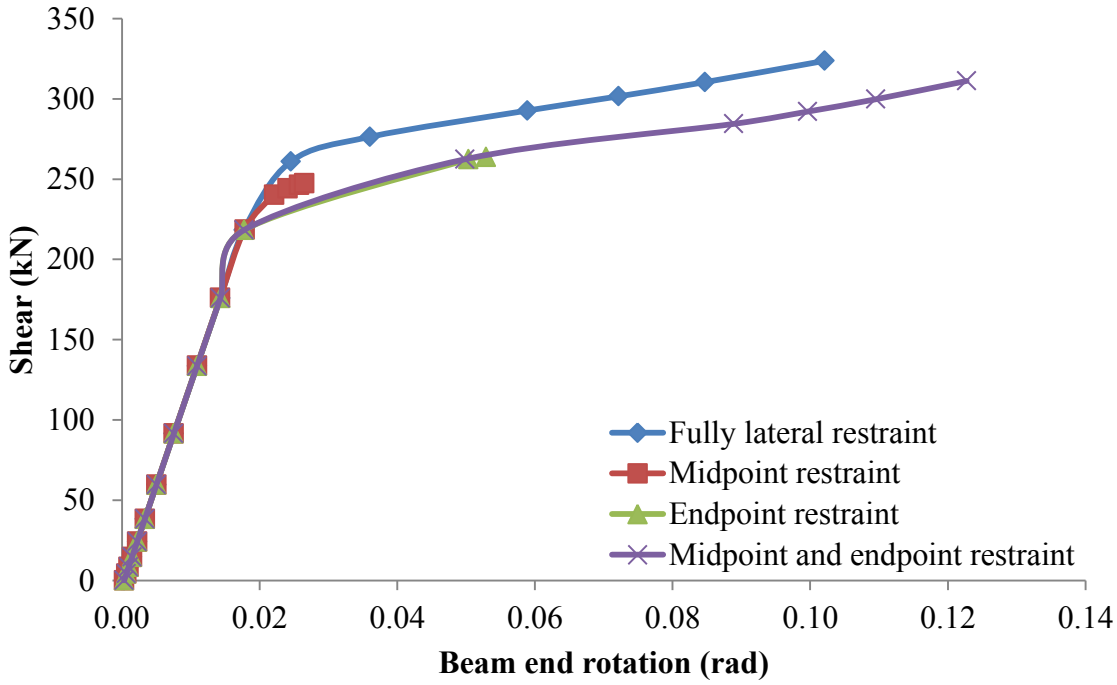

Figure 5.33 Beam end rotation for lateral restraint parameter

Figure 5.34 shows the connection shear versus the shear tab rotational twist for all cases. It can be seen that the inclusion of a lateral restraint at the end of the beam effectively controls the lateral twisting of the shear tab as shown in simulations 3, 16 and 17. The exclusion of the end restraint as in simulation 15 influences the connection behaviour and ultimately the connection capacity. The connection shear versus rotational twist curve for simulation 15 levels off at a load of 245 kN whereas simulations 3, 16 and 17 continue to resist higher load with no sign of a rotational twist failure. Simulations 3 and 17 were governed by the shear failure of the bolt. Simulation 16 attained a lower ultimate load

than simulations 3 and 17. Since simulation 16 was laterally restrained at the end points only, the beam experienced a substantial lateral deflection at mid-span due to lateral instability of the beam. This deflection has attributed to the reduction of the connection capacity. Simulation 16 failed by lateral torsional buckling of the beam prior to reaching the bolt shear strength. The FE predicted ultimate loads of 368, 263 and 322 kN for simulations 3, 16 and 17, respectively. Figure 5.35 illustrates the lateral torsional buckling at midspan of the beam.

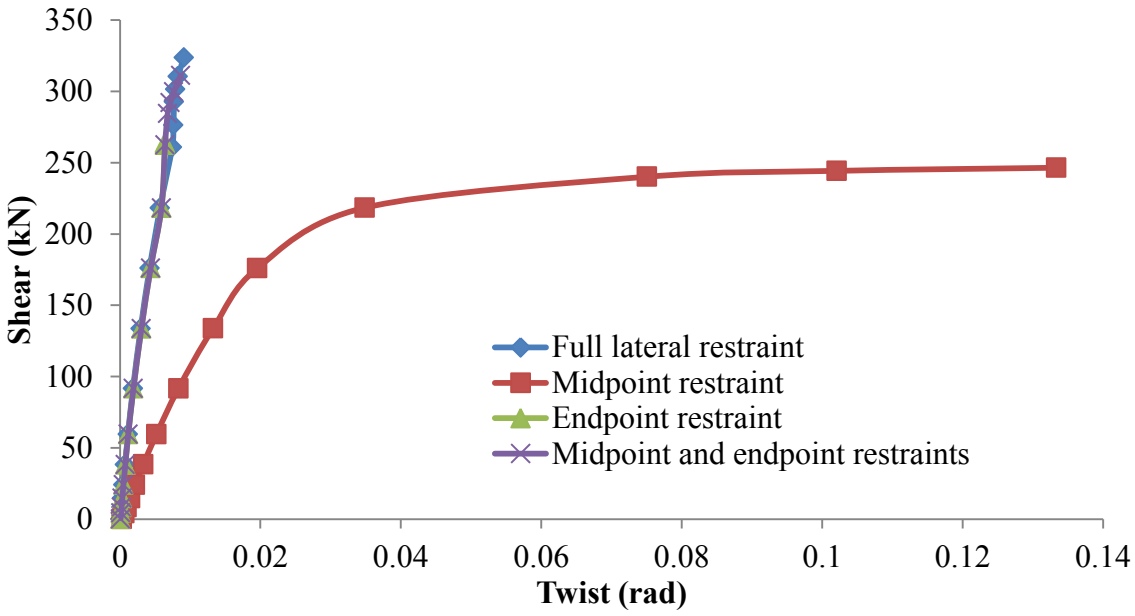

Figure 5.34 Connection shear versus rotational twist of shear tab

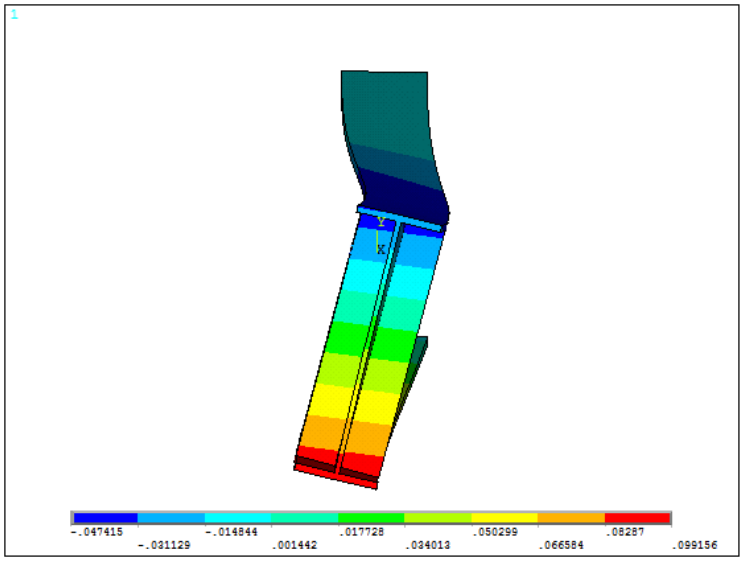

Figure 5.35 Lateral torsional buckling demonstarted in simulation 16

For simulation 15 where the lateral restraint is not provided at the tab location, the connection failed by tab twist at 245 kN. This value is in line with theoretical value of 240 kN obtained from Equation [2.8] proposed by Sherman and Ghorbanpoor (2002).

5.7 Beam Length-to-Depth Ratio

The length to depth ratio, L/D, was varied to examine the slenderness of the beam on the connection capacity. The length of the beam is varied while the beam depth is maintained. For simulations 3, 18, and 19, the beam lengths are 9 m, 5 m and 7 m, respectively. Figure 5.36 shows a comparison of the beam end rotation of FE models. Simulations 18, 19 and 3 contained both a linear and nonlinear portion along the loading history of the FE models. Naturally, beams with a longer span resulted in larger rotations at the ends. At failure, simulations 18, 19 and 3 had end rotations of 0.118, 0.135, and 0.150 rad, respectively.

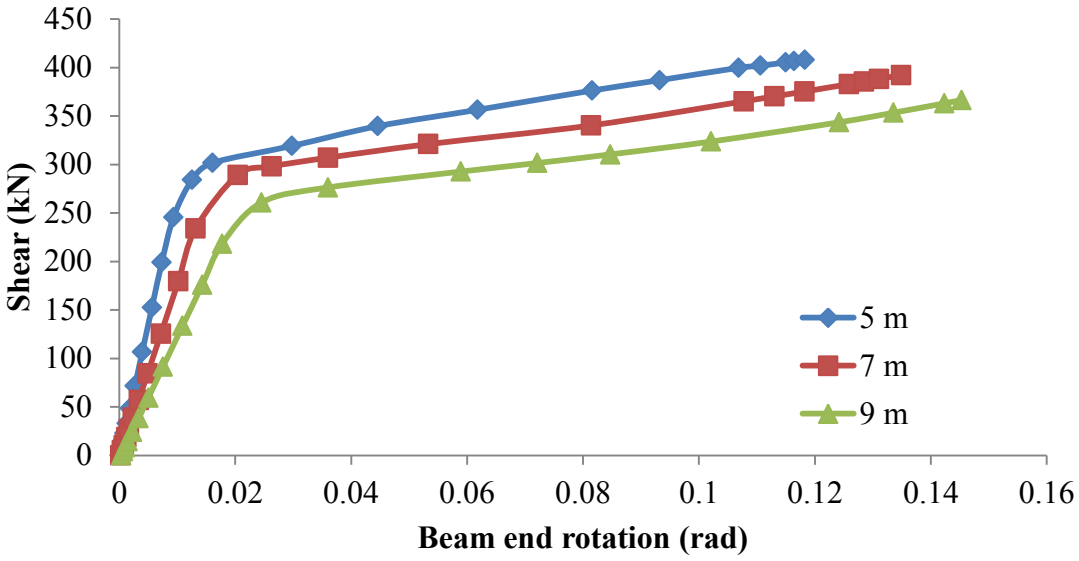

Figure 5.36 Shear versus beam end rotation for length to depth ratio parameter

Figures 5.37 and 5.38 illustrate the shear stress distribution for simulations 18 and 19. Bolt shear failure governed both cases. The bolt shear failure occurs at 400 kN and 392 kN for the 5 m and 7 m beams, respectively. A decrease in the bolt group shear capacity is observed with the increase in beam length.

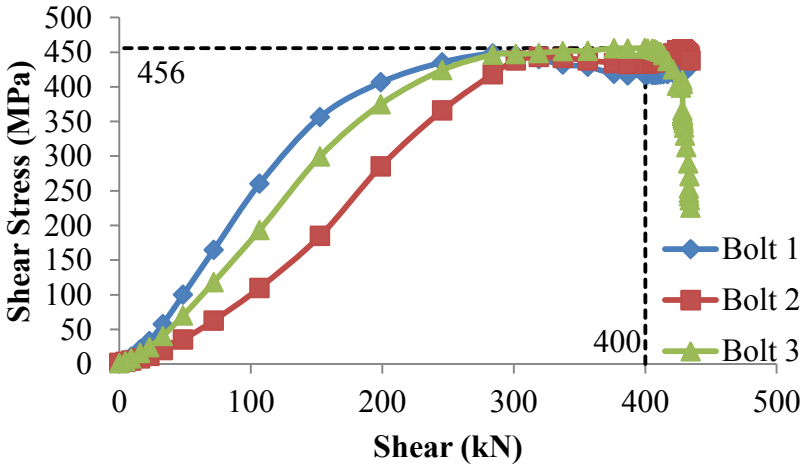

Figure 5.37 Shear stress versus connection shear for simulation 18 (5 m beam)

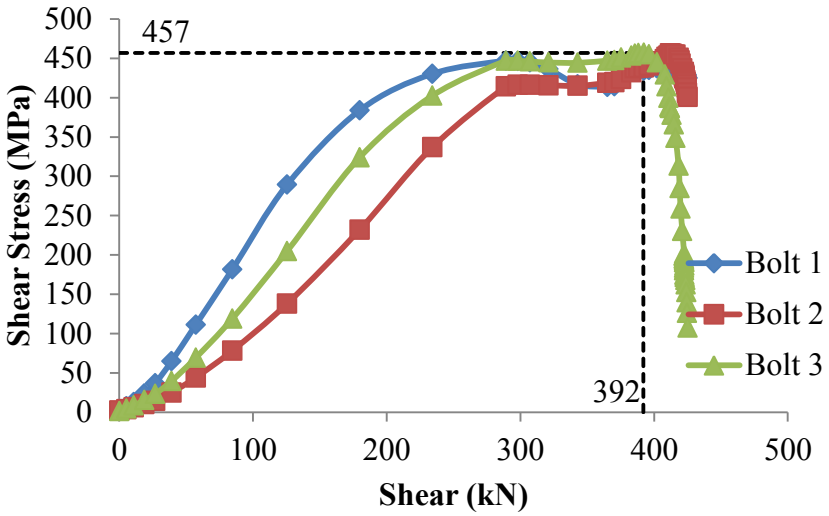

Figure 5.38 Shear stress versus connection shear for simulation 19 (7 m beam)

Table 5.11 lists the shear stress values at ultimate load for each of the simulations. The table shows that the shear stress is distributed across all three bolts in a similar manner and the maximum shear stress occurs in the bottom bolt at failure for all simulations.

Table 5.11 Shear stress distribution for beam length-to-depth ratio

Simulation	**18**	**19**	**3**
Beam Length (m)	5	7	9
Top Bolt	432	448	451
Middle Bolt	433	438	443
Bottom Bolt	456	457	457
Standard Deviation	13	9	7
Ultimate Load (kN)	400	392	368

Figure 5.39 plots the movement of the inflection point versus connection shear load. The fluctuation follows a similar trend as in the previous parameters; movement of the inflection point towards the support until the beam yield region in which the inflection point reverses direction and moves away from the support. Although following slightly

different paths, the effective bolt eccentricities at ultimate are close for all three simulations.

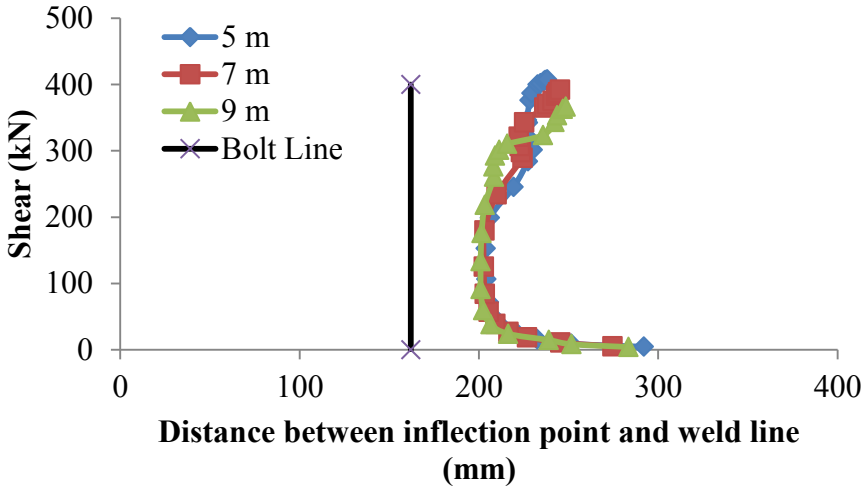

Figure 5.39 Distance of point of inflection to weld line for varying beam length-to-depth ratios

Figure 5.40 shows the L/D ratio versus the measured effective bolt eccentricity, e_b, at failure. For the given beam slenderness, the e_b increases in an approximately linear manner with the increase in the beam slenderness.

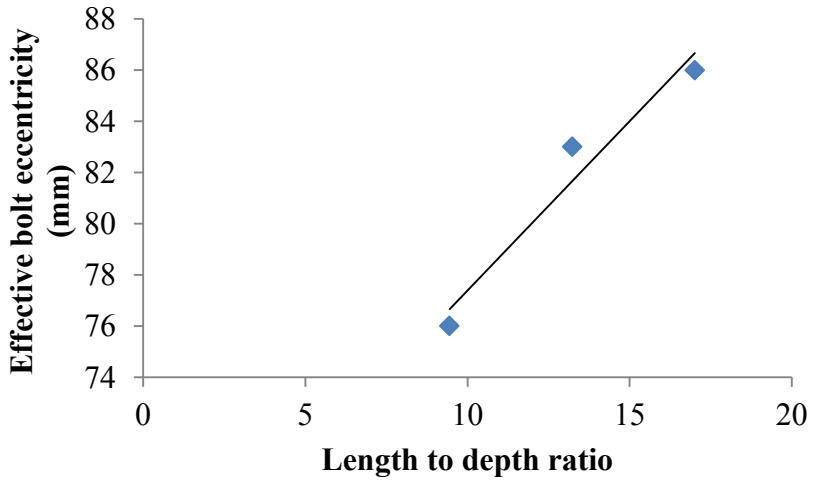

Figure 5.40 length-to-depth ratio versus measured e_b

The ultimate bolt shear capacity using the AISC manual 2011 design procedure are compared with that obtained using the measured e_b from the FE analysis in Table 5.12. The FE ultimate connection capacities are 368 kN, 400 kN and 392 kN for simulations 3, 18, and 19, respectively. The AISC design procedure predicted bolt shear failure at 139 kN. The AISC method does not take the beam rotational stiffness into consideration when determing the connections ultimate capacity. The use of the measured e_b better predicted the bolt shear capacity than using distance 'a' as the eccentricity. The FE measured e underestimated bolt shear by 35% whereas the AISC procedure underestimated the capacity by 65%.

Table 5.12 Summary of effect of beam length-to-depth ratio

Simu. No.	L (m)	Beam end rotation (rad)	$e_{b,FE}^{(1)}$ (mm)	$e_{b,AISC}^{(2)}$ (mm)	$F_{u,FE}^{(3)}$ (kN)	$F_{u,AISC}^{(4)}$ (kN)	$F_u^{(5)}$ (kN)	$F_{u,FE}/F_u$	$F_{u,AISC}/F_u$
3	9	0.150	86	162	244	139	368	0.66	0.38
18	5	0.118	76	162	270	139	400	0.66	0.34
19	7	0.135	83	162	253	139	392	0.65	0.35

1 Bolt effective eccentricity according to FE simulation, mm
2 Bolt effective eccentricity according to AISC 2011, mm
3 Bolt shear including bolt group reduction factor based on $e_{b,FE}$, kN
4 Connection ultimate capacity based on AISC 2011 design procedure, kN
5 Ultimate connection shear for FE simulation, kN

5.8 Number of Bolts

This section studies the effect of number of bolts on the distribution of forces and the influence it has on the ultimate capacity of the connection. The connections consisting of three, four, five and six 20 mm, A325 high strength bolts in a single row are studied. The bolt spacing and the horizontal and vertical edge distances are maintained for all

simulations according to AISC Specification 2010. The shear tab height for the 3, 4, 5 and 6 bolted connections were 229, 305, 381, 457 mm, respectively.

Figure 5.41 illustrates the beam end rotation for the 3, 4, 5 and 6 bolted connections. All connections have the same stiffness in the linear portion of the graph. Once the beam enters the nonlinear portion, connections with a greater number of bolts have a higher post yield stiffness.

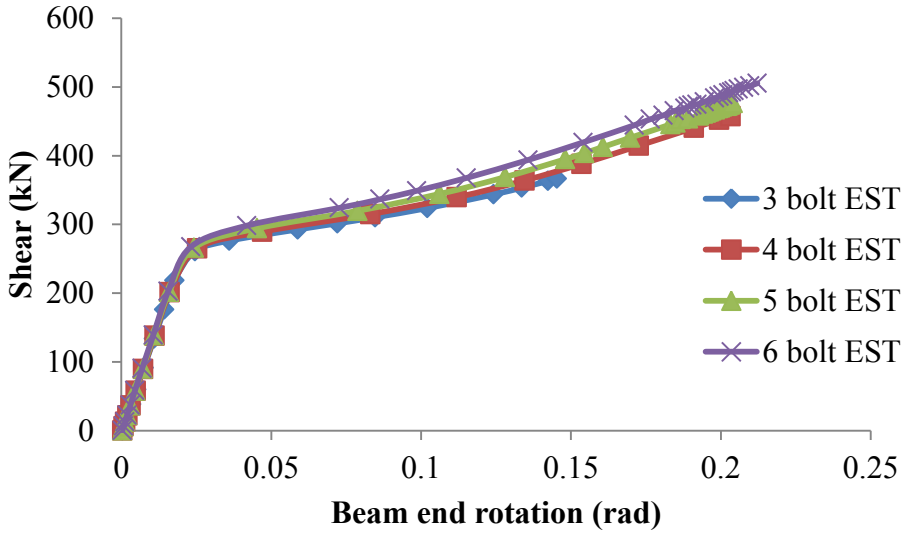

Figure 5.41 Coneection shear versus beam end rotation for number of bolt parameter

The shear stress plot of all bolts for the 4, 5 and 6 bolted connections are presented in Figures 5.42 to 5.44. All connections were governed by bolt failure. The connection capacity increases as the number of bolt increases. The 4, 5 and 6 bolted connections reached failure at 457, 474 and 505 kN respectively. The percentage increase of the connection capacities for the 4, 5 and 6 bolted connections in comparison with the 3 bolted connection are 24%, 29%, 37%. The 4-bolt EST connection was govern by bolt

fracture of the bottom bolt, similar to the 3 bolted connection presented earlier. However, bolt shear failure for the 5 and 6 bolted connections occurred in the topmost bolt.

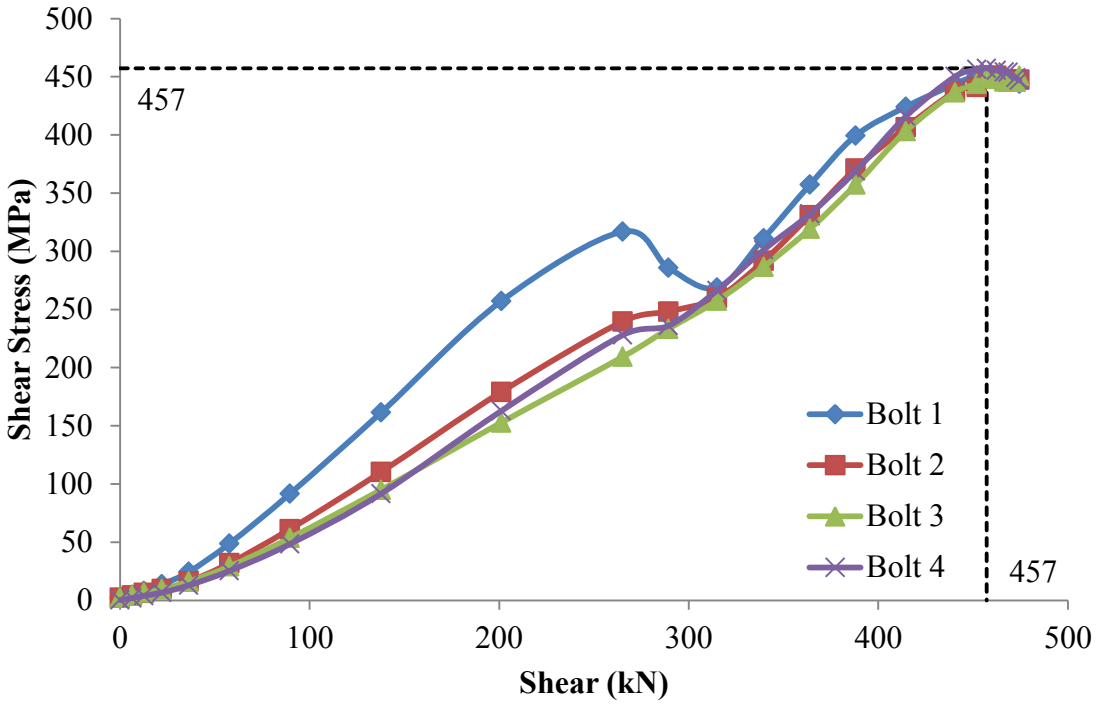

Figure 5.42 Shear stress versus connection shear for simulation 20 (4-bolt EST)

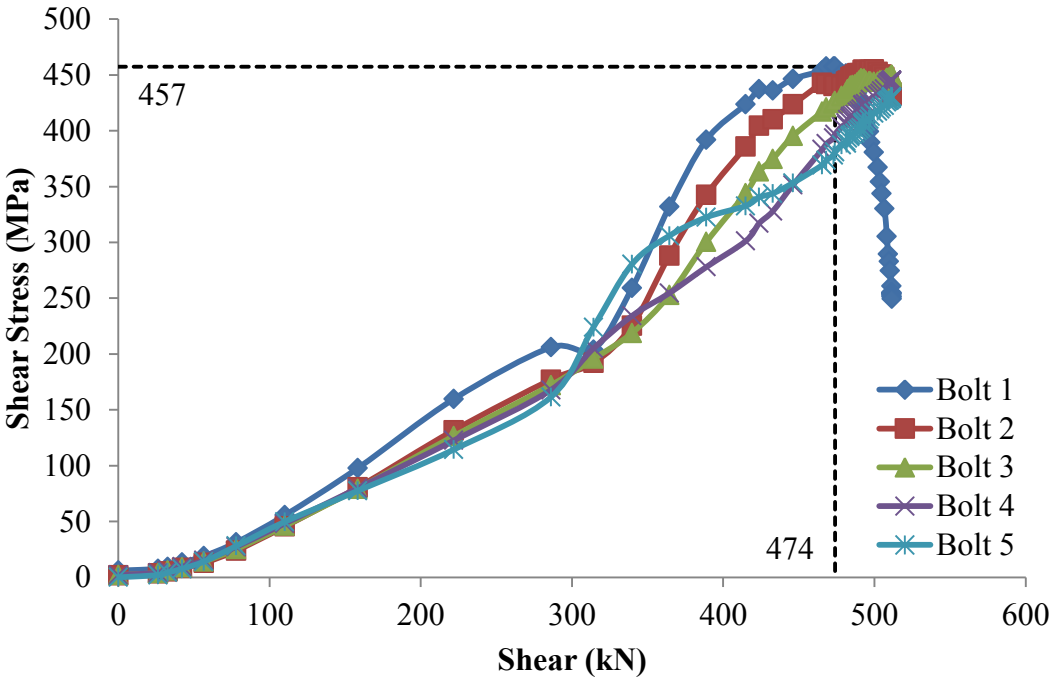

Figure 5.43 Shear stress versus connection shear for simulation 21 (5-bolt EST)

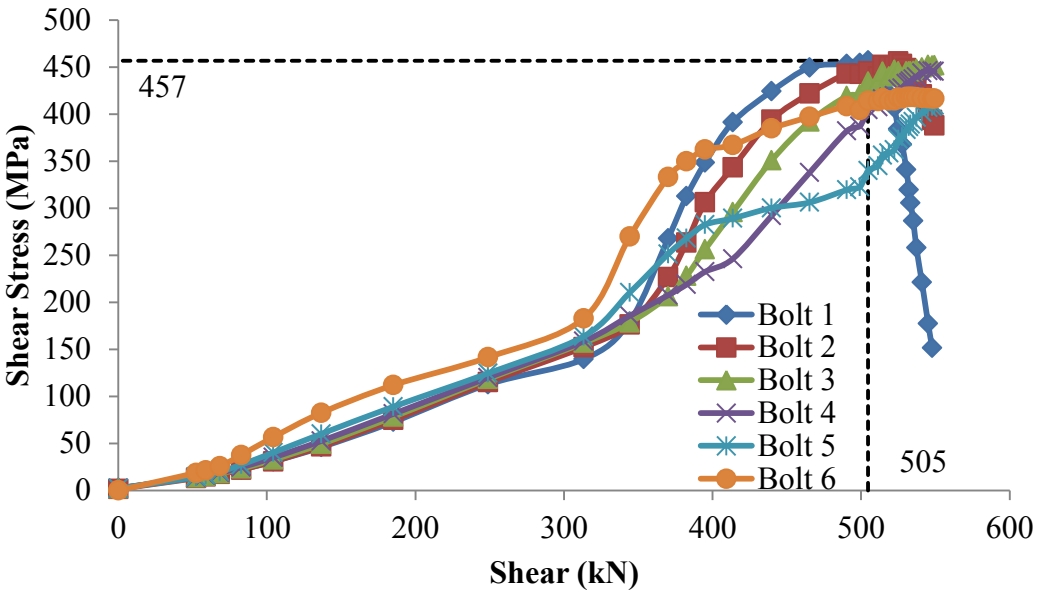

Figure 5.44 Shear stress versus connection shear for simulation 22 (6-bolt EST)

The movement of the inflection point for the four simulations is presented in Figure 5.45. A similar observation can be made in the movement of the point of zero moment in general. At failure, as the number of bolts increases, the effective bolt eccentricty increases where the effective bolt eccentricity, e_b, was 86 mm, 90 mm, 94 mm, 114 mm for the 3, 4, 5 and 6 bolted connections. This is reasonable since the more bolts in a connection, the stiffer the connection and thus the bigger eccentricity.

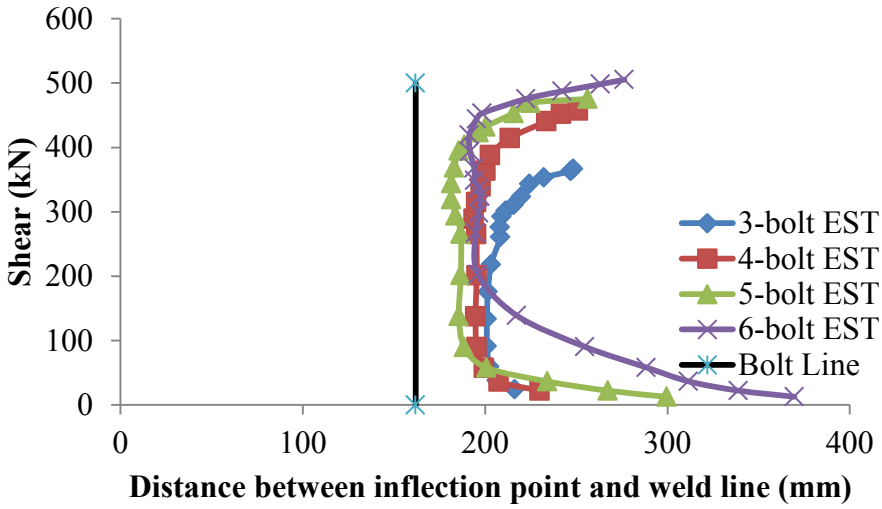

Figure 5.45 Distance of point of inflection to weld line for number of bolt parameter

Figure 5.46 below is a graph of the measured effective bolt eccentricity, e_b, versus the number of bolts in the connection. It shows that a more or less linear relationship is observed between the increase in effective bolt eccentricity, e_b, and the increase in the number of bolts. The eccentricity e_b increases as the number of bolts in the connection increases, which leads to an increased moment applied to the bolt group. However, the added capacity due to more bolts is still achieved.

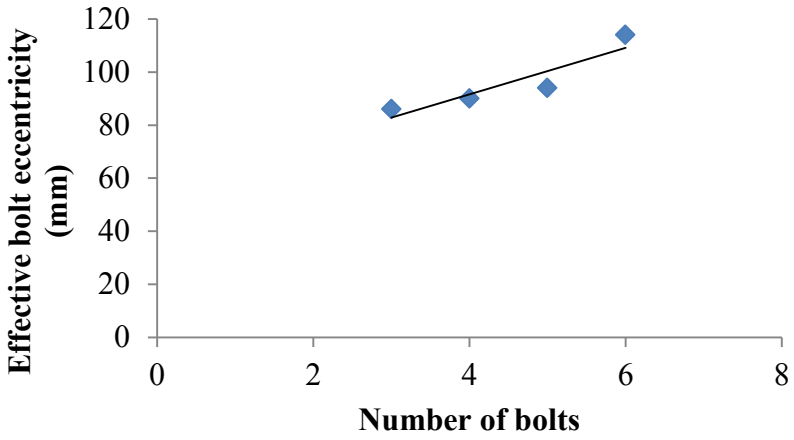

Figure 5.46 Number of bolts versus measured e_b

The bolt group shear strength was the governing limit state for all four simulations as predicted by AISC manual 2011. Table 5.13 summarizes the FE ultimate capacity and the AISC predicted capacity for each simulation. The AISC manual 2011 underestimates the 3, 4 and 5 bolted connections by 62%, 45%, and 31%, respectively when compared with FE results. The AISC manual 2011 predicted the 6 bolted connection capacity within 2% of FE results. When the FE measured e_b was used, the bolt capacities were more accurately predicted for the 3 and 4 bolted connection with improved predicted-to-FE ratio of 0.67 and 0.85, respectively. However, the FE measured e_b used in AISC procedure over predicted the capacity of the 5 and 6 bolted connections, resulting in $F_{u,fe}/F_u$ ratios greater than 1.

Table 5.13 Summary of effect of number of bolts

Simu. No.	Number of bolts	$e_{b,FE}^{(1)}$ (mm)	$e_{b,AISC}^{(1)}$ (mm)	$F_{u,FE}^{(3)}$ (kN)	$F_{u,AISC}^{(4)}$ (kN)	$F_u^{(5)}$	$F_{u,FE}/F_u$	$F_{u,AISC}/F_u$
3	3	86	162	244	139	368	0.66	0.38
20	4	90	162	389	250	457	0.85	0.55
21	5	94	162	538	375	474	1.13	0.79
22	6	114	162	641	517	505	1.27	1.02

This discrepancy may be explained as follows. The AISC manual 2011 design procedure is based on the instantaneaous center of rotation method described in Chapter 2. This method assumes that the center of rotation in line with the centroid of the bolt group. However, according to FE results, the center of rotation for the five and six bolted connections occurs closer to the bottom bolt resulting in added stress in the top bolt causing shear failure. Figures 5.47 to 5.50 illustrate the bolt movement for the 3, 4, 5 and 6 bolted EST connections obtained from FE analysis. The Y-axis represents the initial bolt line location. The circles represent the initial and final bolt location at failure. It can be seen that the center of bolt rotation lies much closer to the bottom bolt (where the dotted black line crosses the Y-axis) for the 5 and 6 bolted connections but close to the middle bolt for 3 and 4 bolted connections. AISC manual 2011 method assumes the dotted black line passes through the origin, a concentric rotation about the vertical centroid of the bolt group. This method fails to recognize the higher stresses generated in the topmost bolts due to the shift of the center of rotation, especially in the case of high number of bolts (>4). Thus, for 3 and 4 bolted EST connections, using FE measured e_b in combination with AISC manual 2011 method improves the bolt shear strength estimate. But for 5 and 6 bolted EST connections, using FE measured e_b in combination with AISC manual 2011 method overestimates the connection shear capacity. The conservative estimate of eccentricity by AISC design procedure, on the other hand, seems to provide reasonably accurate bolt shear strength estimate.

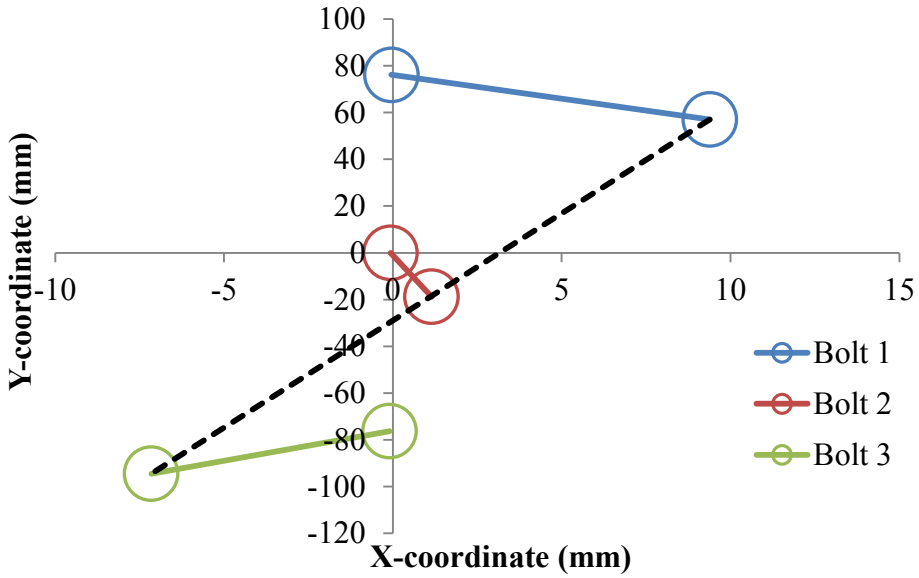

Figure 5.47 Bolt movement for 3-bolt EST connection

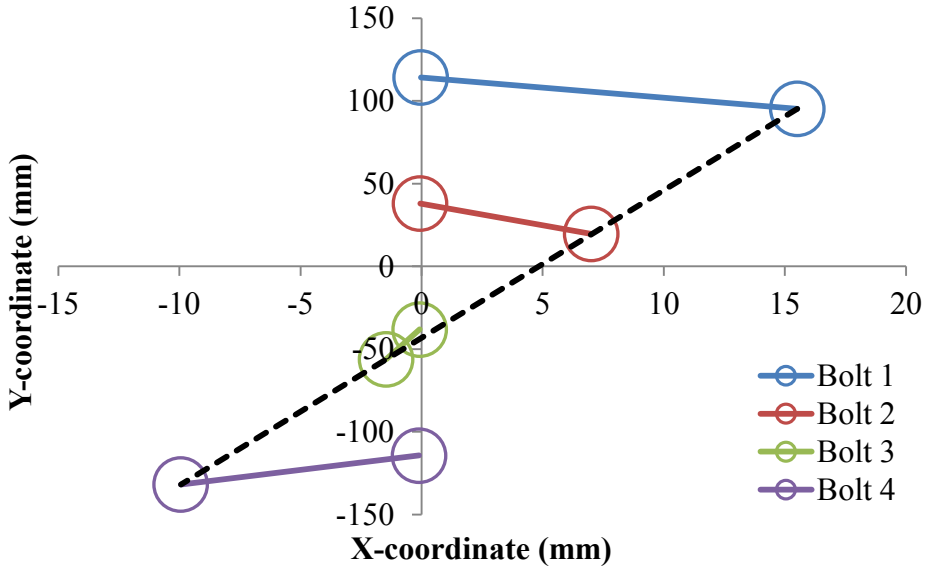

Figure 5.48 Bolt movement for 4-bolt EST connection

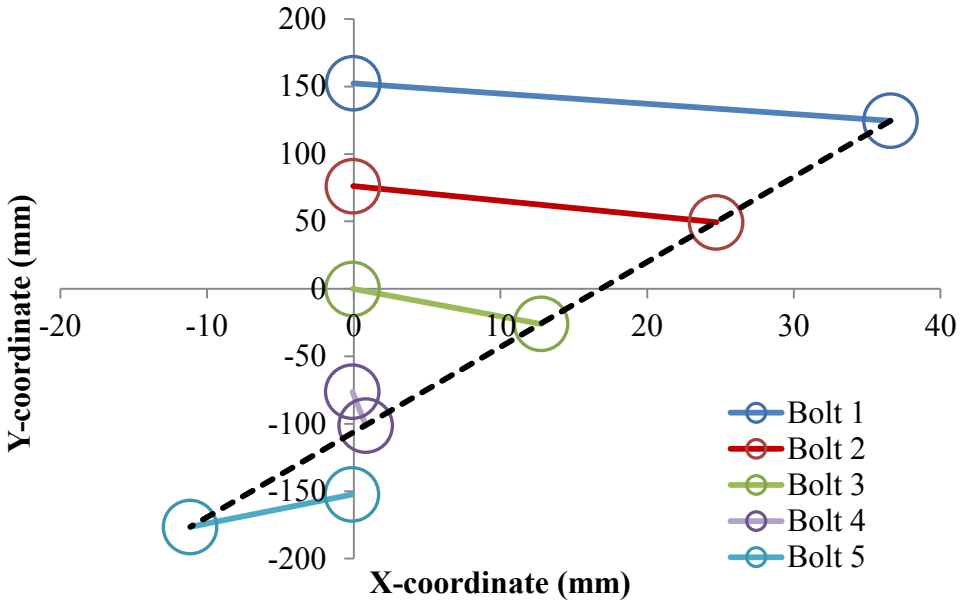

Figure 5.49 Bolt movement for 5-bolt EST connection

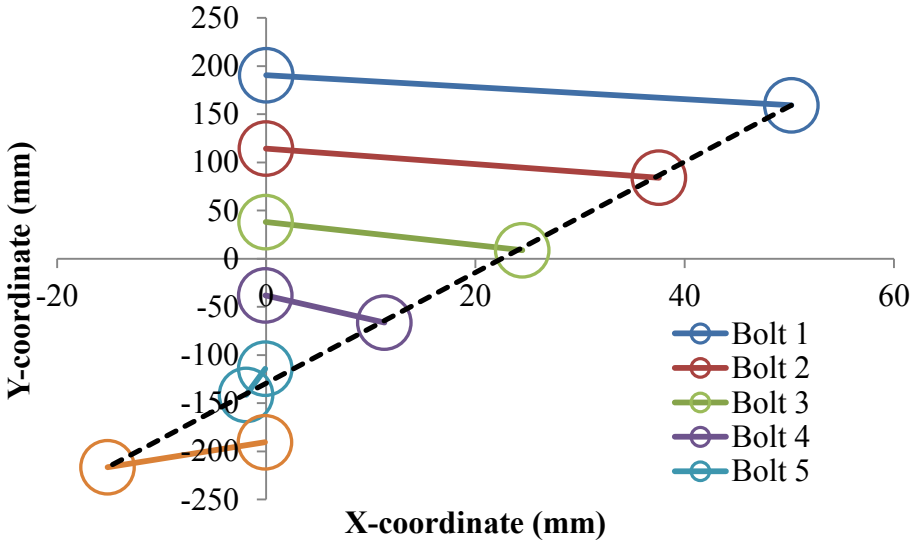

Figure 5.50 Bolt movement for 6-bolt EST connection

5.9 Evaluation of Available Effective Eccentricity Equations

The only exsiting effective eccentricity equation for EST connections is proposed by Sherman and Ghorbanpoor (2002) for EST connections with 6 or less bolts. The recommended equation is shown in Equation [5.2]. The effective bolt eccentricity, e_b, measured in inches, is solely dependant on the number of bolts, n, in the connection with a maximum upper limit of distance 'a'.

$$e_b = n \leq a, \text{ in} \qquad \text{for } n \leq 6 \qquad [5.2]$$

The effective eccentricity for 3 bolted EST connections obtained from this study is compared with values ontained using this equation and AISC manual 2011 values in Figure 5.41. The solid blue line in the figure indicates the e_b value suggested by the AISC manual 2011, which is 162 mm for the given parameters. The red line represents e_b recommended by Sherman and Ghorbanpoor (2002), which is 76.2 mm. The dots in green are the measured eccentricities at bolt failure extracted from the FE model. A total of nine 3-bolt EST connection simulations were used. It can be seen that the measured bolt eccentricities are much smaller than the value suggested by the AISC 2011 design procedure. The equation proposed by Sherman and Ghorbanpoor (2002) seems to provide a lower bound value of the effective bolt eccentricity. The purple crosses marked in Figure 5.51 were obtained by back-calculating the effective bolt eccentricities using the FE ultimate loads if AISC 2011 method is used. The average of the eccentricities obtained from the back-calculation of the FE ultimate load is represented as a solid purple line, which is around 47 mm.

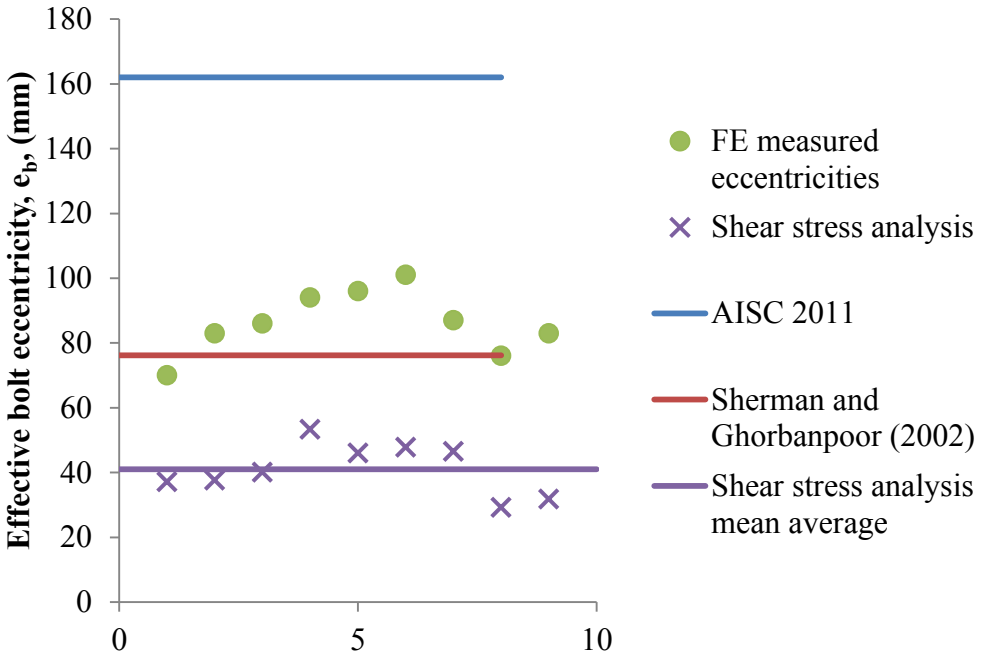

Figure 5.51 Effective bolt eccentricity, e_b, for all EST connections governed by bolt fracture

As for the 4-bolt, 5-bolt, and 6-bolt EST connections, the AISC 2011 design procedure suggests a bolt eccentricity of 162 mm for all cases. The equation by Sherman and Ghorbanpoor (2002) yields a bolt eccentricity of 102 mm, 127 mm, and 152 mm, respectively. The FE analyses predicted bolt eccentricities of 90 mm, 94 mm, 114 mm for the 4-bolt, 5-bolt and 6-bolt EST connections.

CHAPTER 6 Summary and Conclusion

6.1 Summary

The purpose of this study was to investigate the behaviour and strength of unstiffened extended single plate shear connections focusing on the bolt shear strength. A finite element model was developed in ANSYS to simulate the EST connection behaviour in a typical beam to column web connection situation. The FE element model was verified using experimental test results obtained from Astaneh et al. (1989) on CST connections and from Sherman and Ghorbanpoor (2002) on EST connections. A parametric study was subsequently carried out to study effects of seven parameters on the strength of EST connections. The behaviour in the from of connection shear vs. beam end rotation responses is discussed; the effective eccentricity obtained from FE model is presented and the validity of AISC manual 2011 design procedure is assessed.

6.2 Conclusion

6.2.1 Web Slenderness Ratio of the Supporting Column

An increase in the slenderness of the web, h/w, results in a increase in the effective eccentricity for the bolt group and a reduction in the shear capacity of the connection. Columns with a low web slenderness (i.e. stiffer support) had more evenly distributed shear stresses. A minimum h/w ratio should be placed to avoid the web yielding.

6.2.2 Distance ‘a’

An increase in distance “a” results in an increase in the bolt eccentricity and hence a decrease in the connection strength. However, the rate of the increase in the effective eccentricity decreases and it seems that the maximum effective bolt eccentricity levels off at 105 mm.

6.2.3 Plate Thickness

For the studied thickness, an increase in the plate thickness results in an increase in the connection shear strength and also more even distribution in the shear stress among all bolts. The failure of the connection using a thin plate may be governed by plate yielding rather than bolt fracture as in the case of thicker plate.

6.2.4 Double-Row of Bolts

A sufficiently thick plate needs to be used with double-row bolts to ensure bolt shear failure. When a thin plate (10 mm) is used, the failure of connections using double-row bolts was governed by the tensile yielding of the shear tab due to flexure at the top of the shear tab whereas when a thicker plate (12 mm) is used, the failure of connection is governed by bolt shear. However, the AISC manual 2011 design procedure predicted bolt fracture to be the governing limit state for both cases. A minimum plate thickness requirement should be developed for multi-row bolt arrangement.

6.2.5 Lateral Restraint

The presence of a lateral restraint at the beam end effectively controls the twisting of the EST. Excluding the end restraint can significantly decrease the connection capacity. A 35% decrease in connection capacity for the 3-bolt EST connection is observed when end restraint was absent.

6.2.6 Beam Length-to-Depth Ratio

The beam end rotation increases with the increase in length-to-depth ratio of the beam. The increased beam end rotation results in an increase in the effective eccentricity and a reduction in the connection capacity.

6.2.7 Number of Bolts

An increase in number of bolts results in an increase in the FE measured bolt eccentricity. However, the connection capacity increase is realized with the increase in the number of bolt. The instantaneous center of rotation for the 3 and 4-bolt EST connections occurred close to the centroid of the bolt group whereas this location for the 5 and 6-bolt EST connections occured close to the bottom bolt resulting in increased stresses on the top bolts.

6.2.8 Evaluation of AISC manual 2011

In general, the AISC design procedure only permits 34% to 42% of the available 3-bolt connection capacity and 55% of the available 4-bolt connection capacity when compared with finite element results.. This conservatism is due to the large values used in the AISC

bolt eccentricity. When the finite element determined eccentricity is used in combination with AISC design procedure, the prediction of bolt shear capacity of the connection can be improved by about 30%. In the case of 5 and 6-bolt connections, the AISC procedure predict the capacity within 12 and 2% of the finite element results, respectively. It suggests that the AISC procedure is more accurate for the use of EST connections with higher number of bolts.

6.3 Recommendations for Future Work

Extended single plate shear connection simulation by finite element modeling allows the study of various parameters without the need of costly physical experimental studies. The following are recommendations for further research.

- Additional studies on the effect of double and triple bolt rows on the single plate behaviour.
- This series of FE modeling focused on single plate shear connections to flexible column supports. Additional work should be done to flexible girder supports.
- Assess the influence of larger bolt diameters on the bolt eccentricity and connection capacity.
- Investigate stiffened extended single plate shear connections, where the shear tab is stiffened with a plate that is welded between the column flanges.

REFERENCES

ANSYS (2010), User Manual, Version 13.0, ANSYS, Inc., SAS IP, Inc.

CISC (2010), Handbook of Steel Constructions, 10th ed., Canadian Institute of Steel Construction

AISC (1994), *Manual of Steel Constrcution LRFD*, Vol. II, 2nd ed., American Institue of Steel Construction, Chicago, IL.

AISC (2005), *Steel Construction Manual*, 13th ed., American Institute of Steel Construction, Chicago, IL.

AISC (2010), *Specification for Structural Steel Buildings,* ANSI/AISC 360-10, American Institute of Steel Construction, Chicago, IL.

AISC (2011), *Steel Construction Manual*, 14th ed., American Institute of Steel Construction, Chicago, IL.

Ashakul, A. (2004), "Finite Element Analysis of Single Plate Shear Connections,"*Doctor of Philosophy Dissertation*, Virginia Polytechnic Institute and State University, Blacksburg, Virginia.

Astaneh, A., Call, S.M. and McMullin, K.M. (1989), "Design of Single Plate Shear Connections," *Engineering Journal*, American Institute of Steel Construction, Vol. 26, No. 1.

Astaneh, A. and Porter, K.A. (1990), "Design of Single Plate Connections with Snnug-Tight Bolts in Short Slotted Holes," Report No. UCB/SEMM-90/23, Department of Civil Engineering, University of California, Berkeley.

ASTM (2013),"Specification for Structural Bolts, Steel, Heat Treated 830MPa Minimum Tensile Strength," ASTM International, WestConshohocken, PA, 2013, DOI: 10.1520/C0033-03

Crawford, S.F and Kulak, G.L. (1968), "Behavior of Eccentrically Loaded Bolted Connections," Studies in Structural Engineering, No. 4, Departmentof Civil Engineering, Nova Scotia Technical College, Halifax, NS.

Creech, D. (2005), "Behavior of Single Plate Shear Connections with Rigid and Flexible Supports," *Master of Science Thesis,* North Carolina State University, Raleigh, NC.

Hormby, D.E, Richard, R. M., and Kriegh, J. D. (1984). "Single-Plate Framing Connections with Grade 50 steel and Composite Construction," *Engineering Journal*, American Institute of Steel Construction, Vol. 21, No. 3.

Kulak, G.L. and Grondin, G.Y. (2010), "Limit States Design in Structural Steel," Canadian Institute of Steel Construction

Lipson, S.L., (1968), "Single-Angle and Single-Plate Beam Framing Connections," *Canadian Structural Engineering Conference*, Toronto, ON, Canada, pp. 141-162

Muir, L.S. and Thornton, W.A. (2011), "The Development of a New Design Procedure for Conventional Single-Plate Shear Connections," *Engineering Journal*, American Institute of Steel Construction, Vol. 48, No. 2.

Rahman, A., Mahamid, M., Amro, A. and Ghorbanpoor, A. (2003), "3D FE Model of Extended Shear Tab Connections," 16th Engineering Mechanics Conference, ASCE, Seattle

Rahman, A., Mahamid, M., Amro, A. and Ghorbanpoor, A. (2007), "The Analyses of Extended Shear Tab Steel Connections, Part I: The Unstiffened Connections," Engineering Journal, American Institute of Steel Construction, Vol 44, No.2.

Richard, R. M., Gillett, P. E., Kriegh, J. D., and Lewis, B. A. (1980), "The Analysis and Design of Single-Plate Framing Connections," *Engineering Journal,* American Institute of Steel Construction, Vol. 17, No. 2.

Richard, R. M., Kriegh, J. D., and Hormby, D. E. (1982), "Design of Single Plate Framing Connections with A307 Bolts," *Engineering Journal*, American Institute of Steel Construction, Vol 19, No. 4.

Sherman, D.R., and Ghorbanpoor, A. (2002), "Design of Extended Shear Tabs" *Research Report RR3095*, American Institute of Steel Construction, Inc., Chicago, IL.

Yarimci, E. and Slutter, R.G. (1963), "Results of Tests on Riveted Connections," Report No. 200.63.401.1, Fritz Engineering Laboratory, Lehigh, Betlehem, Pa.

Young, N. W., and Disque, R. O. (1981), "Design Aids for Single Plate Framing Connections," *Engineering Journal*, American Institute of Steel Construction, Fourth Quarter, 129-148.

APPENDIX A

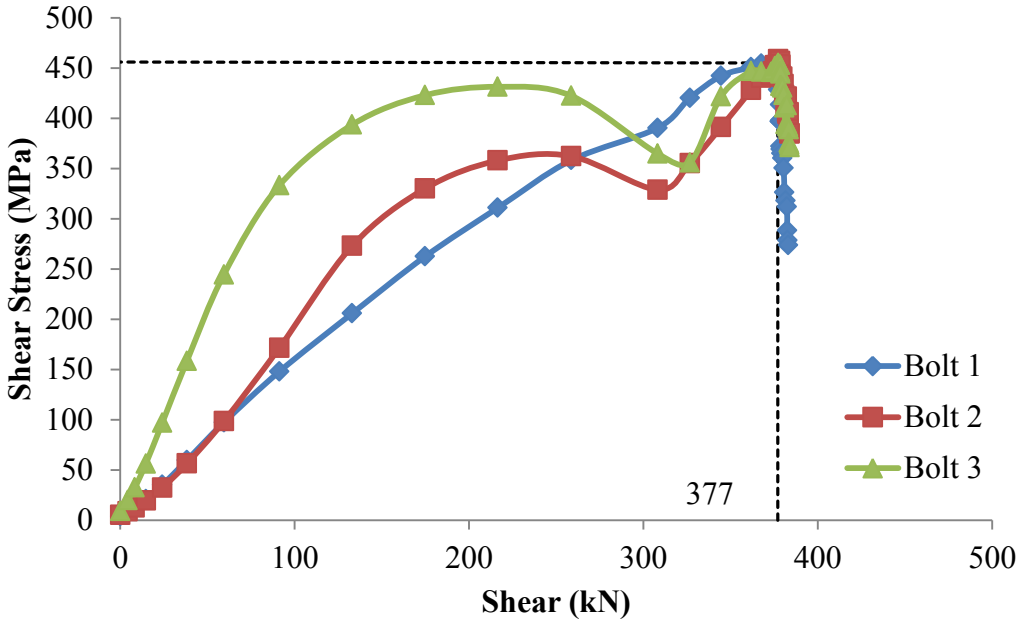

Figure A.1 Shear stress versus connection shear for simulation 1

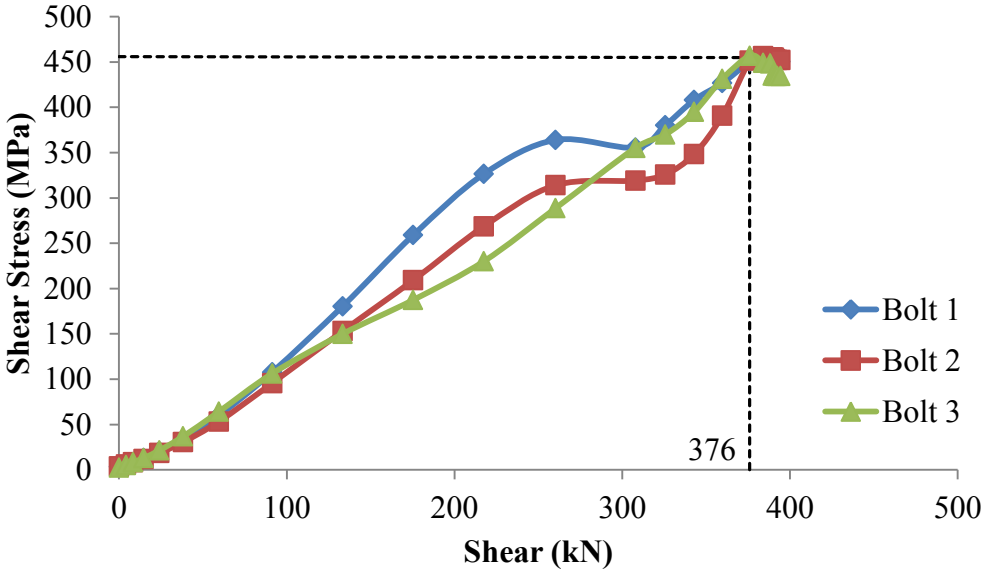

Figure A.2 Shear stress versus connection shear for simulation 2

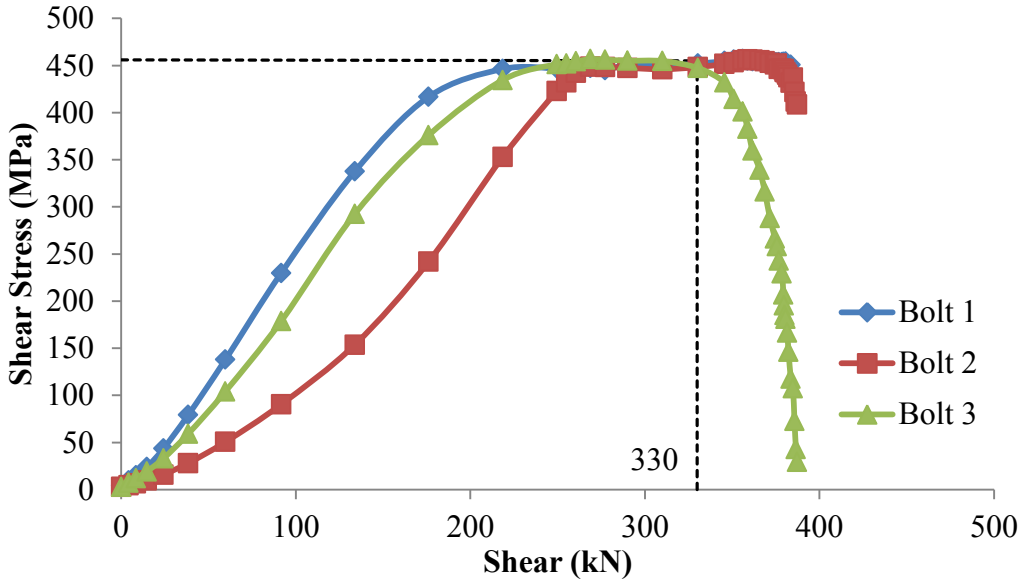

Figure A.3 Shear stress versus connection shear for simulation 4

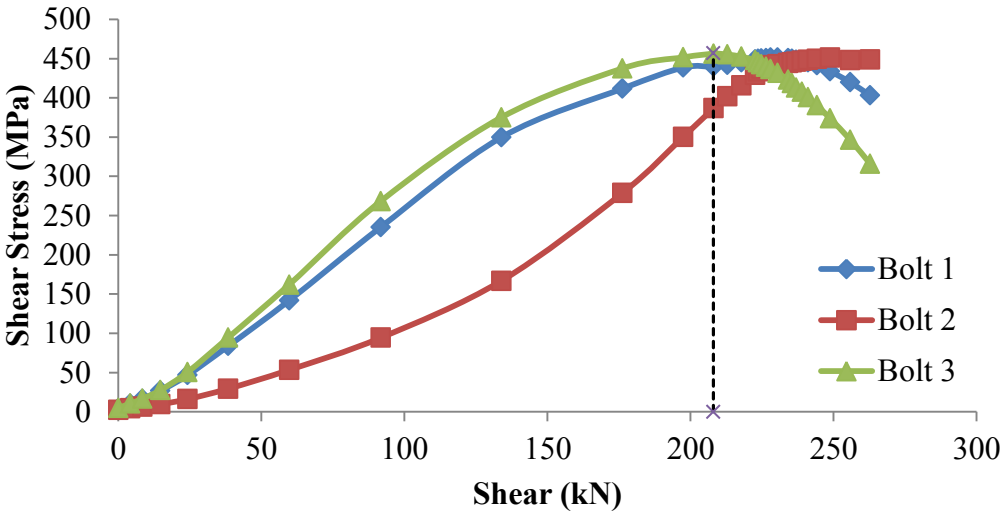

Figure A.4 Shear stress versus connection shear for simulation 5

APPENDIX B

Appendix B contains an sample calculation of how the critical limit state according to AISC manual 2011 design procedure was determined for the extended single plate configuration. The calculations presented are for simulation 3. The limit states considered in the calculations for each connection are:

1. Bolt shear.
2. Bolt bearing.
3. Plate shear yielding.
4. Plate shear rupture.
5. Plate block shear.
6. Shear yielding, shear buckling and yielding due to flexure of plate.
7. Plate buckling.

The material resistance factor, φ, is excluded from all calculations.

Example Calculation: Simulation 3

1) **Bolt shear:**

$\mathbf{R_n = C * F_v * A_b}$ (AISC 2011 Eqn J3-1)

$A_b = 0.442\ in^2$ (Table 7-1)

$F_u = 137\ ksi$

$F_v = 0.563 f_u = 77.2\ ksi$

e_b = 6.37 in

C = 0.918 (Interpolation in Table 7-6)

R_n = $C*f_v*A_b$

= $0.918*77.2kips*0.442in^2$

= 31.3 kips

= 139 kN

2) Bolt Bearing:

R_n=C*lesser of ($1.2*L_c*t*F_u$,$2.4*d_b*t*F_u$) (AISC 2011 Eqn J3-6a)

Lc = 1.5-(13/16)/2 in = 1.09 in

t_{plate} = 0.394 in

F_u = 87.0 ksi

d_b = 0.75 in

C = 0.918

$1.2*L_c*t*F_u$ = 44.8 kips → governs

$2.4*d_b*t*F_u$ = 61.7 kips

R_n = 0.918*44.8 kips = 41.1 kips

= 183 kN

3) Plate shear yielding:

$R_n=0.6*F_y*A_{gv}$ (AISC 2011 Eqn J4-3)

F_y = 50.8 ksi

d_{plate} = 9 in

t_{plate} = 0.394 in

A_{gv} = 9 in *0.394 in = 3.54 in^2

Rn = 0.6*50.8 ksi*3.54in^2 = 108 kips

= 480 kN

4) Plate shear rupture:

$R_n=0.6*F_u*A_{nv}$ (AISC 2011 Eqn J4-4)

F_u = 87.0 ksi

d_{plate} = 9 in

t_{plate} = 0.394 in

d_{bolt} = 0.75 in

n = 3 bolts

A_{nv} = t_{plate}*(L-n(d_{bolt}+1/8))) = 0.394*(9-3*(0.75+1/8))

= 2.51 in^2

R_n = 0.6*87 ksi * 2.51in^2 = 131 kips

= 582 kN

5) Plate block shear

$R_n = U_{bs}F_uA_{nt}$ + lesser of ($0.6F_uA_{nv}$, $0.6F_yA_{gv}$) (AISC 2011 Eqn J4-5)

F_y = 50.8 ksi

F_u = 87.0 ksi

t_{plate} = 0.394 in^2

d_{bolt} = 0.75 in

U_{bs} = 0.5

A_{nt} = t_{plate}*(1.5-(d_{bolt}/2+(1/16)))

= 0.394in*(1.5in-(0.75in/2+(1/16in))) = 0.42 in^2

A_{gv} = 0.394in*(9in-1.5in) = 2.96in^2

A_{nv} = t_{plate}*(7.5-2.5*(d_{bolt}+1/8))

= 0.394in*(7.5in-2.5*(0.75in+1/8in)) = 2.09in^2

$0.6F_uA_{nv}$= 0.6*87 ksi*2.09 in = 109.1 kips

$0.6F_yA_{gv}$= 0.6*50.8 ksi*2.96 in = 90.2 kips →governs

R_n = 0.5*87.0 ksi*0.42 in^2+90.2 kips

= 108.5 kips

= 482 kN

6) Shear yielding, shear buckling and yielding due to flexure of plate.

$$\left(\frac{V_r}{V_c}\right)^2 + \left(\frac{M_r}{M_c}\right)^2 \leq \mathbf{1.0}$$ (AISC 2011 Eqn 10-5)

F_y = 50.8 ksi

Dplate = 9 in

Tplate = 0.394 in

Zplate = (0.394in)*(9 in)^2/4 = 7.98 in^3

M_c = F_yZ_{pl} = 50.8ksi*7.98in^3 = 405 kips

Vc = 31.3 kips

E = 6.37 in

Mr = Vr kips * 6.37 in = 6.37Vr kip-in

Solve for Vr:

(Vr/(31.3kips))^2 + (Vr * 6.37 in/405kips)^2 = 1

0.001021Vr^2 + 0.000247Vr^2 = 1

0.001268Vr^2 = 1

Vr = 34.08 kips

7) Plate Buckling

$$\lambda = \frac{h_o\sqrt{F_y}}{10t_w\sqrt{475 + 280\left(\frac{h_o}{c}\right)^2}}$$

h_o = 9 in

c = 6.374 in

F_y = 50.8 ksi

t_{plate} = 0.394 in

λ = 0.506 < 0.7 There plate buckling doesn't govern